NPS-69-82-003

NAVAL POSTGRADUATE SCHOOL
Monterey, California

TRAILING VORTICES IN STRATIFIED FLUIDS

by

T. SARPKAYA
S. K. JOHNSON

June 1982

82 07 19 112

NAVAL POSTGRADUATE SCHOOL
Monterey, California

J. J. Ekelund, RADM, USN
Superintendent

D. A. Schrady
Acting Provost

Reproduction of all or part of this report is authorized.

This report was prepared by:

TURGUT SARPKAYA
Distinguished Professor of
Mechanical Engineering

Reviewed by: Released by:

Paul J. Marto, Chairman   William M. Tolles
Department of Mechanical   Dean of Research
Engineering

11

SECURITY CLASSIFICATION OF THIS PAGE (When Data Entered)

REPORT DOCUMENTATION PAGE	READ INSTRUCTIONS BEFORE COMPLETING FORM
1. REPORT NUMBER NPS-69-82-003 2. GOVT ACCESSION NO.	3. RECIPIENT'S CATALOG NUMBER
4. TITLE (and Subtitle) TRAILING VORTICES IN STRATIFIED FLUIDS	5. TYPE OF REPORT & PERIOD COVERED Progress Report
	6. PERFORMING ORG. REPORT NUMBER
7. AUTHOR(s) Professor Turgut Sarpkaya LCDR Steven Kenneth Johnson	8. CONTRACT OR GRANT NUMBER(s) ARPA Order 3925
9. PERFORMING ORGANIZATION NAME AND ADDRESS Naval Postgraduate School Monterey, California 93940	10. PROGRAM ELEMENT, PROJECT, TASK AREA & WORK UNIT NUMBERS
11. CONTROLLING OFFICE NAME AND ADDRESS Defense Advanced Research Projects Agency (DARPA) 1400 Wilson Blvd., Arlington, VA 22209 (ATTN: Dr. A. J. Bruckheim)	12. REPORT DATE June 1982
	13. NUMBER OF PAGES iv + 162
14. MONITORING AGENCY NAME & ADDRESS(if different from Controlling Office)	15. SECURITY CLASS. (of this report) UNCLASSIFIED
	15a. DECLASSIFICATION/DOWNGRADING SCHEDULE

16. DISTRIBUTION STATEMENT (of this Report)

Approved for public release; distribution unlimited.

17. DISTRIBUTION STATEMENT (of the abstract entered in Block 20, if different from Report)

18. SUPPLEMENTARY NOTES

19. KEY WORDS (Continue on reverse side if necessary and identify by block number)

Stratified Flow; Trailing Vortices; Delta Wings; Vortex Pair

20. ABSTRACT (Continue on reverse side if necessary and identify by block number)

Experiments were conducted with two Delta wings and a streamlined body with lifting surfaces to investigate the evolution of turbulent trailing vortices in stratified and unstratified water. The vortex trajectories were determined as a function of the relative depth D/b_0, normalized time $V_0 t/b_0$, and the stratification parameter $N b_0/V_0$. The results have shown that the vortices rise only to a finite height as they gradually demise under the influence of turbulence, sinusoidal instability, and the vortex

DD FORM 1473   EDITION OF 1 NOV 68 IS OBSOLETE
(Page 1)   S/N 0102-014-6601

iii

SECURITY CLASSIFICATION OF THIS PAGE (When Data Entered)

 # 20 - ABSTRACT - (CONTINUED)

breakdown. The effect of stratification is to reduce the lifespan of vortices and the maximum height attained by them. Various approximate analyses have been examined and new ones have been proposed to determine the lifespan of the vortices. Finally, an exploratory numerical analysis of the two-dimensional, unsteady laminar vortices has been carried out with encouraging results.

Accession For		
NTIS GRA&I	☒	
DTIC TAB	☐	
Unannounced	☐	
Justification		
By		
Distribution/		
Availability Codes		
Dist	Avail and/or Special	
A		

SUMMARY

Experiments were conducted with two Delta wings and a streamlined body with lifting surfaces to investigate the evolution of turbulent trailing vortices in stratified and unstratified water. The vortex trajectories were determined as a function of the relative depth D/b_0, normalized time $V_0 t/b_0$, and the stratification parameter Nb_0/V_0. The results have shown that the vortices rise only to a finite height as they gradually demise under the influence of turbulence, sinusoidal instability, and the vortex breakdown. The effect of stratification is to reduce the lifespan of vortices and the maximum height attained by them. Various approximate analyses have been examined and new ones have been proposed to determine the lifespan of the vortices. Finally, an exploratory numerical analysis of the two-dimensional, unsteady, laminar vortices has been carried out with encouraging results.

PREFACE

The work reported herein is part of a basic research on trailing vortices in stratified and unstratified fluids and was performed during the period 1 January 1982 to 30 June 1982. The principal investigator is Dr. Turgut Sarpkaya, Distinguished Professor of Mechanical Engineering. Sponsorship was provided by the Defense Advanced Research Projects Agency (DARPA) under ARPA Order 3925. The contract technical monitor was Dr. Arthur J. Bruckheim, Program Manager, Tactical Technology Office, DARPA.

The authors wish to acknowledge the generous support of DARPA and the valued interaction with Dr. Arthur J. Bruckheim and Dr. I. E. Alber. A special note of thanks is extended to Mr. Jack McKay for his most skillful work in the construction and alterations of the test facilities and models.

TABLE OF CONTENTS

4

LIST OF FIGURES

6

LIST OF TABLES

9

TABLE OF SYMBOLS AND ABBREVIATIONS

B — The model base chord length

b_o — Vortex separation distance

C — Salt concentration

D — Initial depth of the vortices

d — Layer thickness

E — Kinetic energy

g — Acceleration of gravity

H — The height of the vortices above the original position

H_{max} — Maximum vertical height attained

N — Brunt-Vaisala frequency for gravity

P — Potential energy

p — Pressure

r_o — Initial vortex core radius

SP — Stratification parameter (Nb_o/V_o)

T — Temperature

t — Time

U — Speed of the model

u,v — Fluid velocity in the x and y directions

V_o — The vortex rise velocity at the moment of its generation

$W_{Fr.Water}$ — Weight of the fresh water

$W_{n,salt}$ — Weight of salt in the n-th layer

Y — Vertical distance from the streamlined body

Z — Distance downstream from the lifting surface

z — Complex variable

α -   Angle of attack of the model

α_t -   Thermal diffusivity

Γ -   Vortex strength

γ -   Angular vortex separation

ε -   Angle of the vertex of the model

ζ -   Vorticity

θ -   Temperature difference between ambient and local

ν -   Kinematic viscosity

ρ -   Density

σ -   Spread parameter

ψ -   Stream-function

I. INTRODUCTION

Trailing vortices formed by a lifting surface traveling through a stratified or unstratified fluid medium have been the subject of recent interest primarily because of their importance in the determination of safe aircraft separation distances for terminal areas. In recent years this interest has extended to the trailing vortices generated by the control planes of submerged bodies such as a submarine partly because of the effect of these vortices on the motion of the submerged body itself and partly because of the interaction of these vortices with the surrounding fluid medium.

The trailing vortices may be generated by any number of lifting surfaces such as an airplane wing, a missile, single or double Delta wings, or the control·surfaces of a submerged body (sail planes, rudder, and stern). The initial organization or roll-up of a trailing vortex from the vorticity generated by the lifting surface is very rapid and is generally complete within the space of several lifting-surface spans.

Whereas a single vortex is extremely stable, one or more vortices in close proximity exhibit a number of complex interactions and give rise to new phenomena which tend to accelerate the demise of the vortices involved. When a lifting surface starts from rest, a starting-vortex or a Horseshoe vortex is formed since a vortex must be connected either to itself or to a rigid boundary. A Horseshoe vortex is also formed when a lifting surface accelerates or decelerates rapidly, or undergoes a radical change in the angle of attack. When a control surface (e.g., a Delta wing) starts from rest and moves with a constant velocity, the Horseshoe

12

vortex closes on itself, breaks away from the rest of the trailing vortex, links rapidly, and forms a vortex ring. While the first vortex ring undergoes highly complex deformations, a second vortex ring is formed from the Horseshoe vortex connecting the tail end of the trailing vortex. This process does not continue forever for a number of reasons. The speed of the generating surface is much greater than the speed of advance of the vortex rings. Thus, the length of the vortex trail increases rapidly and the motion of the vortices becomes dominated by the mutual interaction of the vortices rather than by the horseshoe vortices at their tail end. The motion of each new vortex ring differs from the one shed previously partly because of the continued aging or diffusion of vorticity (i.e., a weaker ring is formed at succeeding steps) and partly because the motion of each new ring is controlled by all the rings shed previously and by the ever-increasing vortex trail. These phenomena lead to the rapid demise of vortex rings. In fact, shortly after the start of the motion of the lifting surface the horseshoe vortex and the vortex rings play a very minor role on the evolution of the trailing vortex.

The trailing vortices are subjected to three known decay mechanisms: (i) Aging of vortices due to eddy viscosity; (ii) sinusoidal instability leading to the linking of vortices (known as the Crow instability); and (iii) vortex breakdown.

These mechanisms can act independently or in combination. The viscous and turbulent diffusion of vorticity lead to the gradual dissipation of the trailing vortices. Clearly, this phenomenon is strongly influenced by the initial vorticity distribution and the ambient turbulence. Furthermore, the proximity of other vortices, free surface, rigid surfaces

13

(e.g., the submerged body, ground, etc.), ambient shear, stratification of the fluid medium, etc., affect the demise of the vortices. Clearly, the aging of the vortices is ever present and affects the evolution of the trailing vortices regardless of whether the Crow instability and/or vortex bursting take place or not.

Breaking up by linking or sinusoidal instability involves the growth of a rather regular sinusoidal pattern, usually symmetrical for the trailing vortex pair. This is commonly referred to as Crow linking. The time to link (the formation of a series of vortex rings and Horseshoe vortices) has been found to depend, statistically, on atmospheric turbulence within the inertial subrange of eddy sizes (a size range from a few cm to some hundreds of meters). The scale of linking varies around nine times the vortex spacing. Thus, it is the eddy sizes in the range of one to ten times the span or vortex spacing which has the main effect on linking. The formation of vortex rings by linking (distinctly different from those generated at the start of motion) lead to the rapid demise of the vortex trail. Consequently, one would want to accelerate the formation of links (e.g., by periodically changing the angle of attack of the control surfaces) if one is interested in decreasing the hazard posed by the trailing vortices to other aircraft or in decreasing the energy transferred to the fluid medium.

The vortex breakdown is essentially a single-vortex phenomenon, in the sense that it is not necessarily connected with the induced flows associated with the other vortex of the pair. There are, however, frequent occurrences of core bursting in conjunction with the sinuous instability, in which case the sinuous vortex deformation appears to induce core bursting. The effect of vortex breakdown is to flatten the velocity profile by

14

significantly reducing the peak velocity (or the velocity of numerous peaks of several smaller vortices) under the center of the vortex, but without major effect on the speeds away from the vortex center. A definite vortex flow remains in all cases, indicating that core bursting does not totally eliminate the vortex. In fact, the persistence of the outer flow circulation suggests that vortex breakdown may not significantly alleviate the vortex hazard and the energy transfer to the surrounding medium. The understanding of the vortex-breakdown and the determination of how much circulation remains after breakdown remain as critical and vexing questions.

The trailing vortices move downward (downwash) when generated by a lifting surface with a positive angle of attack, as in the case of an airplane, or upward (upwash) when generated by a sail plane with a negative angle of attack, as in the case of a submarine. In either case, the motion of the vortices is determined by the mutual induction, vorticity distribution, the three types of the instabilities or demise mechanisms cited above, stratification effects of the fluid medium, ambient flow turbulence, shear and currents present in the fluid medium, and the proximity effects (e.g., free surface, bottom, ground, other bodies, etc.). An inviscid flow analysis based on concentrated line vortices can help to predict the early stages of motion of the vortices. However, the later stages of the motion become increasingly dominated by the factors cited above and it is not possible to examine the evolution of the trailing vortices without taking into consideration the effect of viscosity, turbulence, stratification, mutual induction, proximity, and all the other phenomena which arise as a consequence of these fundamental variables.

It must also be pointed out that whereas the trailing vortices generated by an aircraft are under each other's influence (in addition to the external non-vortical influences), the trailing vortices generated by a large submerged body may also be under the influence of a complex system of image vortices imbedded in the body.

Density stratification within the fluid medium is of great importance in the migration and ultimate demise of trailing vortices. The atmosphere is less dense at higher altitude while the oceans exhibit various patterns of stratification due to local temperature, salinity, and depth. Generally, a vortex migrates with the fluid in which it was born, retaining most of the original fluid in a so-called recirculation cell. The upwash of the vortices in the ocean environment into a layer of lesser density gives rise to a buoyancy which is in the opposite direction to the velocity resulting from the mutual induction. Furthermore, the motion of the recirculation cell produces oppositely-signed vorticity in the surrounding medium. This, in turn, gives rise to the entrainment and detrainment of fluid from the recirculation cell. Altogether, these additional consequences of stratification help to reduce not only the life of vortices but also the height to which the vortices rise asymptotically. One may also surmise that the stratification will tend to change the occurrence and the resulting characteristics of eddy diffusion, Crow instability, and core bursting. It is evident from the foregoing that the phenomena associated with the generation, migration, interaction, and demise of trailing vortices are very complex. As the review of the previous investigations will reveal, it is not yet possible to devise mathematical models with which some or all of the characteristics of the

phenomena can be predicted. As in many other flow situations, the role played by turbulence and the quantification of the turbulence stresses pose difficult questions. The gradual understanding of the behavior of trailing vortices must rely for the time being on carefully conducted experiments without losing sight of the fact that one must ultimately devise a model to acquire a power of prediction as well as a means to reduce the number of experiments for model verification.

It is clear from the foregoing that the reason for developing as much an understanding as possible of the behavior of trailing vortices is to permit design and improvement of an operational system which properly balances safety and efficiency in the motion of vortex-generating bodies and also to aid in the development of devices to enhance vortex decay, limit vortex upwash, and minimize energy transfer to the surrounding medium. The effort towards the understanding of some of the underlying phenomena forms the basis of the present investigation.

II. REVIEW OF PREVIOUS INVESTIGATIONS

Vortices and vortex wakes have become a major theme of aerodynamics
research since the advent of the large aircraft. The objectives have been
to predict the trajectories and lifetimes of trailing vortices, in order
to relieve the constraint on flight operations imposed by the vortex
hazard. Much of the progress made during the past two decades was dis-
cussed at the Symposium on Aircraft Wake Turbulence and Its Detection
[Ref. 1], held in Seattle in 1970, and at the Aircraft Wake Vortices
Conference [Ref. 2], held in Cambridge, MA in 1977.

The fundamental questions regarding the evolution of the trailing
vortices may be summarized as follows: (i) how does the vorticity gener-
ated by the lifting surfaces organize itself into two or more centers of
vorticity behind and to each side of the lifting surface? (ii) how do
the discrete centers of vorticity interact and affect the stability of
each other? (iii) how does a vortex demise and how does the demise of a
single vortex differ from that of a vortex pair? And finally, (iv) what
is the effect of stable stratification on the generation, roll-up, inter-
action, stability, and demise of vortices?

A. ROLL-UP OF VORTICITY

It is a well known fact that a vortex sheet is trailed from a finite-
aspect-ratio lifting surface as a consequence of the nonuniform spanwise
lift on the wing. The roll-up of this sheet into discrete vortices as
a result of a convective motion was recognized as early as 1907 by
Lanchester [Ref. 3]. Since then there have been numerous studies to
describe this complicated phenomenon. The first mathematical model to

18

describe the inviscid structure of the vortex wake was proposed by Prandtl [Ref. 4]. He based his model on the conservation of mechanical energy and found that the vortex tube radius for an elliptically loaded wing is approximately 8 percent of the wing span. In this analysis the choice of the swirl velocity distribution is somewhat arbitrary, being only constrained by circulation at large radius from the vortex center and the integral constraint on kinetic energy. In other words, the model does not address itself to the determination of the final structure of the wake for a given initial vorticity distribution.

The second model, which overcomes some of the arbitrariness inherent in the Prandtl model, was developed by Betz [Ref. 5]. Betz's model is based on four integral invariants of an incompressible two-dimensional bounded vorticity distribution. The Betz model has now been checked against measurements made behind model and full-scale aircraft and it has been found that the model predicts *distributions which are in far* better agreement than the Prandtl model [Ref. 4].

In more recent times the advent of numerical methods and computer gave impetus to the use of discrete vortex models. In most numerical analyses, the attached boundary layers on the wing surfaces are represented by bound-vortex sheets while the separated free-shear layers are modeled by free-vortex sheets. The free-vortex sheets join the bound-vortex sheets along the separation lines which are known a priori for wings with sharp edges. Furthermore, it is assumed that the vortex breakdown (see e.g., Refs. 6-8) occurs far downstream so that the primary core size and its variation in the vicinity of the wing are negligible. This assumption limits the angle of attack (dependent on

the aspect ratio of the wing) at which the inviscid model is applicable. Furthermore, the flow outside the bound-vortex sheet(s) and the free-vortex sheet(s) is assumed irrotational. Within these limitations, the resulting potential flow model represents the main features of the real flow to a high degree of accuracy. The literature contains several steady and unsteady inviscid-flow models with various degrees of limitations and drawbacks.

The first group of models uses slender-body theory and conical flow assumption [Refs. 9-12]. These models satisfactorily predict the pressure distribution over the front portion of the wing surface. In the rear portion, the models fail to predict a satisfactory pressure distribution because the Kutta-Joukovsky condition is violated at the trailing edge. Such models are limited to simple delta planforms. The second group of models uses a nonlinear discrete-vortex method [Refs. 13-20]. In these models, the bound vortex sheet and the free-vortex sheets are approximated by a set of concentrated vortex lines. The bound vortex sheet is replaced by a bound-vortex lattice, while the free-vortex sheet is replaced by segmented free-vortex lines (in the case of steady flow) or by growing free-vortex lattice (in the case of unsteady flow). The boundary conditions are satisfied at certain control points on the bound- and free-vortex system using an iterative technique.

Although the discrete vortex model has worked well for many years for attached flow problems, when vortex-type separation from leading edges and/or tips occurs, the free-vortex system lies close to the lifting-surface bound vortices and the results are found to be sensitive to variations in the shapes of the vortex elements and the relative lengths of the vortex segments (see e.g., Ref. 21).

20

The third group of models employs doublet-panels (see e.g., Refs. 22-23). In this method, the wing and its free-vortex sheets are divided into networks of quadrilateral panels. Each panel of the networks representing the wing has a biquadratic local doublet distribution and a bilinear local source distribution. Source and doublet splines are used to express the distributions of singularities on the networks in terms of discrete values of singularity strength at certain standard points on each network. The boundary conditions and continuity of singularity strengths across abutting networks are enforced at certain standard points on each network. The results of this method are generally good when the solution converges (see e.g., Refs. 24-25). Apparently, the difficulty in obtaining convergence is due to the failure in satisfying the continuity of the derivatives of the doublet strength across abutting networks. This is equivalent to the existence of concentrated vortex lines between abutting networks. Additional related works are discussed in Ref. 26 in connection with the AGARD Symposium on High Angle of Attack Aerodynamics.

The fourth group of models employs a nonlinear hybrid vortex method (see e.g., Refs. 27-28). In this method, continuous-vorticity and vortex-line representations of the wing and its separated free-shear layers are used. Continuous vorticity is used in the near-field calculations while discrete vortex lines are used in the far-field calculations. The calculated net surface pressure and section normal-force coefficients for wings with tip separation are in good agreement with the experimental data and the nonlinear discrete-vortex method.

The roll-up calculations do not give details of the structure of the tip vortex to be used as initial conditions in a viscous solution. Often

21

the approximate solution of Kaden [Ref. 29] for the unsteady roll-up of
an infinite sheet is used as the basis for the prediction of the decay
of laminar trailing vortices [Ref. 30]. The most obvious drawback of
the existing models is the lack of a realistic model of the leading-
edge core and its feeding sheet. Modeling of the leading-edge core and
its feeding sheet had been first introduced by Brown and Michael [Ref.
31]. This model has been improved by Mangler and Smith [Ref. 32] and
Smith [Ref. 33]. Additional improvements have been made by Moore [Ref.
34] who devised a method to collapse the tightly-wound inner portion of
the vortex sheet into a single tip vortex. This was done primarily to
avoid the numerical difficulties associated with the crossing of the
vortex sheets and with the spurious interaction between the successive
turns of the inner portions of the vortex sheet. Clearly, this sacri-
fices the detail of the tip vortex structure. The latest efforts regard-
ing the calculation of the roll-up process use the method of rediscreti-
zation of shear layers. This method has been devised by Fink and Soh
[Ref. 35] and extensively used by Sarpkaya and Shoaff [Ref. 36]. The
numerical models based on the inviscid flow theory do not account for
the diffusive effects of viscosity and turbulence. Thus, they are not
capable of predicting the evolution of the trailing vortices.

B. TRAILING VORTICES

The vortex sheets roll-up asymptotically and it may be several wing
spans behind the aircraft before the fully rolled-up condition is
reached. With the high Reynolds numbers encountered on lifting surfaces
in free flight, it is likely that their boundary layers, and thus their
trailing vortex sheets, are turbulent. At finite Reynolds numbers,

22

vorticity diffuses, and the sheet becomes a vortex layer of finite, non-zero thickness. Successive turns in the centermost portions of the rolled-up layer merge, the spiral structure disappears and, if the radius of the vortex core is greater than the diffusive length scale, an equilibrium structure ensues. Thus, one anticipates a multi-structured core, the inne:most part of which has effectively reached a state of equilibrium and surrounding this an annulus in which the turns have merged or are in various stages of merging, and an outer region, beyond which discrete turns of the spiral remain evident.

Dynamics of the flow require axial velocities to be present in trailing vortices [Ref. 37] and these can have an important effect on the stability of the trailing vortex systems and play an important role in the occurrence of vortex breakdown. It is also a well-known fact that the occurrence of vortex breakdown in trailing vortices may be delayed or enhanced by the acceleration or deceleration of the ambient flow due to the proximity of streamlined axisymmetric bodies whose control surfaces may have given rise to the development of trailing vortices. Thus, it is important to make a distinction between the trailing vortices of an aircraft and those of a submerged body. In the case of the former, the trailing vortices are not affected by the proximity of the aircraft body partly because the length of the aircraft in terms of the wing span is relatively small and partly because the wing span is many times that of the body diameter. In the case of a common submerged body, the wing span of the major control surfaces is in the order of the body diameter and the length of the body in terms of the wing span may be in the order of ten. Consequently, the trailing vortices of a submerged body are significantly affected by the

23

flow about the body and by the propulsion system which may modify the flow about the body so as to affect the evolution of the trailing vortices and the occurrence of vortex breakdown. Evidently, the said differences stem from the fact that the wings on an aircraft provide the lift necessary for flight whereas the control surfaces on a submerged body provide only partial lift for depth and attitude control. The major portion of the lift is already provided by the buoyancy of the body.

Numerous attempts have been made to model the behavior of laminar and turbulent trailing vortices. Direct calculation of the structure of the trailing vortices is done by assuming a final flow configuration and requiring conservation of some chosen flow quantities. Most early discussions of the far-field structure were based on the vortex-wake model of Spreiter and Sacks [Ref. 38]. They have assumed that the wake consists of two Rankine vortices, with uniform vorticity inside the core and zero vorticity outside. The circulation and vortex separation are given by Stokes' theorem and conservation of momentum. The core radius is determined by requiring kinetic energy to be conserved. For an elliptically loaded wing this model gives a core radius of about 0.1 times the trailing vortex separation. Test flight data reported that the cores are somewhat smaller than predicted and that all of the vorticity is not in the core [Refs. 1-2].

Donaldson [Ref. 39] noted that the model of Betz [Ref. 5] which assumes that each half of the vortex sheet rolls up into a circular vortex core conserving circulation, impulse, and momentum of impulse, could be used. This conserves the moment of inertia of the vortex distribution about its centroid. Betz further determined the distribution of circulation in the vortex by assuming the vorticity outboard of some point, which will form

24

the core of the vortex inside some radius, conserves its moment of iner-

tia about its own centroid during roll-up. Both Jordan [Ref. 40] and

Donaldson [Ref. 41] have obtained similar solutions. This approach

agrees much better with flight test data than the model of Spreiter and

Sacks [Ref. 38].

C. STABILITY OF TRAILING VORTICES AND THE EFFECT OF STRATIFICATION

If the trailing vortices could be represented as a two-dimensional

vortex pair, the study of their motion may be more straightforward.

Unfortunately, they are most unstable to three-dimensional disturbances

so that the vortices rapidly lose their two-dimensional character. This

is one of the major differences between the motion of a single vortex

and the vortex pair. A single vortex is known to be very stable whereas

a vortex pair suffers from numerous instabilities. Nevertheless, the

study of two-dimensional vortex pairs has continued in hopes of obtaining

a satisfactory solution that will match what little three-dimensional

data are available. The majority of the data have been obtained in large

scale atmospheric tests using aircraft [Refs. 42-43] or from vortex rings

[Refs. 44-45]. Barker and Crow [Ref. 46] and Tomassian [Ref. 47] have

created two-dimensional vortices in a small tank with large circulations

and comparably small separations. There are significant differences

between the experimental results cited. These differences and their

explanations are further compounded by the contradictions of the analyses.

There are fundamental differences in the assumptions made and widely

differing conclusions have been reached regarding the motion of the trail-

ing vortex pair in a stratified medium. The lack of consistent laboratory

data did not help to resolve the differences and to delineate the most

important elements of the physics of the motion. Most models use an oval shaped fluid body carried by the vortices under the influence of their mutual induction and the density difference with the surroundings. There is a significant difference in the accounting of fluid momentum, impulse, energy, viscous and turbulent diffusion, and in the assumptions concerning the buoyancy induced vorticity entrainment and detrainment within the recirculation cell (see Fig. 1). One school of thought holds that the recirculation cell buoys upward in a stably stratified atmosphere [Refs. 48-49], while others maintain that the vortices accelerate downward [Refs. 50-51]. The resolution of the dilemma is important, because of the understanding of wake hazard and of the energy transferred to the surrounding medium.

Table I, adapted from Widnall [Ref. 52], describes the differences in some of these models. The models of Scorer and Davenport [Ref. 50] and Crow [Ref. 51] do not include turbulence effects. The models of Hecht et al., [Refs. 44 and 53] are computer generated flow fields assuming constant recirculation cell areas. Clearly, the differences in these models cannot be resolved until reliable laboratory data are available. It is important that the experiments model the trailing vortices and not just a pair of two-dimensional vortices. The three-dimensional nature of the flow and the importance of the axial velocity in the trailing vortices must be reflected in the proper simulation of the behavior of vortices. It is, thus, important that the differences between the three-dimensional experiments and the two-dimensional analytical or numerical models be clearly delineated. It is only through such comparisons that one would be able to determine as to whether enough physics have been incorporated into the analytical model.

26
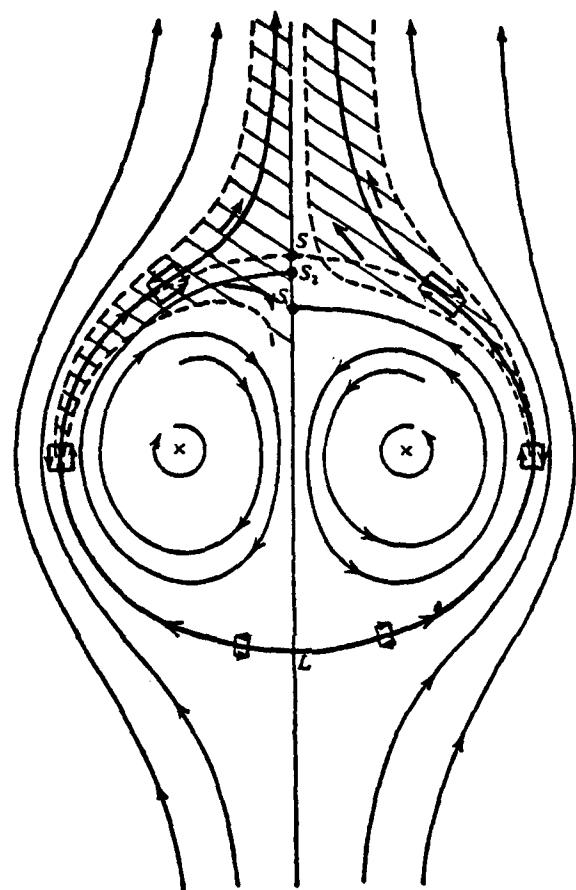
Figure 1. Downward Migrating Recirculation Cell
in a Stratified Atmosphere.

27

TABLE I

Comparison of Theoretical Studies of Vortex Pairs in a Stably Stratified Atmosphere

Author	Vortex Spacing	Migration Speed	Buoyancy Generated Vorticity
Costen [52]			
Weak stability	Decreases	Increases	No Effect
Strong stability	Increases	Stops	-
Kuhn & Nielsen [58]	Decreases	Increases	Partly Ent.
Saffman [49]	Increases	Stops	Entrained
Scorer & Davenport [50]	Decreases	Increases	Detrained
Tombach [59]			
Strong stability	Increases	Stops	Entrained
Weak stability	Decreases	Increases	Entrained
Tulin & Shwartz [48]	Increases	Stops	Entrained & Annihilated
Crow [51]	Decreases	Increases	Created in Wake
Narain & Uberoi [60]	Decreases	Decreases	Entrained
Hecht et al. [44]	Decreases	Stops	Created at Boundary
Hecht, Bilanin, Hirsh [53]	Not Appreciable	Stops	Created at Boundary

The first quantitative analysis of the three-dimensional sinusoidal instability observed in trailing vortices in an ideal homogeneous fluid was given by Crow [Ref. 54]. His results showed good agreement with the observations of the general features of aircraft vortex instability. Crow and Bate [Ref. 55] explored the growth of vortex-pair instability when driven by ambient turbulence. They have calculated the time to linkage as a function of the Kolmogorov turbulence parameter. The possibility of exciting the vortex-pair instability by changing the lifting surface span-load distribution was suggested by Crow and demonstrated in flight by Chevalier [Ref. 56] by changing aircraft pitch angle periodically.

The trailing vortices may also suffer from instabilities inherent to single vortices, i.e., from vortex breakdown. Although the mechanism is not well understood, the presence of axial velocities in the trailing vortices and the proximity of the body from which the vortices are emanating play significant roles in the occurrence of vortex breakdown. The vortex breakdown has been studied in detail for single vortices (see e.g., Refs. 6-8). It is not known what would be the effect of mutual induction and straining of vortices on the breaking of one or both of the vortices. Furthermore, it is not clear as to what happens after the breakdown. It was assumed that the breakdown leads to the total dissipation of circulation and thus its occurrence is most desirable. However, observations [Ref. 2] have shown that the vortex breakdown does not totally dissipate the existing circulation. Thus, the determination of how much circulation remains in a vortex after the breakdown constitutes one of the major questions. One would also like to determine as to how long the remaining circulation persists. Qualitatively, it is now clear

29

that the path to the ultimate destruction of trailing vortices has not
yet been charted. The Crow instability, laminar and turbulent diffusion,
entrainment and detrainment of oppositely-signed vorticity, vortex break-
down or a cascade of vortex breakdowns, and the proximity effects (body
or ground) play significant roles. For a submerged body, the deceleration
of the ambient flow toward the tail of the body may give rise to vortex
breakdown at a fixed point relative to the body. This, in turn, results
in a series of vortex breakdowns as the body moves at a constant speed,
leaving behind a cascade of breakdowns. Since each breakdown separates
a supercritical swirling flow from a subcritical flow (downstream of the
breakdown) (see Ref. 7) and since the subcritical flow cannot sustain
waves, each breakdown rapidly moves upstream to catch up with the newest
breakdown. This, in turn, leads to rapid weakening of the trailing vortices.
The quantification of these qualitative observations constitute the essence
of future research efforts.

D. SUMMARY OF THE PREVIOUS INVESTIGATIONS

It is clear from the foregoing that a great deal of additional work
is needed to understand the rolling-up of vortices in both the strati-
fied and unstratified fluid medium, the evolution of trailing vortices,
the demise mechanisms, and the processes leading to the ultimate destruc-
tion of vortices. Analytical studies must be based on reliable experimental
data in order to incorporate as much relevant physics as possible into
the models. Furthermore, the analyses must be based on the observations
and measurements of three-dimensional trailing vortices rather than those
of two-dimensional vortices in order to bring into focus the important
role played by the three-dimensionality of the flow and the axial velocity

30

in the vortices. In fact, a rigorous investigation of the entire phenomenon might begin with trailing vortices generated by relatively simple bodies (such as a Delta wing or rectangular wing) in an unstratified medium and then expanded to include the effect of stratification. At present there are no extensive experiments in either medium and no detailed calculations have been reported.

III. EXPERIMENTAL EQUIPMENT AND PROCEDURES

It is clear from the foregoing that there is very little or no data regarding the motion of trailing vortices in stratified and unstratified fluids. It is also clear that the analytical models and numerical calculations can be judged, validated, and upgraded only through the use of data obtained with three-dimensional trailing vortices under controlled laboratory conditions. This, in turn, requires the use of a large water basin in which various models may be towed at desired speeds.

The test facility used in the present investigation was developed with the following specific objectives in mind: (i) the establishment of the parameters governing the phenomenon and the scaling laws; (ii) the understanding of the characteristics of the sinusoidal instability in three-dimensional trailing vortices with axial velocity; (iii) the determination of the role played by the vortex breakdown or cascade of breakdowns and of the circulation remaining in the trailing vortices following breakdown; (iv) the establishment of any interaction between the sinusoidal instability and the vortex breakdown; (v) the investigation of the effect of ambient stratification, ambient turbulence, and model-induced turbulence on the evolution and demise of trailing vortices; (vi) the determination of the characteristics of internal waves generated by the body and/or trailing vortices prior to, during, and after the onset of sinusoidal instability and/or vortex breakdown; (vii) to examine the behavior of trailing vortices generated by a lifting surface undergoing time-dependent oscillations (with or without the body-proximity effects); (viii) to study the evolution of Horseshoe vortices and vortex rings; (ix) to examine the effect of the alterations in the axial velocity of the vortices at the time of their

32

generation; and (x) to investigate the interaction of the trailing vortices with the vortices generated by the body and/or control surfaces.

The experimental equipment consists of the water basin, the stratification system, and the test models.

A. WATER BASIN

The basin is 36 feet long, 3 feet wide and 5 feet deep and is made of 0.5-inch thick aluminum plates, welded appropriately (see Fig. 2). The back wall of the tank is reinforced to prevent bulging under hydrostatic pressure. The front wall is fitted with square windows of 1.0-inch thick plexiglass for flow visualization.

Vertical and horizontal scales of 0.5-inch increments are marked on the central window. The scales are used during the experiments to evaluate the position of the trailing vortices (see Fig. 3).

The aluminum interior of the tank is painted with marine epoxy to prevent corrosion. In addition, the inside face of the back wall is painted with flat white paint to provide better contrast and make the flow visualization easier with the dye used.

The filling pipes lie on the bottom of the tank. They are plastic pipes 2.0-inch diameter, perforated along their entire length with holes of 1/16-inch diameter (see Fig. 4).

Two drains are provided at the bottom at each end of the basin. Two parallel rails of 1.0-inch diameter are mounted along the bottom of the tank. A carriage rides smoothly on these rails and provides the test body with a constant velocity through the use of an endless cable and a 3/4 Hp DC motor (see Fig. 5). The velocity of the model is measured and continuously monitored through the use of a magnetic velocity sensor,

33
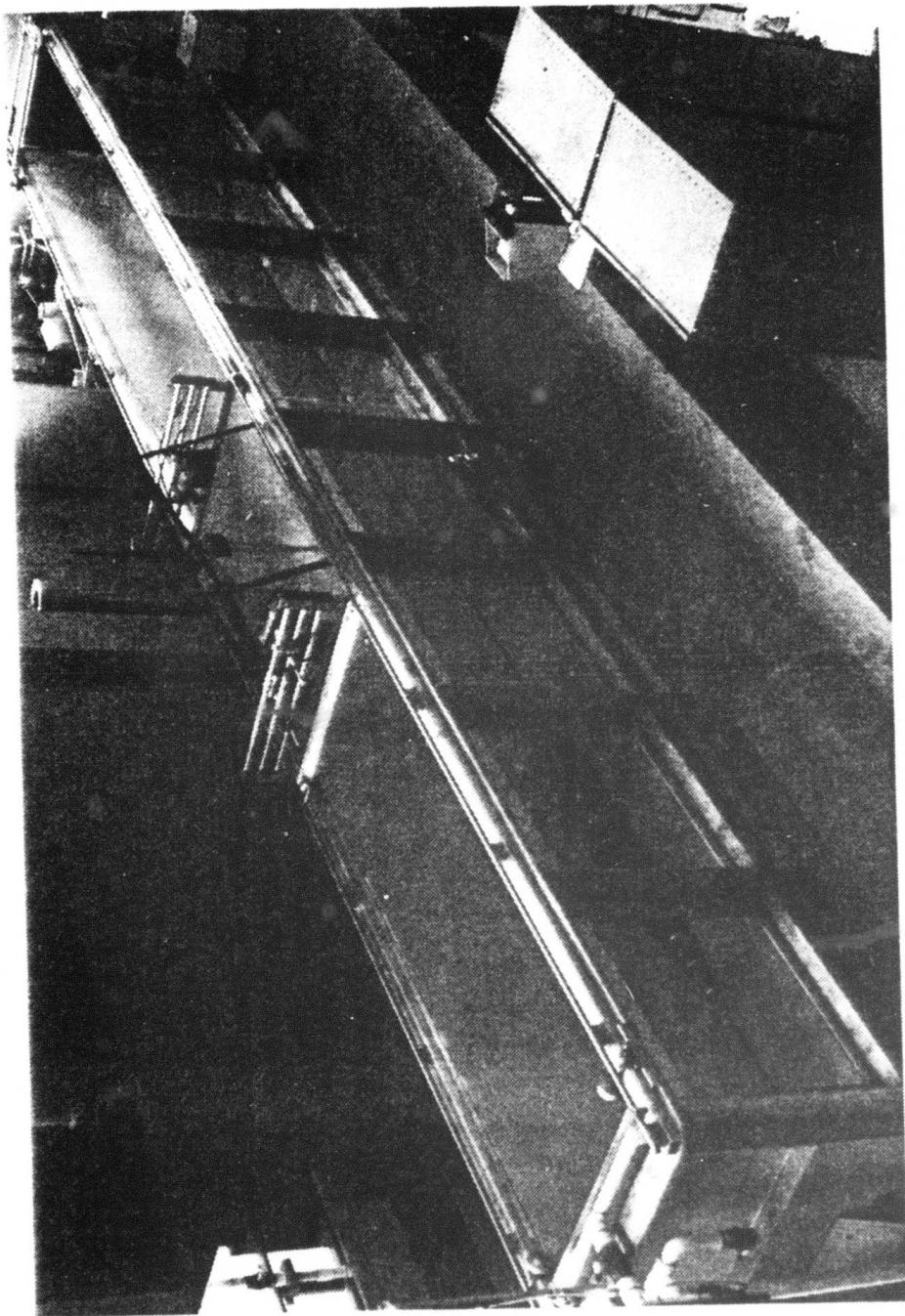
Figure 2. Water Basin.
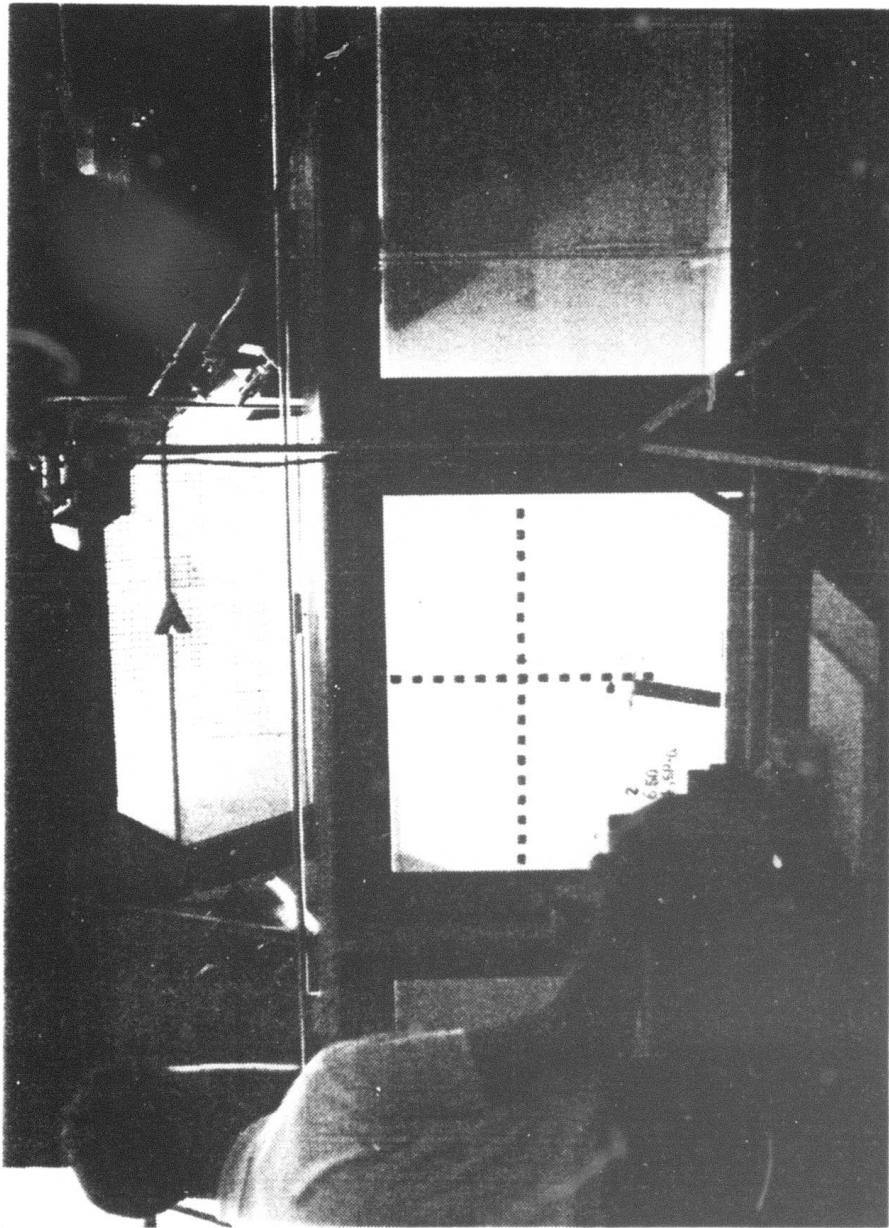
Figure 3.   Central Window and the Horizontal and Vertical Scales.
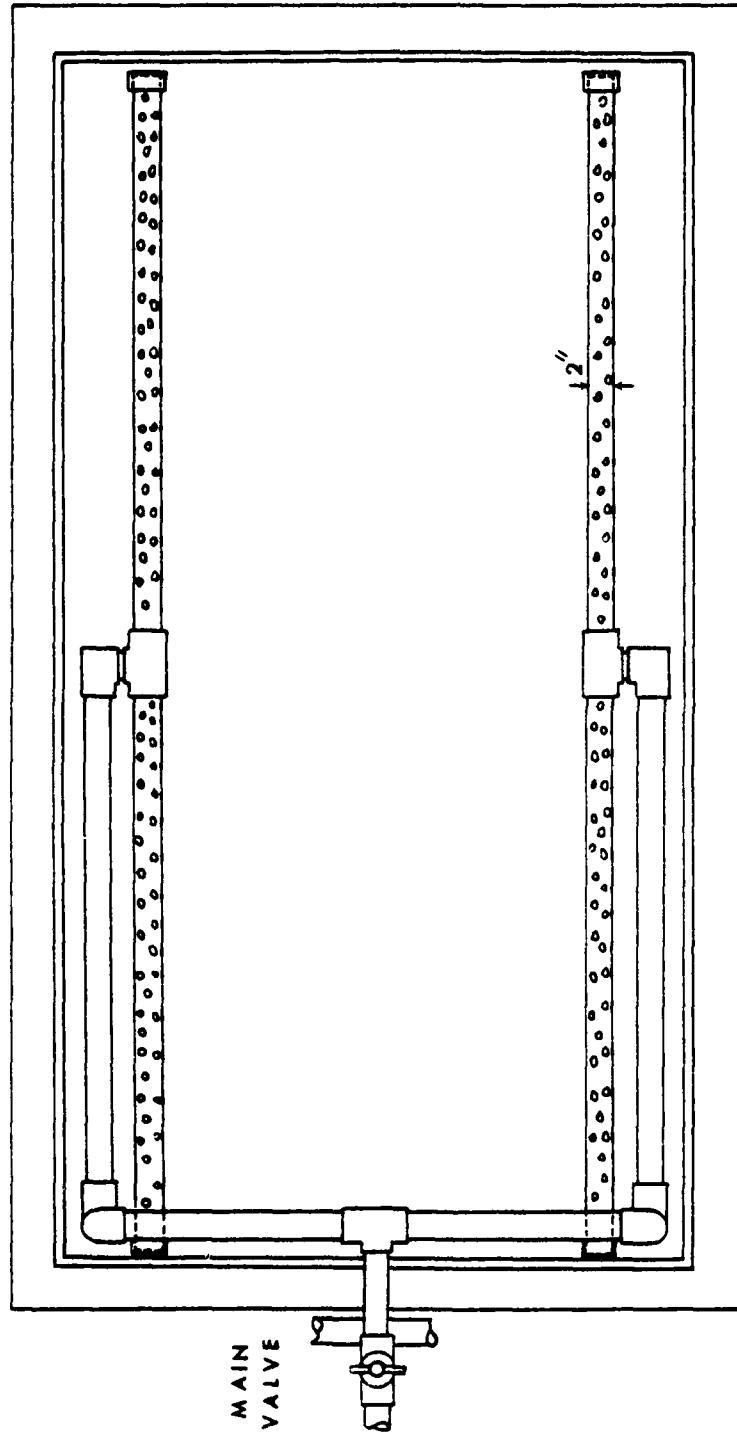
Figure 4. Top View of Stratification System.

MAIN
VALVE

2"
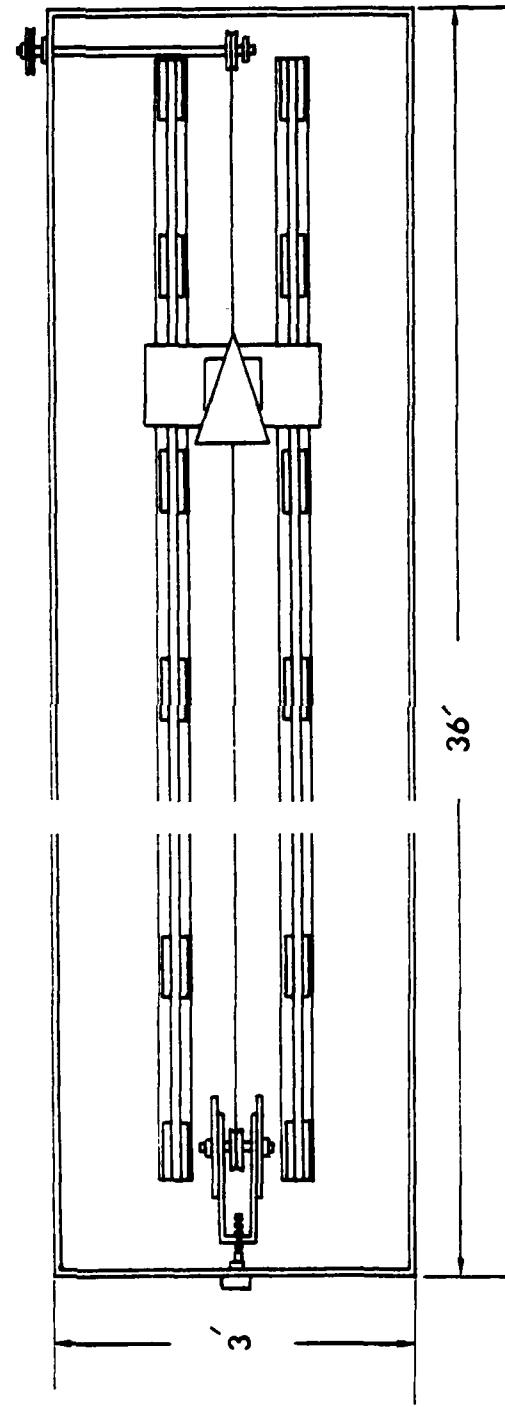
Figure 5. Towing Mechanism.

37

mounted above a precision gear. The sensor counts the number of teeth
and yields and instantaneous velocity proportional to the velocity of
the model.

The two rails, the carriage and the filling pipes are located on or
near the bottom of the basin and under a turbulence management system.
This system consists of a one-inch-thick polyurethane foam, sandwiched
between two perforated aluminum plates (see Fig. 6).

B. STRATIFICATION SYSTEM

The stratification system consists of four tanks (60-gallon capacity
each) and the necessary tubes and valves.

First, brine water of certain salt concentration is prepared in one
of these tanks. Then precalculated amounts of brine water are added to
the other three tanks, depending on the desired density gradient and the
number of the layers. The calculation of the amount of salt needed, for
a certain density gradient or for a certain stratification parameter, is
discussed in Appendix A.

The resulting solution is drained into the basin at a rate of 2.1 CFM.
Necessary precautions have been taken to prevent air entrainment and
subsequent bubble generation. Furthermore, two air-bubble traps have
been, installed, one just before the main valve of the filling system
and one at the middle point of the delivery pipes.

This system can fill the water basin and establish a desired stratifi-
cation in about three hours. There is no difficulty regarding the desired
density gradient, even for the lower gradients (e.g., $d\rho/dy = 5 \times 10^{-5}$
slug/ft^3/inch). The density discontinuity between the 0.9-inch layers
disappeared by diffusion after a short time for the stratifications of

38
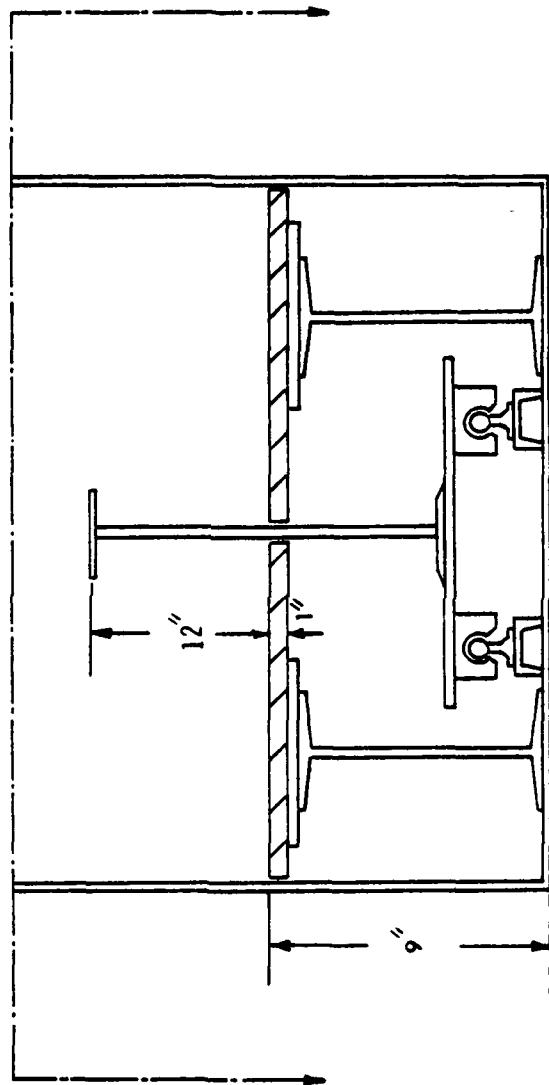
Figure 6. Turbulence Management System.

39

interest. Smooth density gradients were obtained as verified by a salinity meter. The parts of the stratification system are shown in Figs. 4 and 7.

C. MODELS

Three models were used in the experiments. The first two models are Delta wings, made of 1/8-inch thick aluminum with hollow interiors. Each model cavity is filled with dye prior to the filling of the basin with water. The two holes at the rear edge of each model and the third hole in the middle of the upper surface are plugged prior to an experimental run to prevent dye leakage (see Fig. 8). The dye consisted of food coloring and proper amounts of alcohol. The density of the mixture was such that the dye was only extremely slightly buoyant relative to its surroundings.

The models are mounted on their bases by means of a streamlined thin aluminar bar (its cross section was a NACA 0006 foil) and set at the desired angle of attack. The models are placed at a level 9 inches above the foam. The first Delta wing had a vertex angle of 39.5055 degrees and a base length of 7.9 inches. The second model had a vertex angle of 50 degrees and a base length of 5.071 inches.

The third model is a submerged planing surface made of plexiglass and attached to a streamlined body. The body is cut in half longitudinally with the bottom half removed to allow testing at greater depths with negligible hydrodynamic ground effects. The planing surface has a base length of 6.96 inches with an aspect ratio of 2.20 (Aspect ratio = [base length]^2/Area). The model is mounted to the carriage such that the plane

FRESH WATER

60 GAL

FILLING PIPE

DRAIN
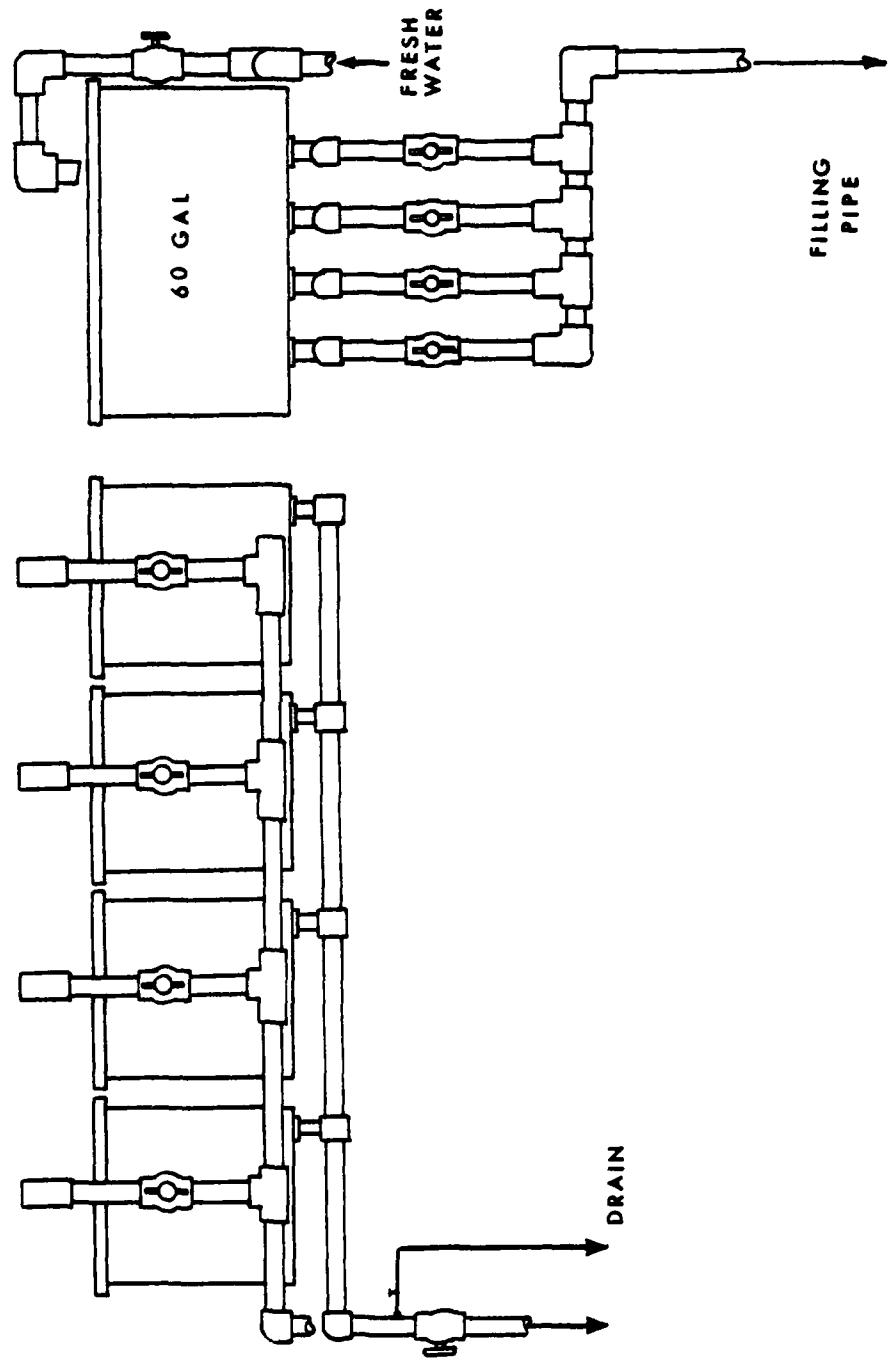
Figure 7. Stratification System Auxiliary Tanks.

41

dye holes
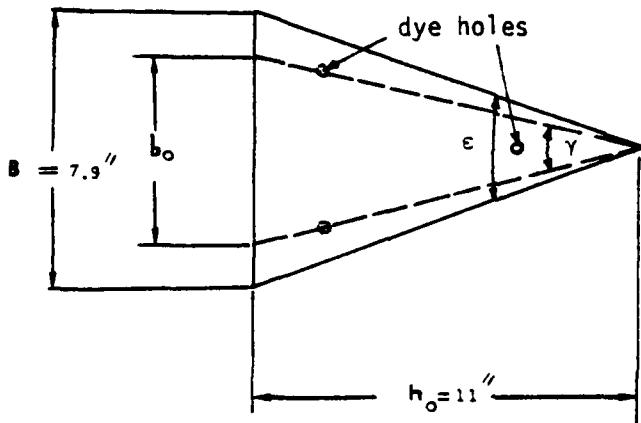
DIMENSIONS

Delta 1:

B = 7.90"

b_o = 5.585"

h_o = 11.00"

ϵ = 39.5 deg.

$B = 7.9''$

b_o

ϵ

γ

$h_o = 11''$

Delta-wing Model No. 1

Delta 2:

B = 5.07"

b_o = 3.70"

h_o = 6.00"

ϵ = 50.0 deg.

ΔH_o

$B/2$

α
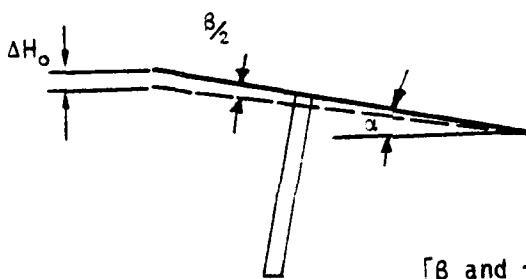
[β and γ are from Ref. 61]

Figure 8. Delta-Wing Models.

bottom of the body is flush with the top of the aluminum plate above the foam.

A hollowed core within the supporting column of the planing surfaces is filled with dye. The dye is dispensed from the tips of the planing surfaces with small holes connected to the dye reservoir (i.e., the hollow core).

As noted earlier all models are pulled by means of a DC motor, pulley, and cable system at the desired speed (ranging from 1.0 to 5.0 ft/sec). The entire arrangement is shown in Figs. 9 and 10.

D. TEST PROCEDURES

The model is initially filled with dye and all the fill and drain holes on the model are closed with wooden pegs. Then the basin is filled gradually either with fresh water (for unstratified flow experiments) or with salt water (for stratified flow experiments) to the desired level. After sufficient period of waiting for the elimination of any internal currents in the basin the model was set in motion at a desired speed.

The motion of the trailing vortices are recorded on high-speed Polaroid film at the test section (one of the plexiglass panels near the middle of the basin). Each picture included two clocks accurate to 0.01 second, the vertical and horizontal scales on the plexiglass window and, of course, the side view of the trailing vortices as they rose from the model after formation (see Fig. 11). The time interval between successive pictures is determined from the two clocks. The vertical rise of the vortices is determined from the vertical scale. Attention has been paid to the fact that the vortices are farther away from the scale on the plexiglass window and that the scale placed vertically in the middle of the test

43
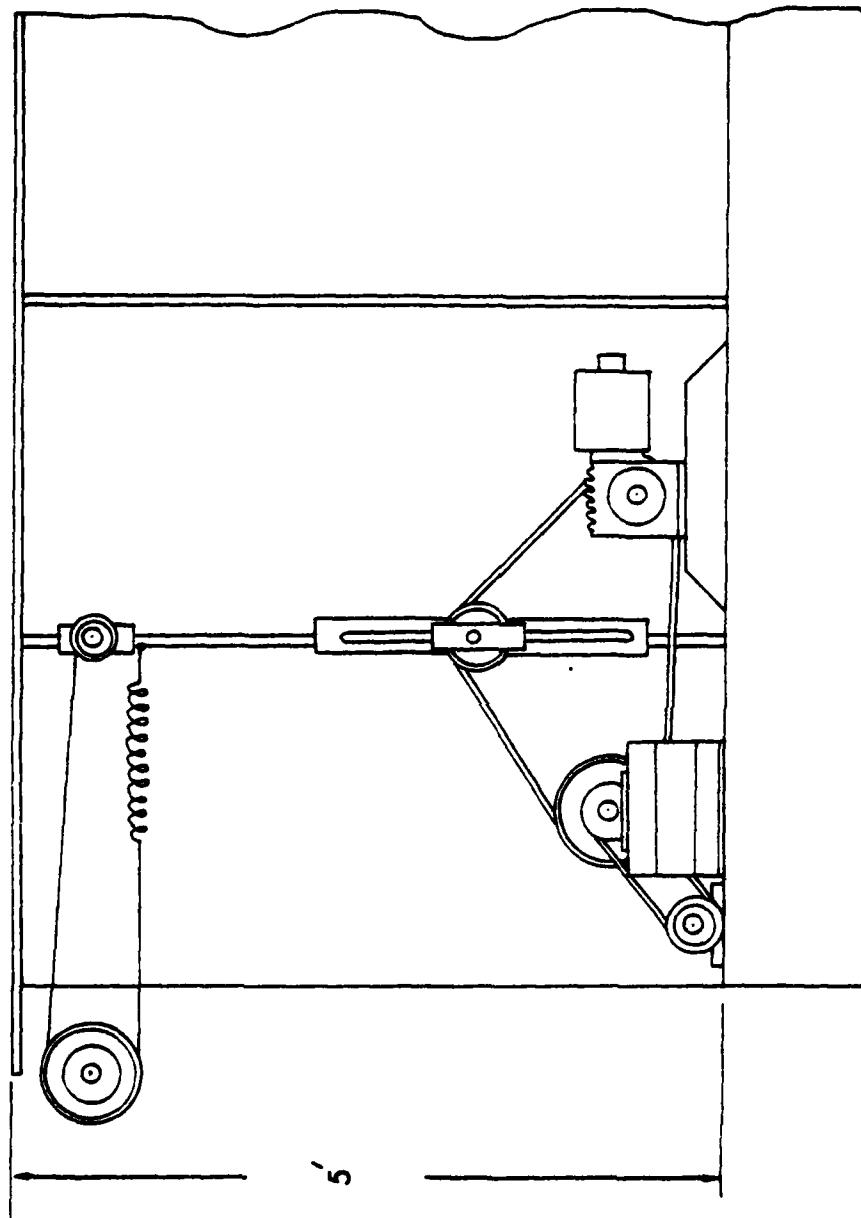
Figure 9. Motion Generation Mechanism.

44
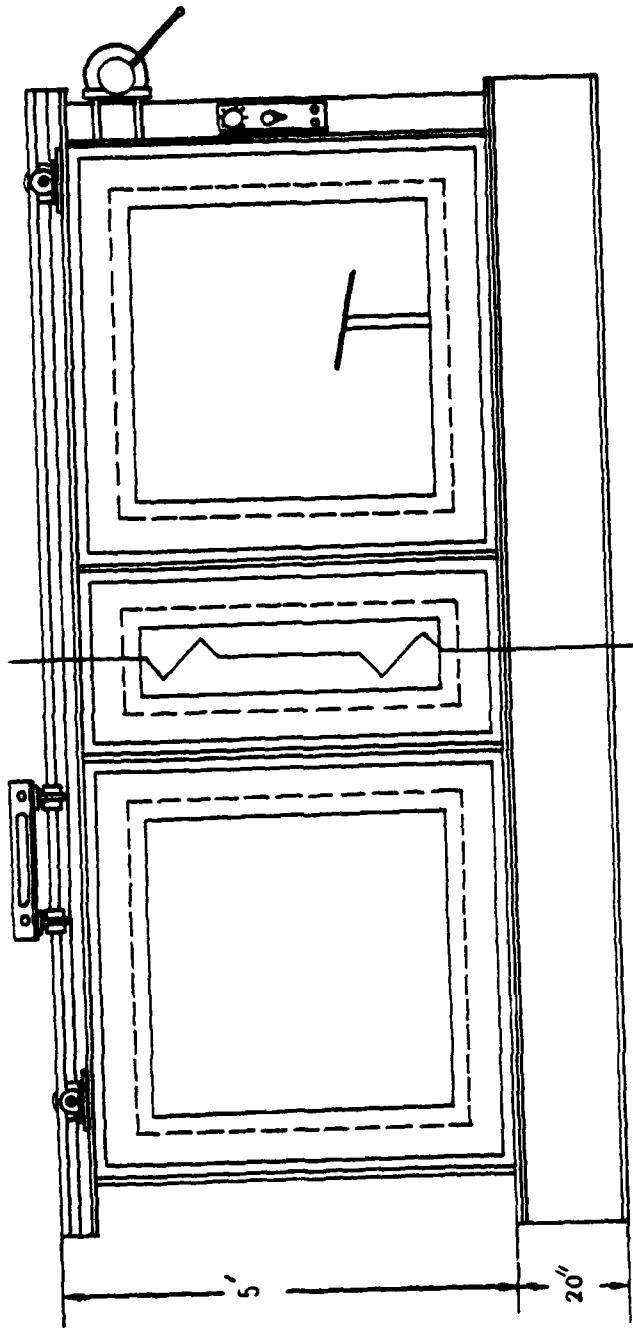
Figure 10. Front View of the Basin.

45

MODEL- 2
$D/b_o = 6.50$
$U = 4.04$, $SP = 0$.
$\alpha = 10°$
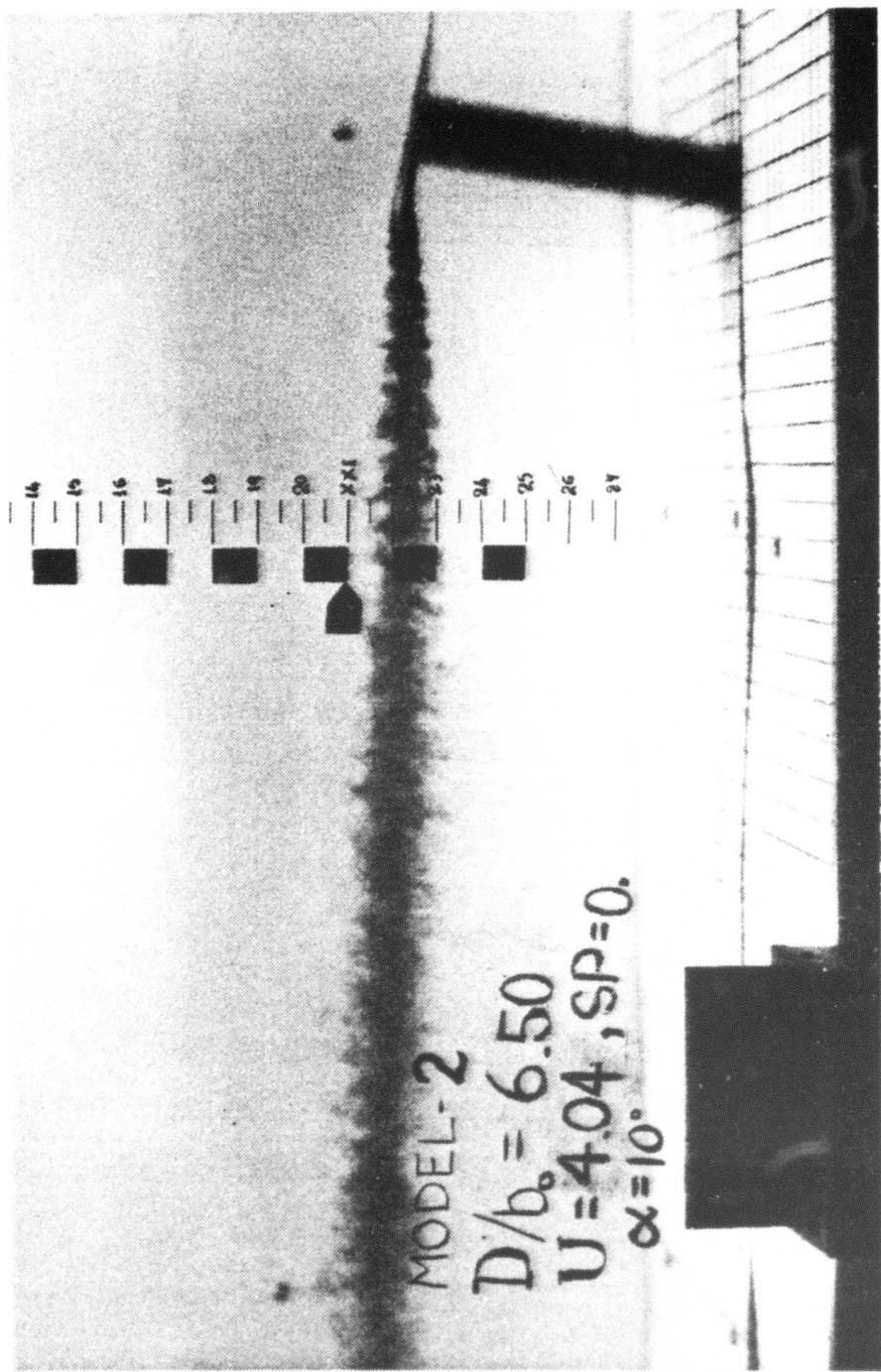
Figure 11. Side View of the Trailing Vortices.

46

section does not exactly correspond to the scale marked on the plexiglass window due to refraction and parallax. The necessary correction was made by photographing a scale placed in water in the middle of the test section together with the scale marked on the plexiglass window. This resulted in a simple conversion table which enabled the determination of the actual position of the vortex from the scale reading on the photograph.

The results are non-dimensionalized and plotted in various forms and compared with those obtained in the previous runs. Each experiment was repeated at least twice to ascertain that the experiments were repeatable.

The experiments with the formation of Horseshoe vortices and vortex rings were conducted in the manner described above with the exception that the model was initially placed closer to the test section, rather than at one end of the basin, and that both the horizontal and vertical scales were used to determine the velocity components of the translation of the vortices.

All trailing vortices and vortex rings were recorded on film until the time they have completely dissipated either due to aging (diffusion of vorticity due to viscosity, turbulence, entrainment, and detrainment), or due to Crow instability (sinusoidal instability and linking leading to the formation of vortex rings), and/or due to vortex breakdown (core bursting). It was thus possible to determine the life span of vortex cores from their formation to their final demise.

IV. RESULTS

A. DIMENSIONAL ANALYSIS

The experimental procedure is based on a careful dimensional analysis of the parameters entering into the phenomenon.

The dependent parameter of major importance is the displacement H of the vortex in the vertical direction and it may be expressed as a function of the following independent parameters for a given body shape:

$$H = f(t, U, D, \rho_0, \frac{\partial \rho}{\partial y}, \nu, B, \varepsilon, \alpha, g) \tag{1}$$

where t denotes the time; U, the forward velocity of the model; D, the initial depth of submergence of the vortex pair; ρ_0, the fluid density; $\partial \rho / \partial y$, the density gradient; ν, the kinematic viscosity of water; B, the base width of the model (see Fig. 8); ε, the vertex angle; α, the angle of attack; and g, the gravitational acceleration. The other parameters such as the vortex strength Γ, the core radius of the vortices r_0, the vortex separation b_0, and the velocity of vertical migration of vortices V_0, are determined by the same parameters governing the variation of H.

A dimensional analysis of Eq. (1) yields

$$\frac{H}{B} = f(\frac{Ut}{B}, \frac{D}{B}, \frac{NB}{U}, \frac{U^2}{gB}, \frac{UB}{\nu}, \varepsilon, \alpha) \tag{2}$$

in which

$$N = (\frac{g}{\rho_0} \frac{\partial \rho}{\partial y})^{1/2}$$

48

and is known as the Brunt-Vaisala frequency. The other dimensionless parameters appearing in Eq. (2) are self-explanatory.

In the present investigation B, ϵ, α, and D were determined by the model being investigated. The velocity of the model was varied from 0.32 ft/s to 4.04 ft/s in experiments with fresh water ($N = 0$). The experiments with stratified water were carried out by varying N ($N = 0.0974 \text{ s}^{-1}$ to 0.2101 s^{-1}) at various velocities.

The dimensionless parameter NB/U is often replaced by another parameter Nb_0/V_0, known as the stratification parameter. It should be noted that both b_0 and V_0 are dependent parameters. b_0 is determined by the shape of the body and its angle of attack. V_0 is determined by

$$\frac{V_0}{U} = f(\frac{D}{B}, \frac{NB}{U}, \frac{U^2}{gB}, \frac{UB}{\nu}, \epsilon, \alpha) \tag{3}$$

Thus, Eq. (2) may be recast as

$$\frac{H}{b_0} = f(\frac{V_0 t}{b_0}, \frac{D}{b_0}, \frac{Nb_0}{V_0}, \frac{V_0^2}{gb_0}, \frac{V_0 b_0}{\nu}, \epsilon, \alpha) \tag{4}$$

Of the parameters appearing in Eq. (4) only t, D, N, g, and ν are independent and may be varied irrespective of the shape of the body. However, the remaining parameters with the exception of α depend on the shape, aspect ratio, and the velocity of the body. The variation of ϵ and α are imbedded in the variation of V_0 and b_0. Experiments were performed with a given body by varying the angle of attack and the speed of the body for a given Brunt-Vaisala frequency, N. Then V_0 and H were determined from the pictures. The parameters ϵ and b_0 were obtained from the

49

existing experimental data [Ref. 61]. Subsequently, the data were plotted in terms of H/b_0 versus $V_0 t/b_0$ for various values of D/b_0, and Nb_0/V_0. The measurements have shown that the dimensionless parameters V_0^2/gb_0 and $V_0 b_0/\nu$ are not important within the range of the parameters encountered in the experiments. With the foregoing arguments, Eq. (4) may be written as

$$\frac{H}{b_0} = f(\frac{V_0 t}{b_0}, \frac{D}{b_0}, \frac{Nb_0}{V_0}) \qquad (5)$$

This equation formed the basis for the analysis of the entire experimental data.

B. DELTA-WING GENERATED VORTICES IN UNSTRATIFIED WATER

Sample data obtained with the first Delta-wing (referred to hereafter as Delta 1) in unstratified water ($Nb_0/V_0 = SP = 0$) are shown in Fig. 12 for two values of V_0 and for $D/b_0 = 5.19$. Two symbols, identifying two independent runs, show that there is very little scatter in the data. Had the vortices maintained their strength and spacing, as they would in an ideal fluid, H/b_0 would have been equal to $V_0 t/b_0$. This straight line relationship is also shown in Fig. 12. Clearly, all the data points are below the ideal line and show that the vortices do not retain their original characteristics. One may argue that this may be as a consequence of several factors such as the decrease of circulation, the increase of the vortex spacing b, and the proximity of the free surface. The variation of b with time may be excluded from this discussion because the observations and measurements have shown that it remains practically constant for large

50
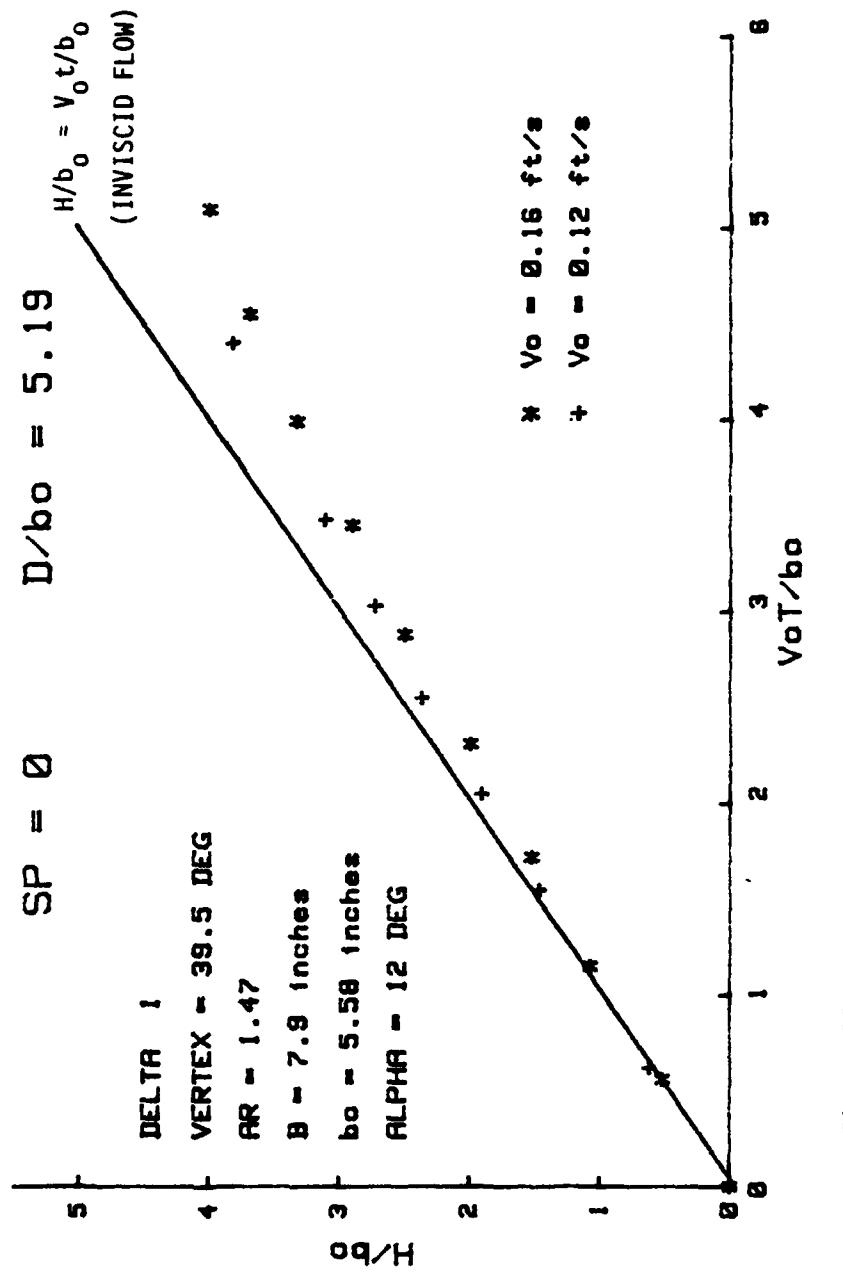
Figure 12. Vertical Vortex Rise for Delta 1, SP = 0, D/b_0 = 5.19.

51

enough values of D/b_0. As to the free surface effects, it will be shown that they do not play any role in the rise of the vortices for D/b_0 larger than about 4.3. Thus one may conclude that for large D/b_0 values, the difference between the actual and the ideal values of H/b_0 is due to the decrease of the circulation of vortices with time. This decrease, as noted in connection with the discussion of previous studies, is a consequence of eddy diffusion of vorticity, Crow instability, and vortex breakdown. This fact has not been recognized in the past because of lack of reliable data and it was often assumed that the vortex strength remained constant. This in turn gave rise to conflicting conclusions cited in Table I.

Figure 13 shows a composite plot of the data obtained with Delta 1 for various values of V_0 at a fixed value of $D/b_0 = 4.31$. The primary purpose of this figure is to substantiate the assertion that the dimensionless parameters V_0^2/gb_0 (a representative Froude number) and V_0b_0/ν (a representative Reynolds Number) do not play experimentally detectable roles in the variations of H/b_0 with V_0t/b_0, at least for unstratified flow experiments. The two-fold variation of V_0 for constant values of b_0, g, and ν yields a four-fold variation in the Froude number and a two-fold variation in the Reynolds number. Clearly, Fig. 13 does not exhibit such a dependence on the said two parameters. In fact, it is because of this finding that the governing parameters were finally reduced to that given by Eq. (5).

The next question to be addressed is the dependence of H/b_0 on D/b_0. In other words, at what D/b_0 does the free surface affect the rise of the vortices and in what form does this effect exhibit itself?
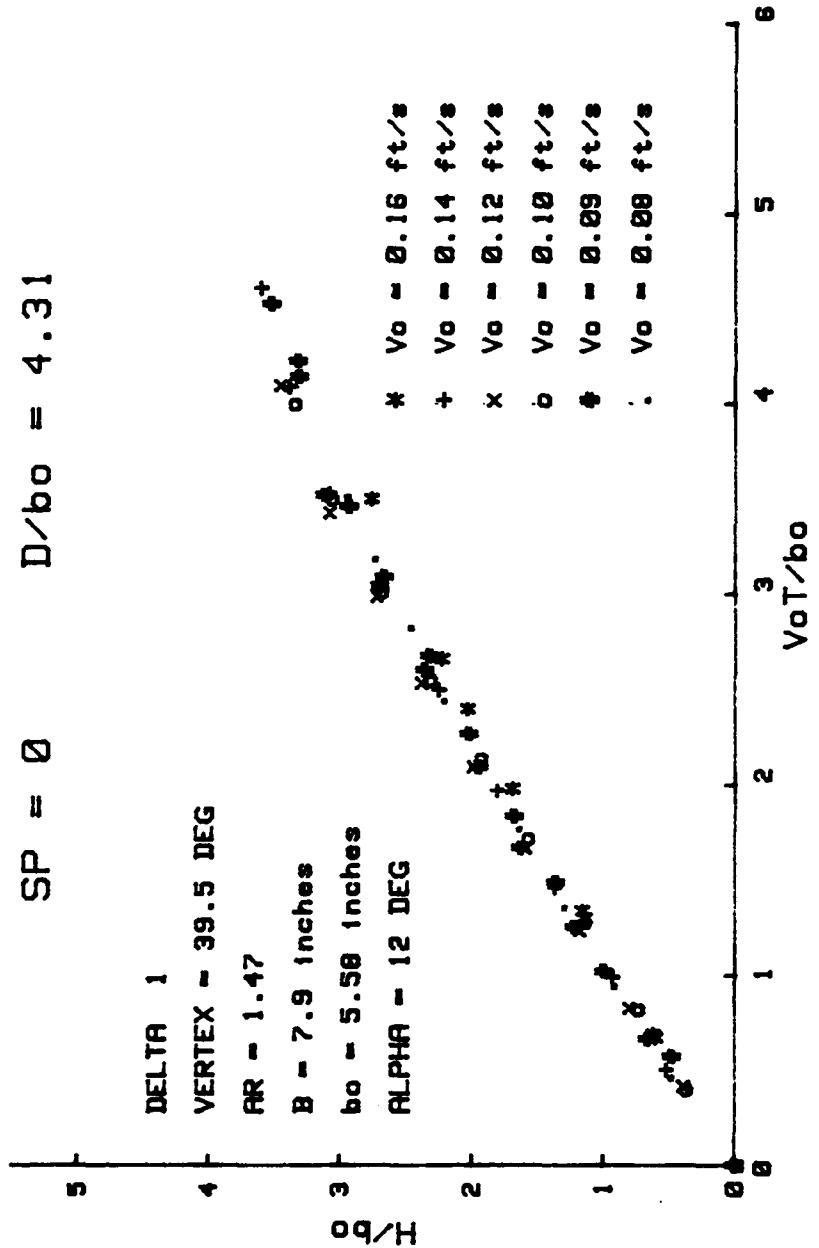
Figure 13. Vertical Rise for Delta 1, SP = 0, $D/b_0 = 4.31$.

Figure 14 shows the data obtained with D/b_0 values ranging from 2.15 to 5.19, again in unstratified water. Evidently, the variation of H/b_0 versus $V_0 t/b_0$ for $D/b_0 = 4.31$ and $D/b_0 = 5.19$ is such that the differences are negligible and certainly well within the experimental errors. For other values of D/b_0, the vortices reach their limiting height very quickly and then begin to bounce back from the free surface. The smaller the D/b_0, the smaller is the limiting height. These experimental facts may be explained partly in terms of the behavior of inviscid vortices in the vicinity of a plane wall.

The free surface acts as a reflection plane and the motion of the vortex pair is determined not by their mutual induction alone but also by the image vortex pair above the free surface. In other words, the trajectory of the ideal vortices is determined by the mutual induction of four vortices (see Fig. 15). Lamb [Ref. 62] has shown that the trajectories of line vortices in ideal unstratified fluid are hyperbolas given by

$$\frac{1}{(2x/b_0)^2} + \frac{1}{(2y/b_0)^2} = 1 + (\frac{b_0}{2D})^2 \tag{6}$$

where b_0 is the initial spacing of the two real vortices, and D is their initial depth. Equation (6) shows that the vortices move sideways as they approach the free surface. For large values of x and D, y approaches half the initial separation, i.e., the vortex pair does not come closer to the free surface than a distance of $b_0/2$.

A similar analysis cannot yet be carried out in a real fluid including the effects of stratification and turbulence. The strength of the vortices
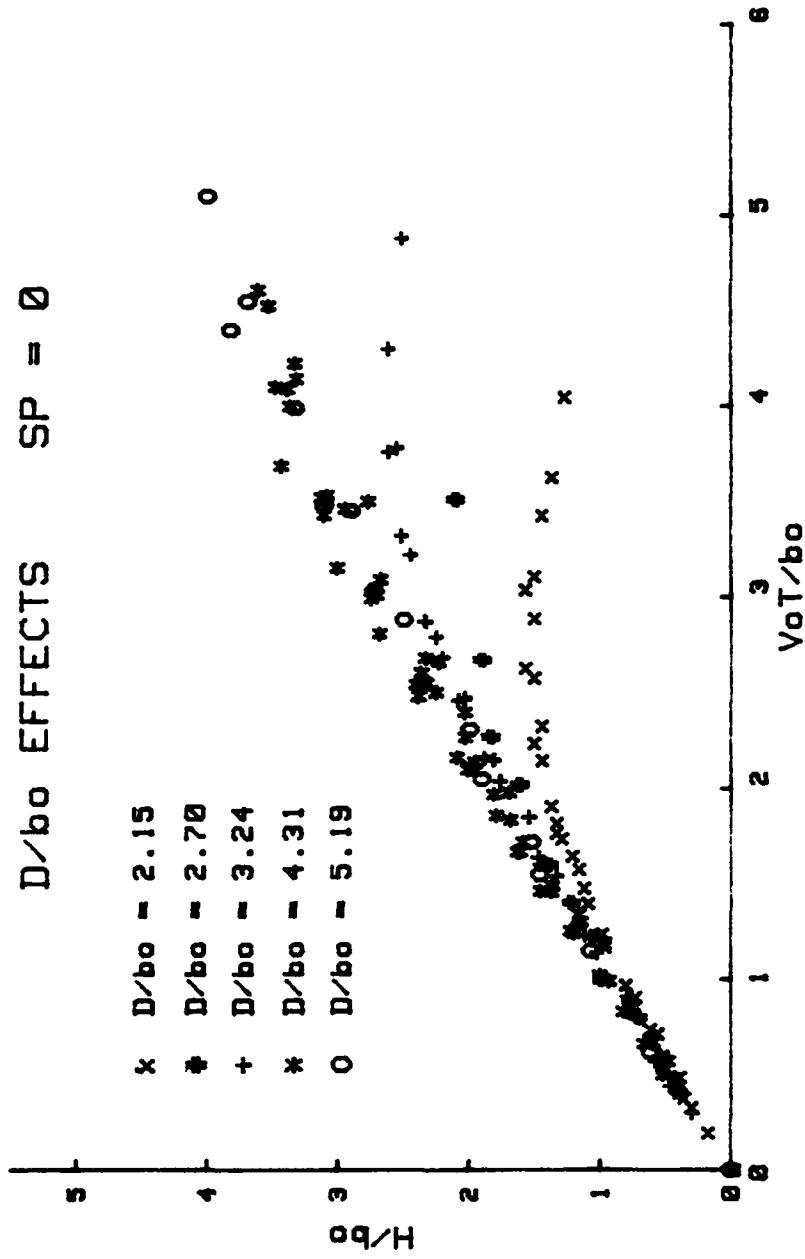
Figure 14. D/b_0 Effects on Vertical Vortex Rise for Delta 1, SP = 0.

55
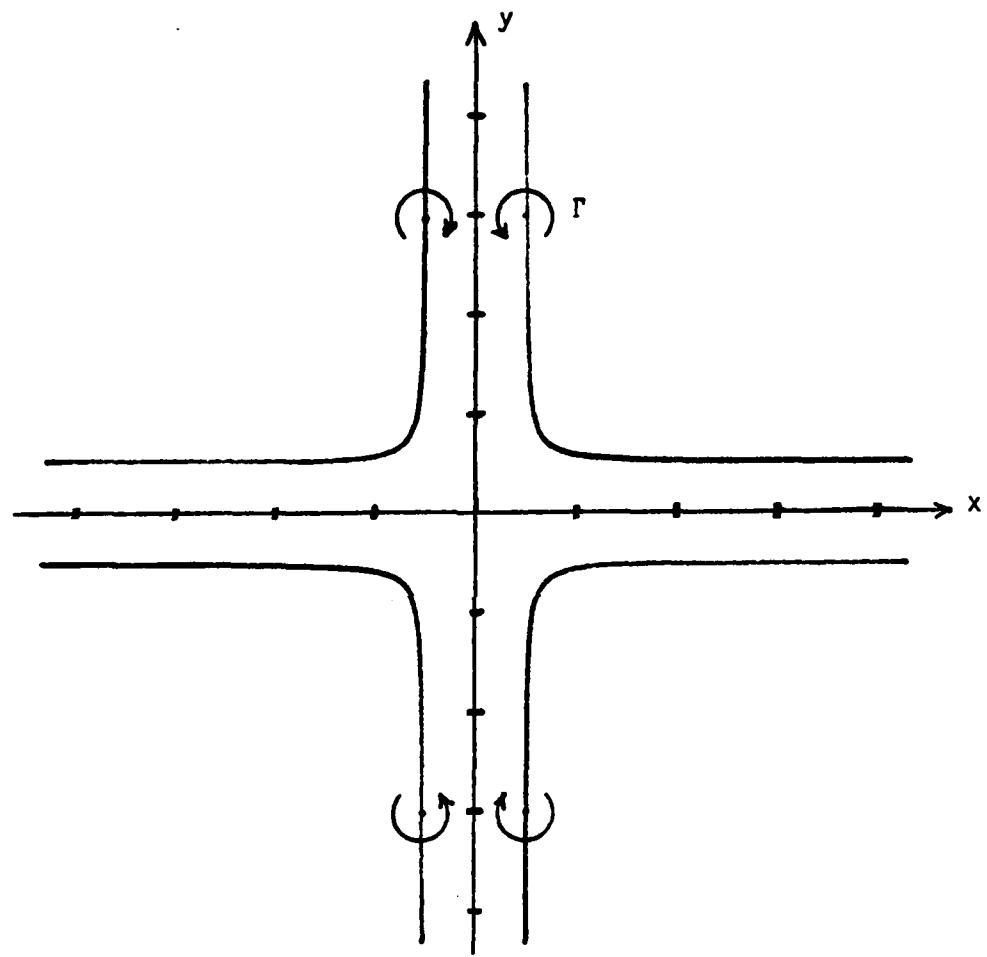
Figure 15. Mutual Induction of Four Vortices and the
Free Surface Effects.

56

and their rise velocity continue to decrease (see the slope of the data for $D/b_0 = 2.15$ in Fig. 14).

As the vortices move too far sideways, they begin to fall under the influence of additional image vortices due to the presence of the side walls. Even though it is not a matter of primary importance, one can show that the combined effect of the image vortices due to the side walls and the free surface is to push the vortices downward. It is not yet possible to verify whether there exists a physical mechanism which will make the vortices bounce from the free surface had there been no side wall effects. It is possible that the decrease in the mutual influence of the trailing vortices may give rise to alterations in the velocity fields in the presence of a movable free-surface boundary and this in turn may result in a bouncing back of the vortices. In any case, only the experiments in a large basin can resolve the question.

An additional fact which can be extracted from Fig. 14 is the lack of importance of the Froude and Reynolds numbers on the rise of vortices even when the free surface effects predominate. The data for all D/b_0 values were obtained at different model speeds even though they have been shown with a single symbol in Fig. 14. The plotted as well as the tabulated data (see Appendix C) show that (see for example the data for $D/b_0 = 2.15$ in Fig. 14) neither the Froude number nor the Reynolds number plays any role on the rise of vortices in unstratified flow with or without free surface effects, within the range of the parameters encountered in this investigation.

The results presented above were obtained with Delta 1. In order to ascertain further the validity of the conclusions reached regarding the

role played by the governing parameters (see Eq. (5)) experiments were carried out with the second Delta-wing model (Delta 2). Figure 16 shows H/b_0 versus $V_0 t/b_0$ for $D/b_0 = 7.73$ in unstratified water for various values of V_0 (Tabulated data are presented in Appendix D). Clearly, the results do not depend on V_0 and hence on the model speed. The comparison of the data obtained with the two models is presented in Fig. 17. Aside from some minor scatter at large values of $V_0 t/b_0$, the results of the two models compare quite well. Thus, it may be concluded on the basis of the extensive data collected from the two models that in unstratified water the rise of the trailing vortices is governed by the dimensionless parameters H/b_0, $V_0 t/b_0$, and D/b_0. In all cases the vortices gradually lose their strength and thus they move upwards with ever decreasing velocities until they are dissipated by various demise mechanisms discussed earlier.

C. DELTA-WING GENERATED VORTICES IN STRATIFIED WATER

Experiments in stratified water were carried out with the same Delta-wing models for various stratification parameters (SP = Nb_0/V_0). First, the results obtained with Delta 1 for five SP values will be presented. Then the results obtained with Delta 2 for three SP values will be shown. Then the results obtained with the two models will be compared.

Figures 18 through 22 show H/b_0 versus $V_0 t/b_0$ for SP values of 0.375, 0.50, 0.625, 0.75, and 1.0 for a fixed value of $D/b_0 = 4.31$. It is important to note that this particular value of D/b_0 was chosen so as to exclude the effects of free surface and thus to concentrate only on the effects of linear stratification. A complete plot of the aforementioned data is presented in Fig. 23. Clearly, the larger the stratification

58
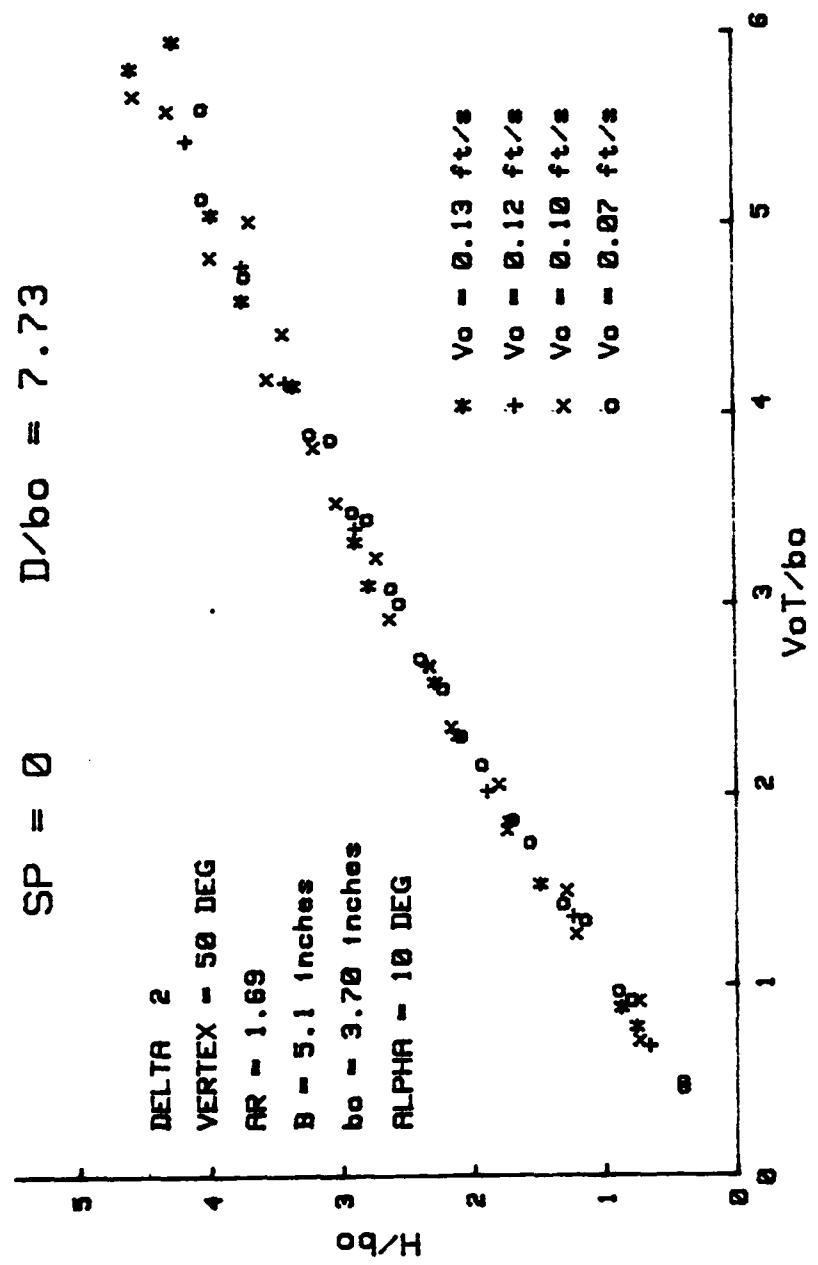
Figure 16. Vertical Vortex Rise for Delta 2, SP = 0, D/b$_0$ = 7.73.
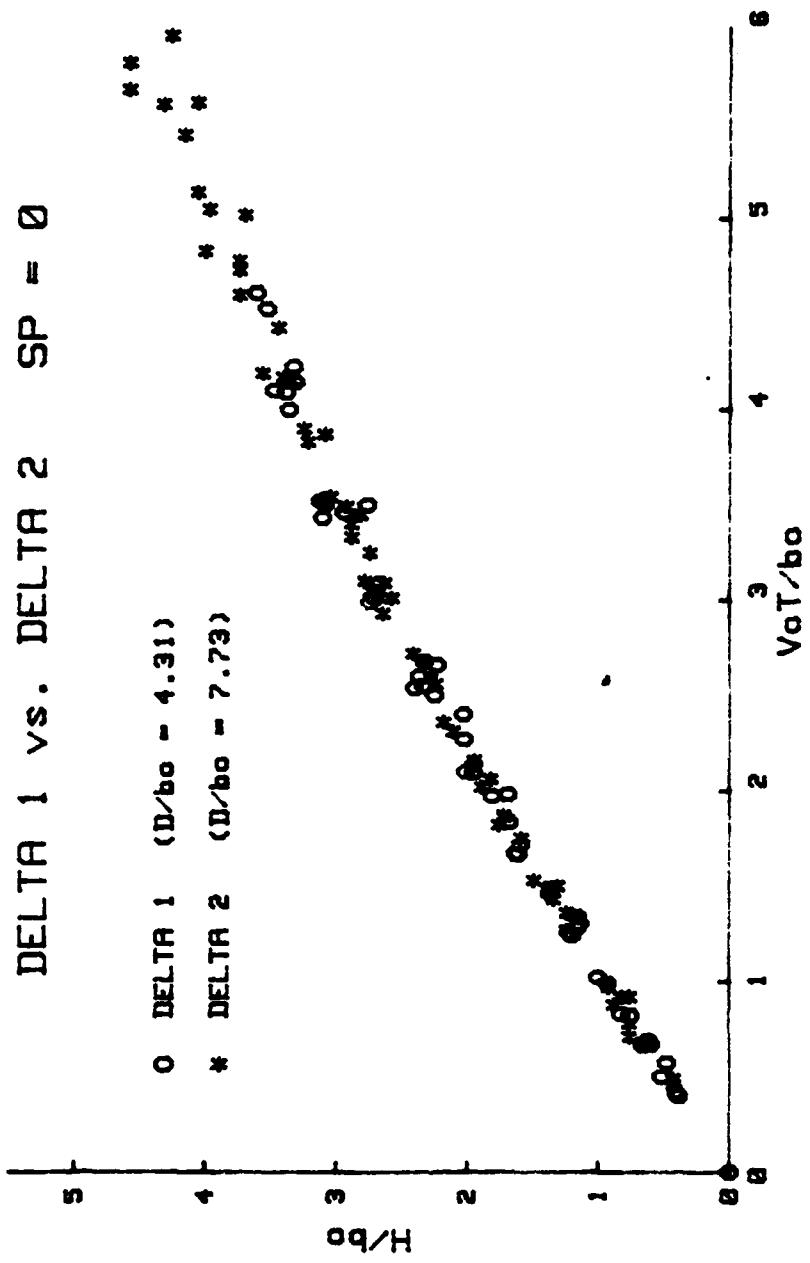
Figure 17. Comparison of the Vortex Rise for Delta 1 and Delta 2 for SP = 0.

SP = 0.375   D/bo = 4.31

DELTA 1
VERTEX = 39.5 DEG
AR = 1.47
B = 7.9 inches
bo = 5.58 inches
ALPHA = 12 DEG

* Vo = 0.16 ft/s

H/bo

VoT/bo
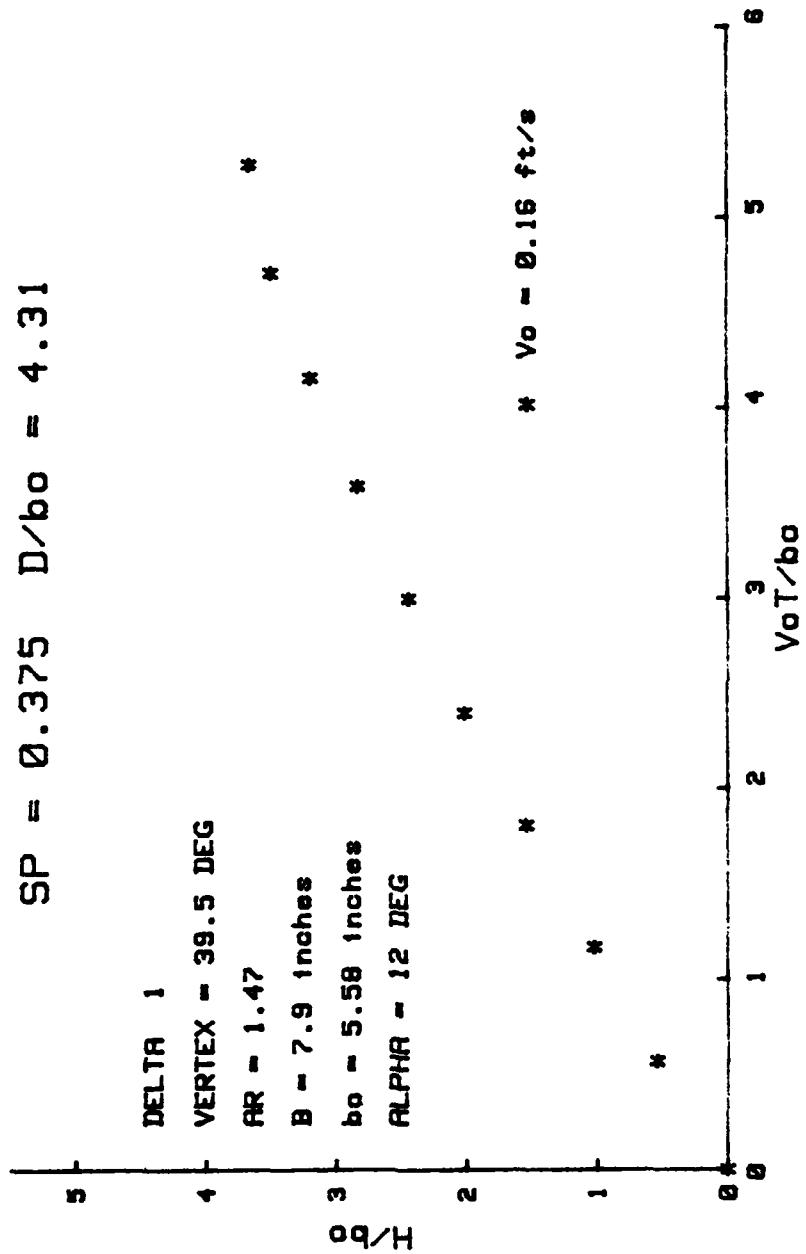
Figure 18.   Vertical Vortex Rise for Delta 1, SP = 0.375, D/b_0 = 4.31.

61
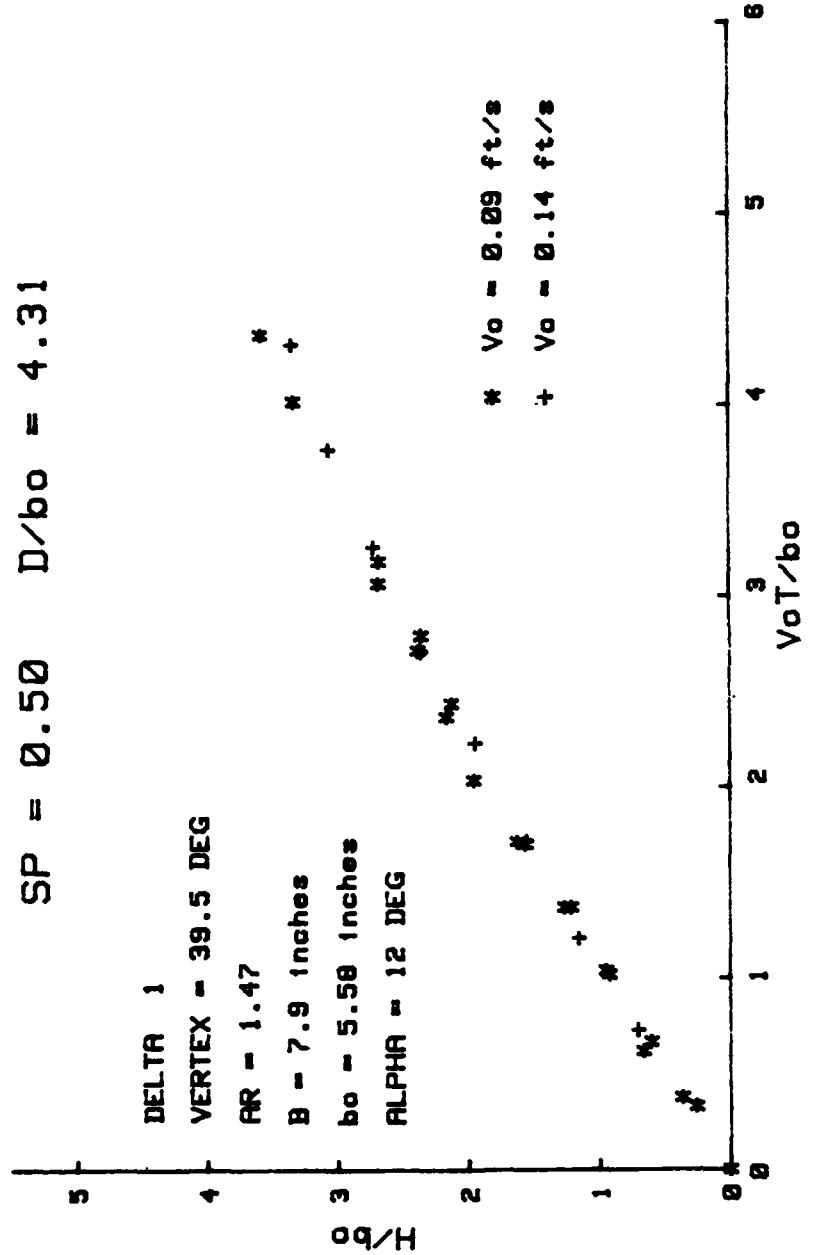
Figure 19. Vertical Vortex Rise for Delta 1, SP = 0.50, D/b_0 = 4.31.

SP = 0.625 D/bo = 4.31

DELTA 1
VERTEX = 39.5 DEG
AR = 1.47
B = 7.9 Inches
bo = 5.58 Inches
ALPHA = 12 DEG

* Vo = 0.09 ft/s

H/bo

VoT/bo
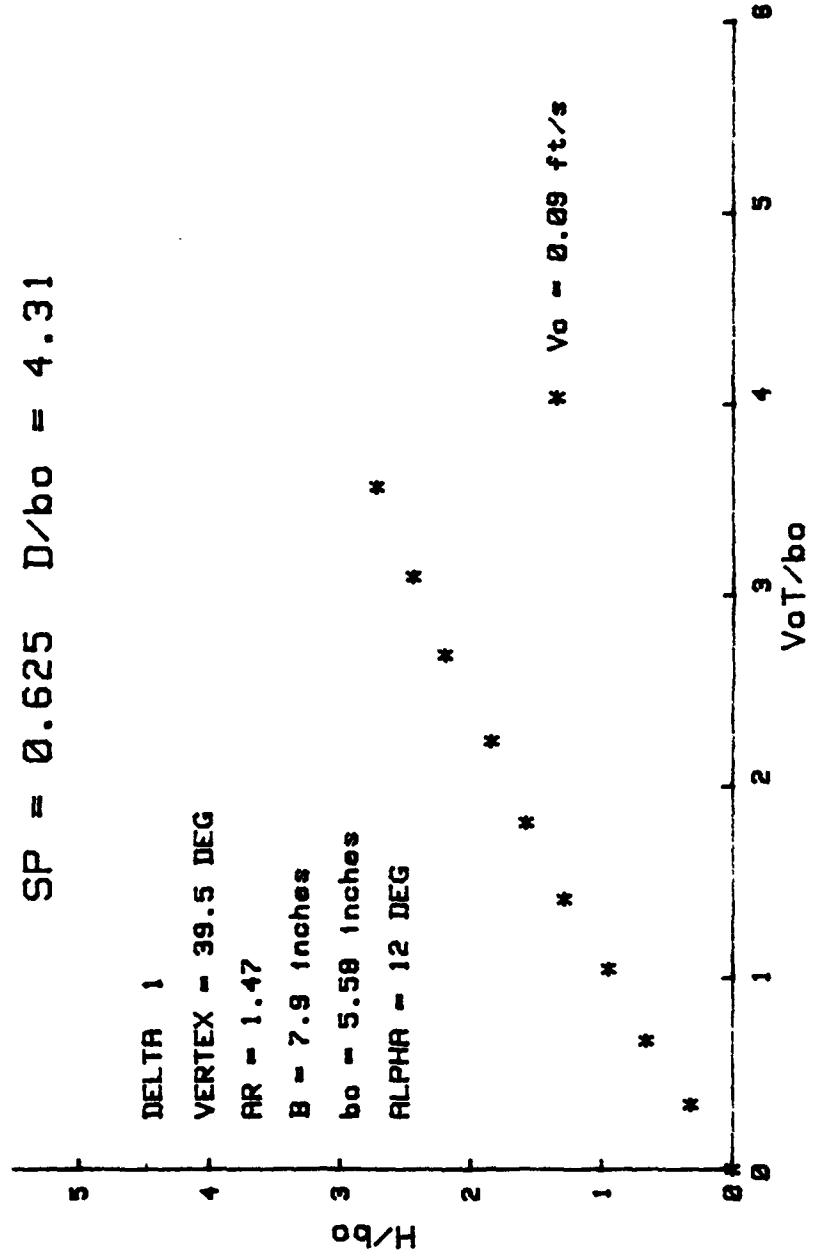
Figure 20. Vertical Vortex Rise for Delta 1, SP = 0.625, $D/b_0 = 4.31$.
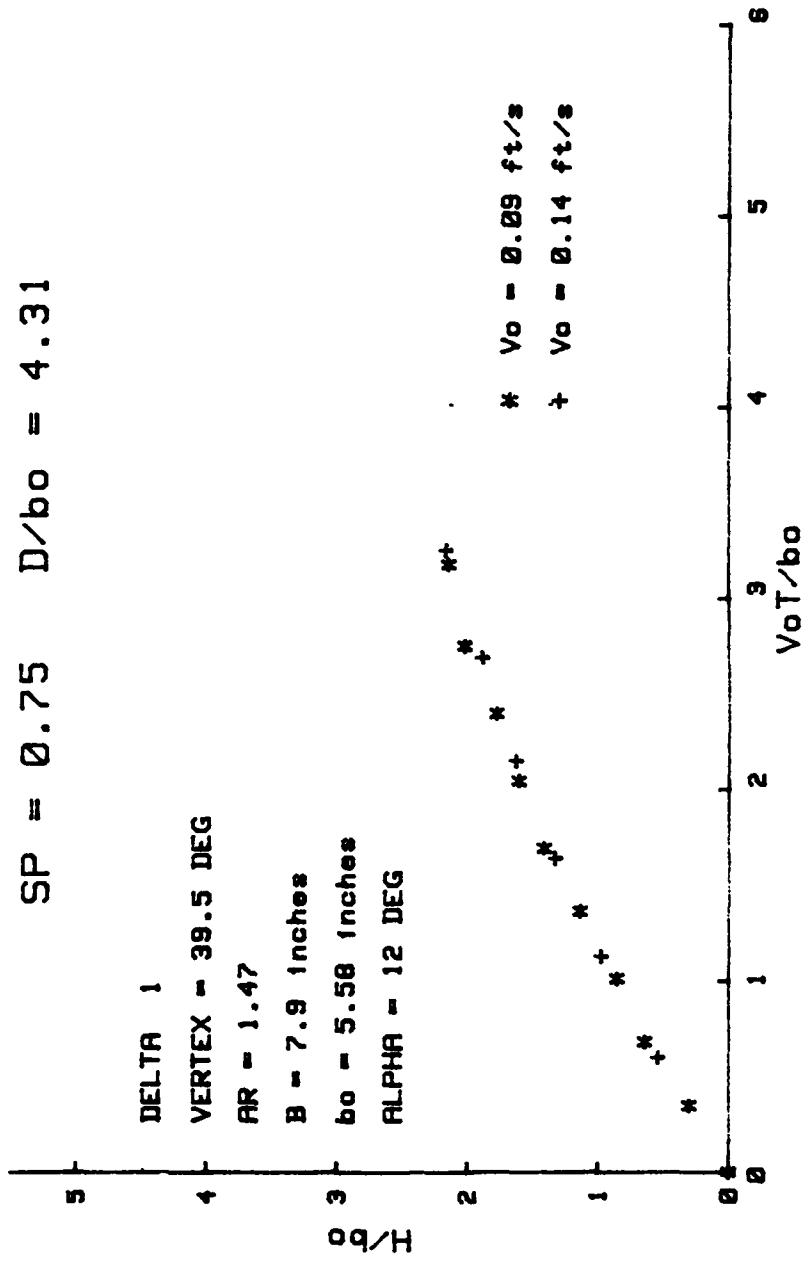
Figure 21. Vertical Vortex Rise for Delta 1, SP = 0.75, D/b$_0$ = 4.31.
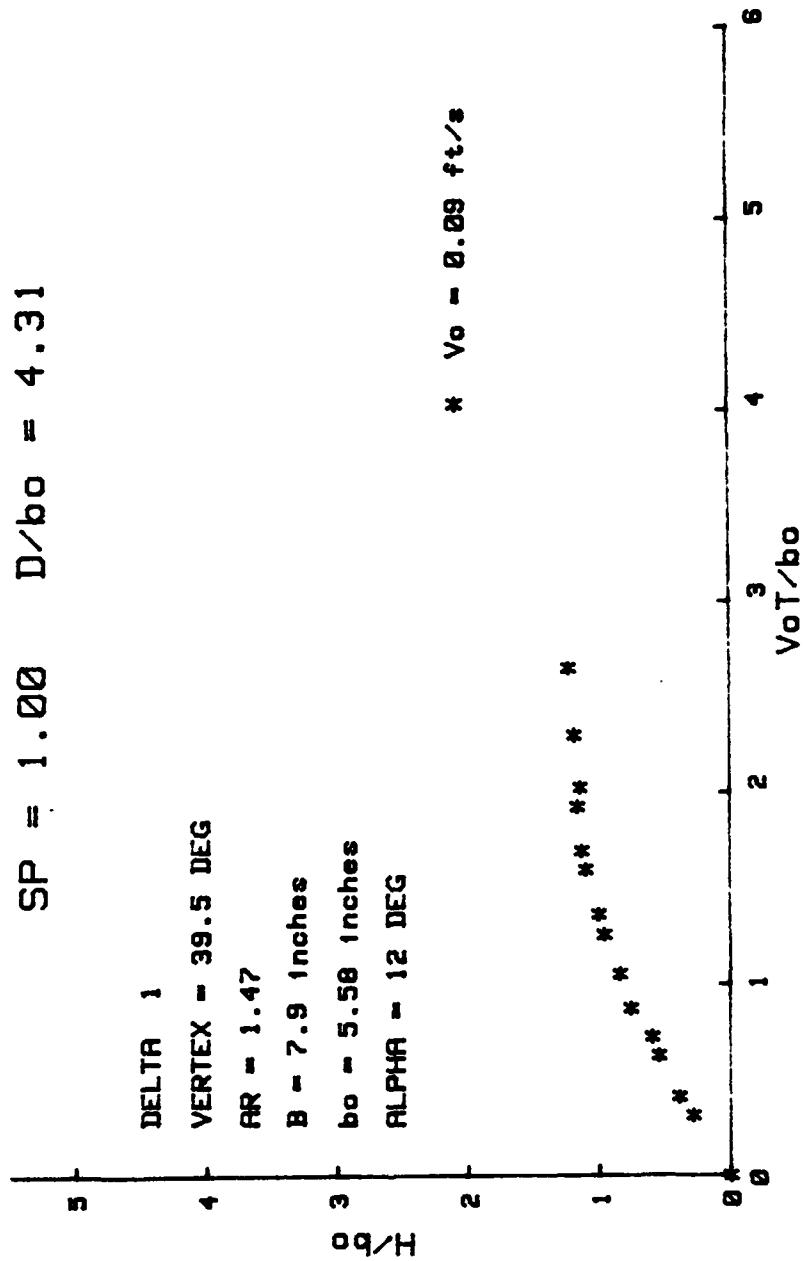
Figure 22. Vertical Vortex Rise for Delta 1, SP =1.0, D/b$_0$ = 4.31.

65
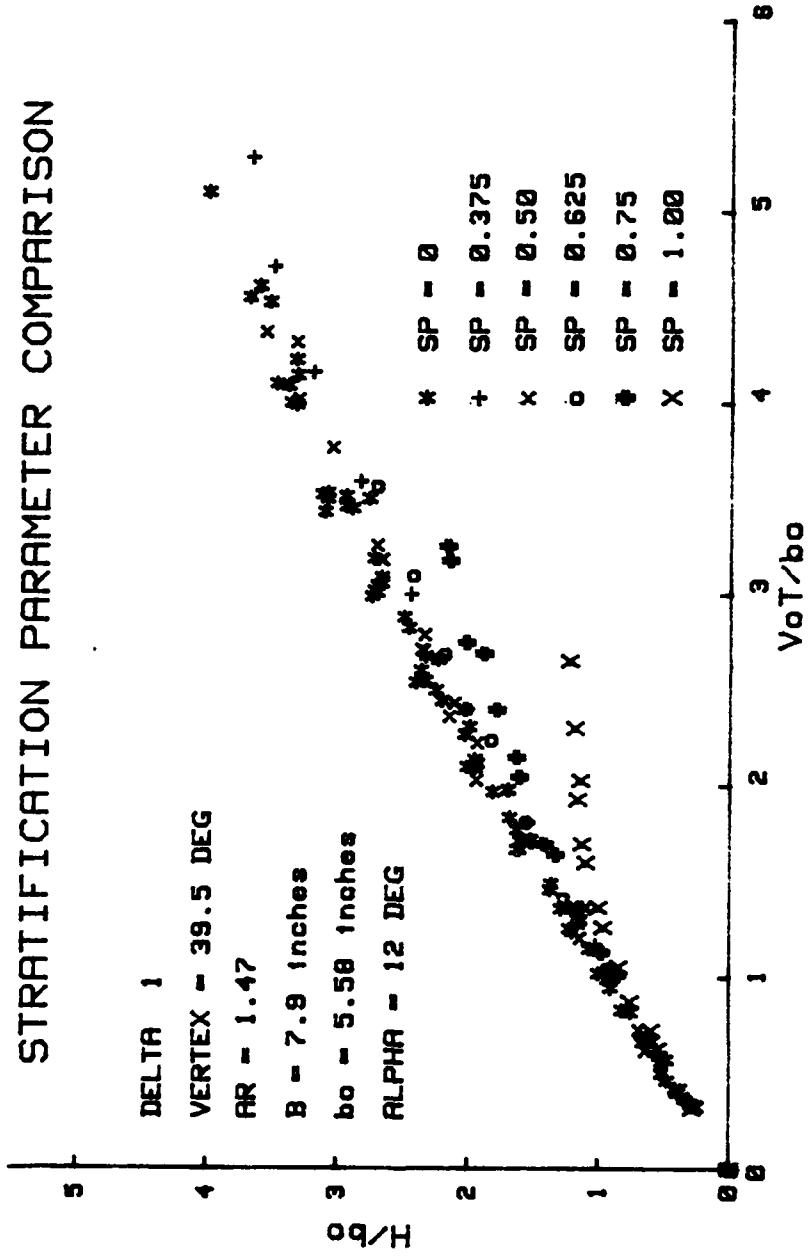
Figure 23. Stratification Effects on Vortex Rise for Delta 1.

parameter, the smaller the rise of vortices. The last data points (of
each particular run) correspond to the state where the vortex core was no
longer discernible and the surrounding dye was randomly diffused with no
sign of circulation. As will be discussed in detail later, this particu-
lar state was reached after the vortices were subjected to one or more
of the demise mechanisms. The fundamental conclusion to be deduced from
Fig. 23 is that the effect of the stable linear stratification is to
inhibit the rise of the trailing vortices. This may be due to a number
of reasons such as: (i) the increase of the downward buoyant force on
the recirculation cell, (ii) the generation of countersign vorticity out-
side the recirculation cell (to be discussed later in Section IV.F),
(iii) the enhanced effect of the entrainment and/or detrainment of the
recirculation cell, (iv) the possible enhancement of the vortex breakdown
and alterations in the circulation distribution after vortex breakdown
due to stratification, (v) the change of the turbulence structure and
hence the eddy diffusion by stratification, and (vi) the enhancement of
the Crow instability, or other as yet unknown demise mechanisms associated
with stratification.

It is evident from Fig. 23 that the vortices in a stratified medium
rise to smaller heights. Thus, the free surface effects become important
at D/b_0 values smaller than that corresponding to the unstratified case.
Clearly, the particular value of D/b_0 at which the free-surface effects
become important in stratified medium depends on the stratification
parameter.

The results obtained with Delta 2 are shown in Figs. 23 through 26 for
three SP values (SP = 0.375, 0.50, and 0.75) and for D/b_0 = 6.50.

67
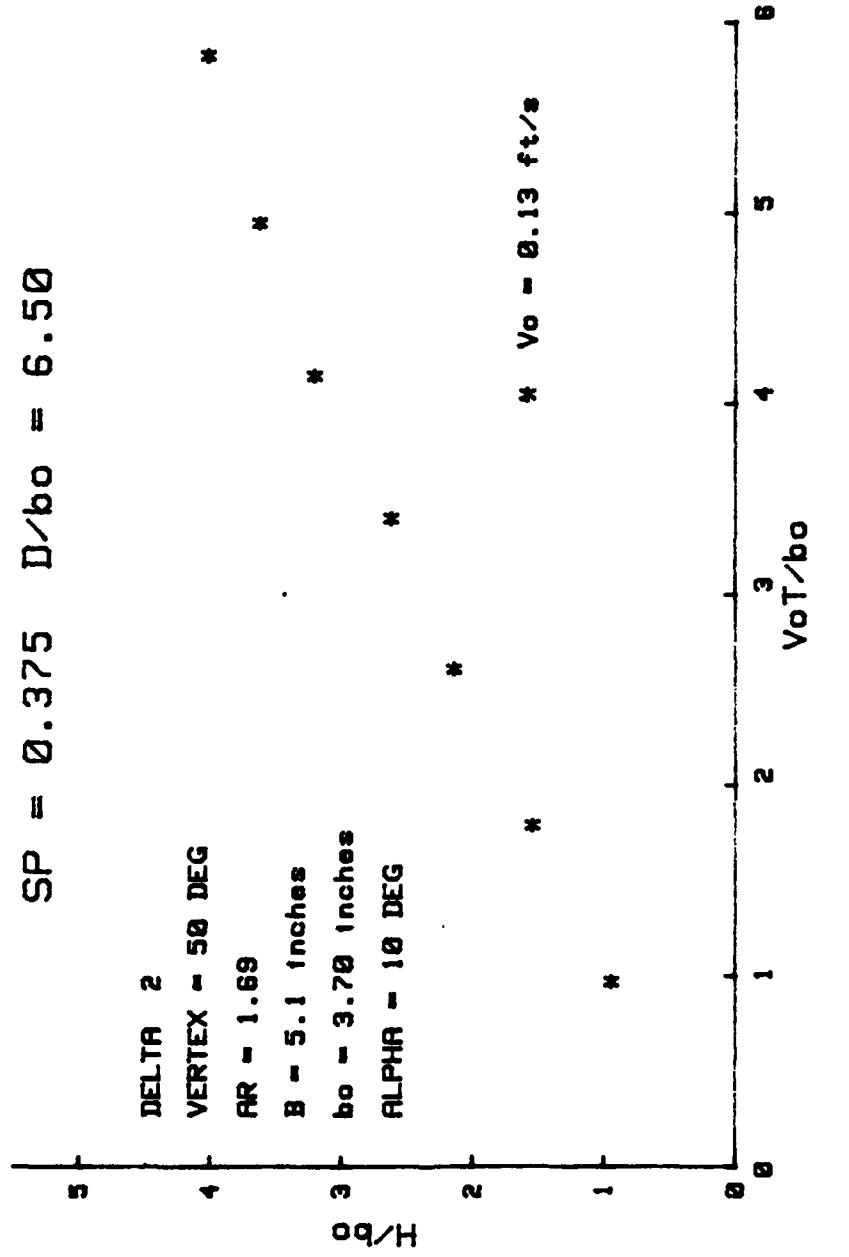
Figure 24. Vertical Vortex Rise for Delta 2, SP = 0.375, D/b_0 = 6.50.
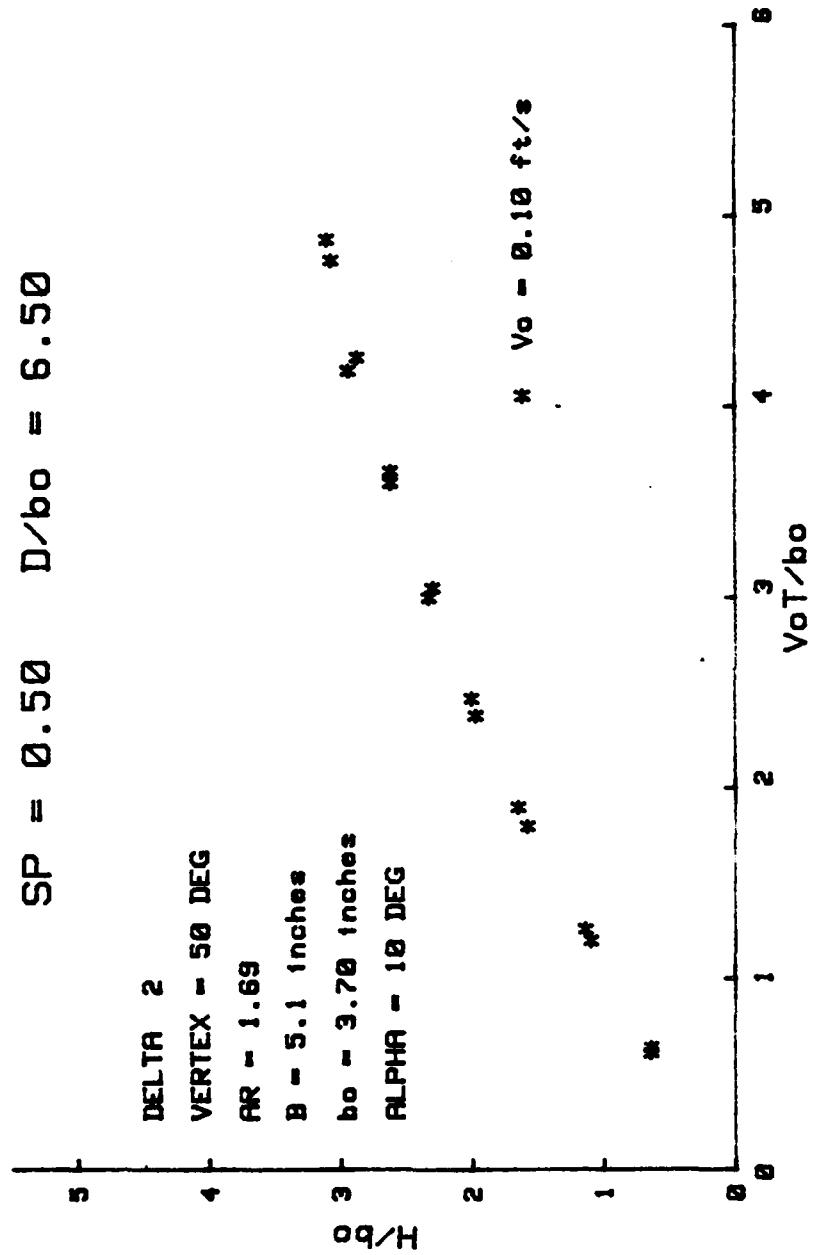
Figure 25. Vertical Vortex Rise for Delta 2, SP = 0.50, D/b_o = 6.50.
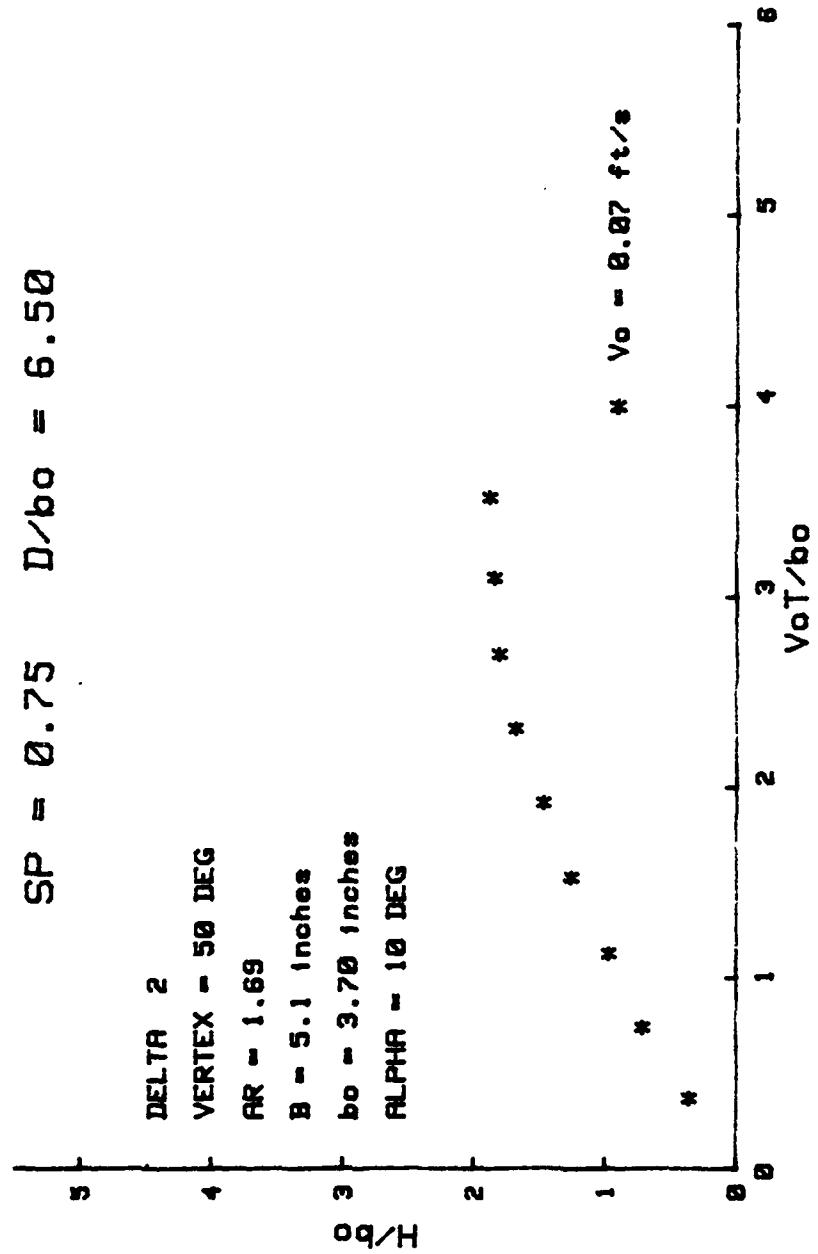
Figure 26. Vertical Vortex Rise for Delta 2, SP = 0.75, D/b_0 = 6.50.

Figure 25 shows the repeatability of the data and all three figures show the general consistency of the experiments.

Figure 27 is a composite plot of the aforementioned figures. A perusal of this figure reveals the same conclusions arrived at earlier in connection with the discussion of Delta 1 (Fig. 23).

Since the purpose of the use of two Delta-wing models was to confirm the independence of the data from the size of the model, Figs. 28 through 30 were prepared for comparison of the data obtained from Delta 1 and Delta 2. In general, the data compare extremely well for a given stratification parameter. The minor differences in H/b_0 for large values of $V_0 t/b_0$ (see Figs. 29 and 30) are thought to be due to the somewhat random influence of the demise mechanisms at the later stages of the life of the trailing vortices. Finally, it should be noted that D/b_0 does not affect the variation of H/b_0 with $V_0 t/b_0$ for D/b_0 larger than at least 4.3, as discussed earlier.

D. DEMISE OF DELTA-WING GENERATED TRAILING VORTICES

The discussion of the demise of the trailing vortices will be carried out first with regard to the initial stages of motion and then to the fully developed trailing vortices.

1. Horseshoe Vortices and Vortex Rings

As the lifting surface is set in motion impulsively from rest the vorticity shed from the surface forms a so-called Horseshoe vortex. Shortly after the formation of this vortex, linking occurs and the Horseshoe vortex transforms into a vortex ring (see Fig. 31, where the Horseshoe vortex is at the point of linking). The observations and

71
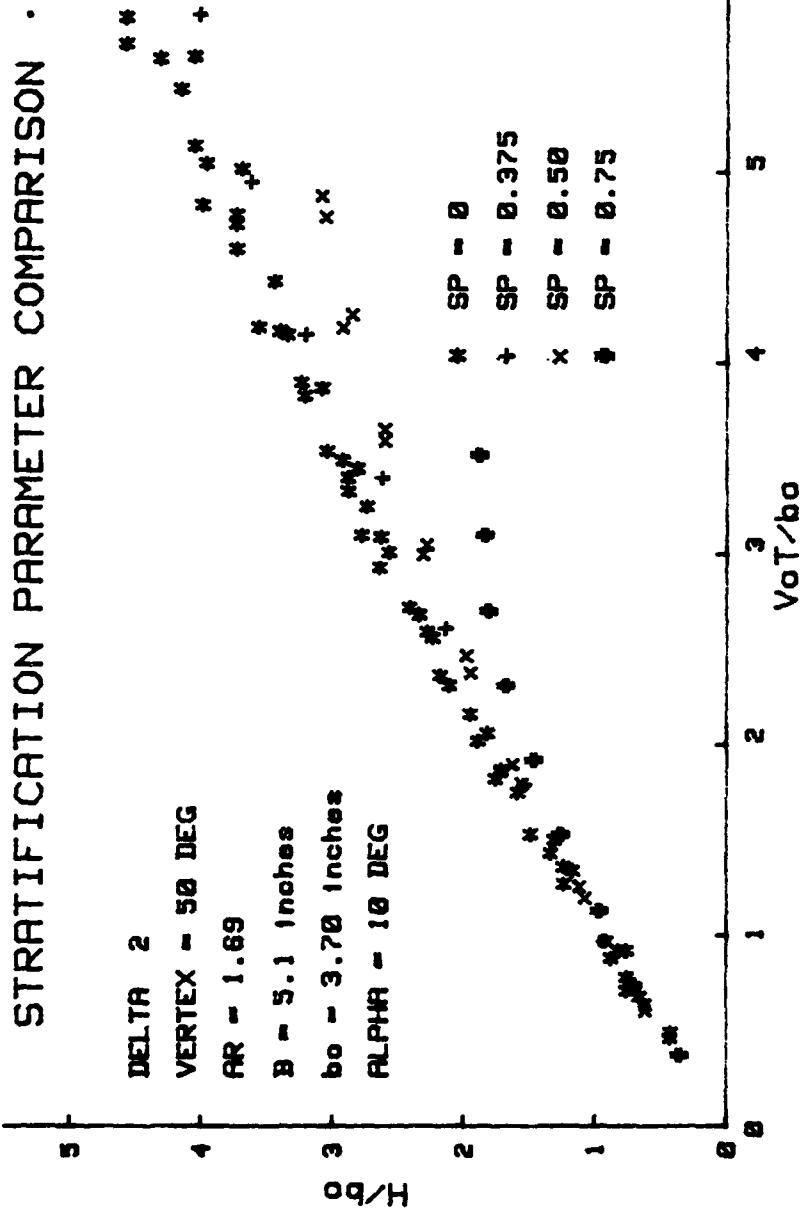
Figure 27. Stratification Effects on Vortex Rise for Delta 2.
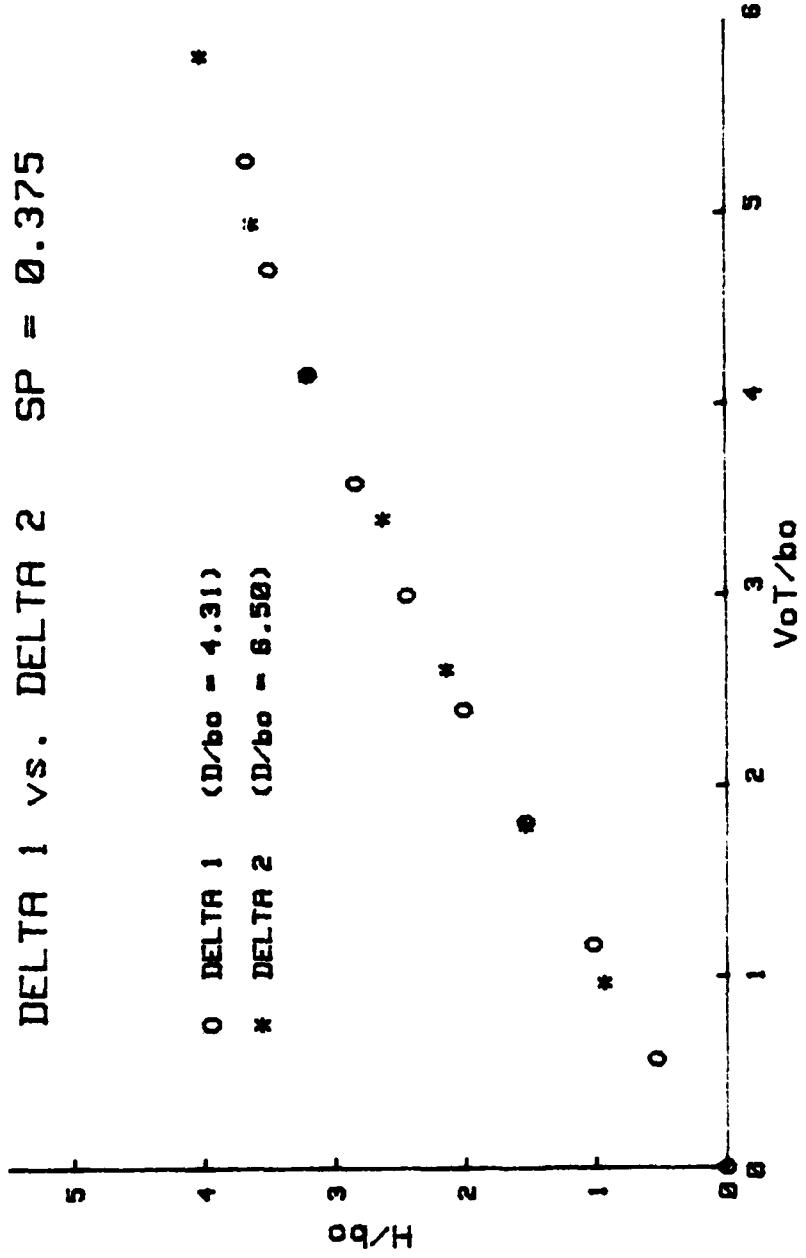
Figure 28. Comparison of the Vortex Rise for Delta 1 and Delta 2 for SP = 0.375.
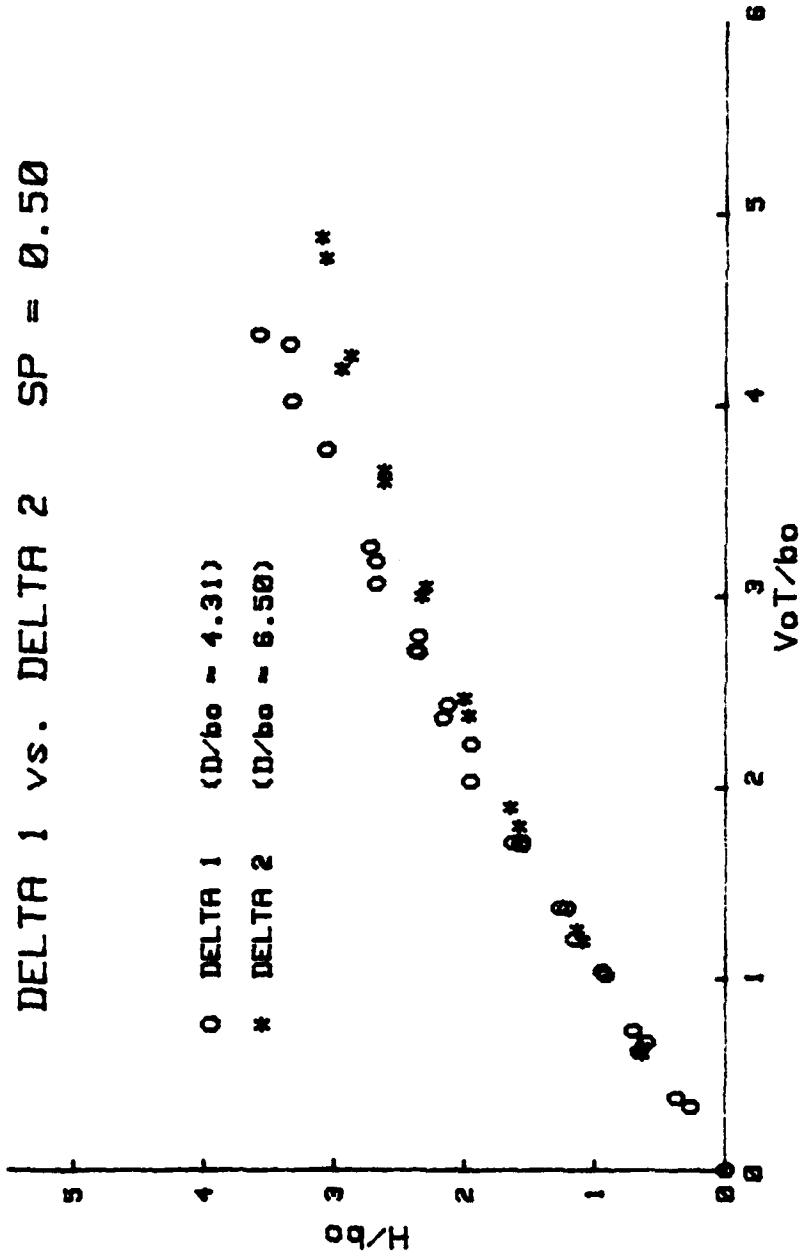
Figure 29. Comparison of the Vortex Rise for Delta 1 and Delta 2 for SP = 0.50.
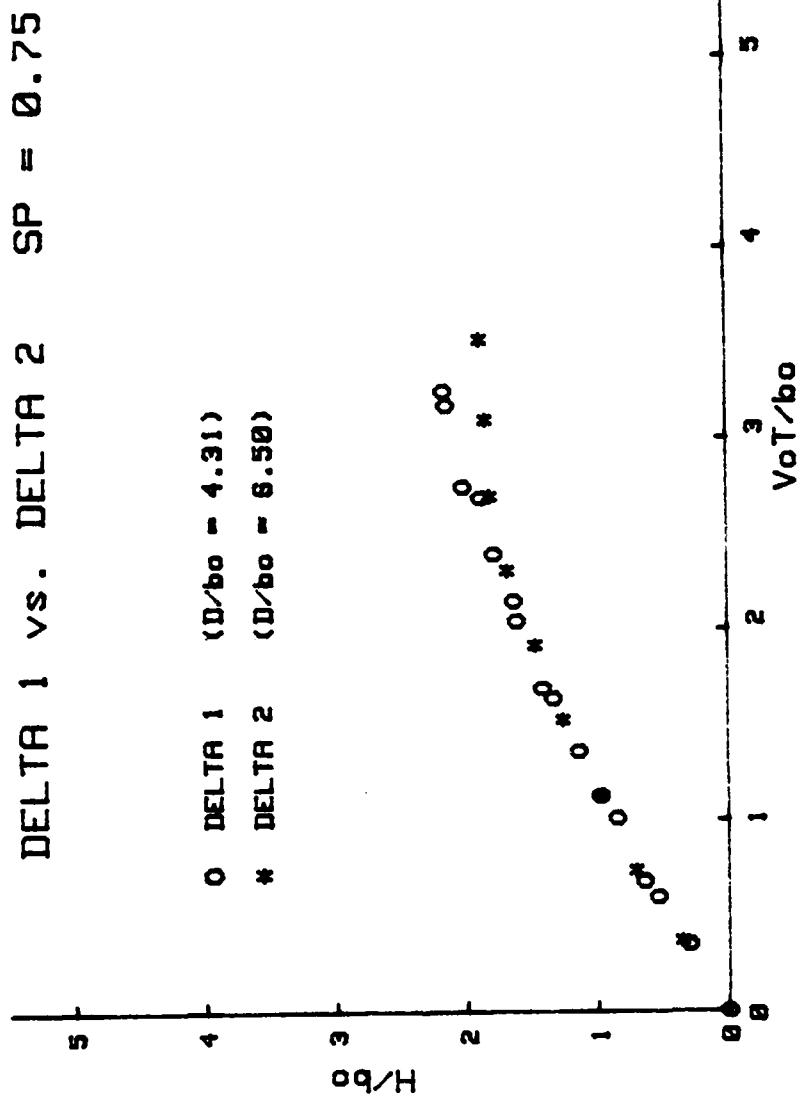
Figure 30. Comparison of the Vortex Rise for Delta 1 and Delta 2 for SP = 0.75.
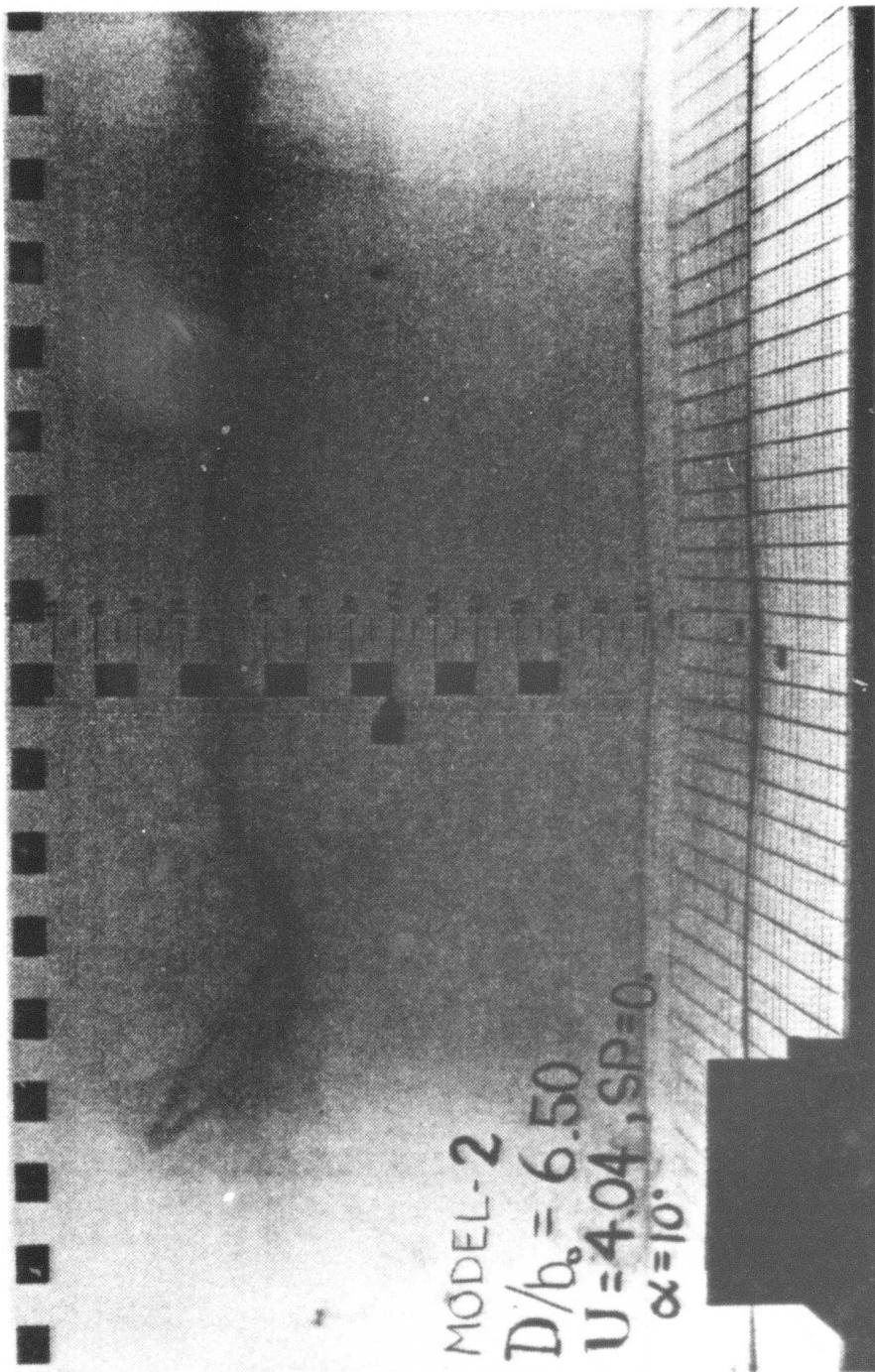
Figure 31. Horseshoe Vortex and the Formation of a Vortex Ring.

MODEL-2
$D/b_0 = 6.50$
$U = 4.04$, $SP = 0$.
$\alpha = 10°$

measurements have shown that the vortex ring inclines itself at an angle of about 45° and undergoes complex deformations partly under the influence of self-induced velocities and partly due to the velocities created by the remainder of the trailing vortex. The complexity of the fluid motion in the vortex ring is such that analyses based on circular vortex rings of constant core and pitch diameter cannot be used to predict the transport velocity of the vortex ring. In fact, attempts made to do so have resulted in an arbitrary selection of the core radius with widely differing velocities. The non-uniformity of the velocities induced on the ring resulted in vortex stretching in addition to gross deformations.

Following the formation of the first ring, the end of the trailing vortices necessarily links and forms a new Horseshoe vortex because of the fact that the vortices cannot end in a fluid. This, in turn, results in a new vortex ring with similar consequences. Repeated experiments have shown that as many as three or four such rings are formed. Several facts must be brought out in connection with their formation, motion, and subsequent demise. Each ring has a character of its own because of a number of reasons. The first ring has the largest circulation because an accelerating body gives rise to the largest accumulation of vorticity. Second, the first ring is formed from that portion of the trailing vortex which is relatively young or not too much affected by aging. Lastly, the first ring is under the influence of its own self-induced velocity plus that of the Horseshoe vortex at the end of the trailing vortex.

The second ring is formed from that part of the vortex trail which is relatively more aged. In other words, the aging and deformation of a vortex ring formed from a relatively young vortex trail (higher

77

concentration of vorticity at the core) are not the same as that of a ring formed from an already aged core. Furthermore, the second ring is influenced not only by the velocities induced by itself, but also by the velocities induced by the first ring and the remainder of the trailing vortex. Extending this discussion to three or four rings one realizes that each ring is different at birth and is subjected to different velocity fields subsequently. Also, one may surmise that the lack of continuation of the formation of a larger number of vortex rings may be related to the demise of the trailing end of the vortices by simple eddy diffusion of vorticity.

From the foregoing, one may postulate that the rings will form at such a frequency that the total length of the trailing vortex between the body and the last ring will remain either constant, or will get larger or smaller. Experiments have shown that not only is the number of rings finite, but also the rate of horizontal progression. The distance as well as the time interval between the successive linkings have been determine and it was found that $(\Delta x)_n/(\Delta t)_n$ is nearly constant (Δx_n is the horizontal distance between the n-th and (n-1)-th link and Δt_n is the corresponding time difference). Comparing the linking velocity given by $(\Delta x)_n/(\Delta t)_n$ with the velocity of the model, it has been found that

$$\frac{U}{(\Delta x)_n/(\Delta t)_n} \cong 16\text{-}20 \tag{7}$$

Thus, one may conclude that the length of the vortex trail increases rapidly and its demise is governed by other mechanisms unrelated to the formation of the Horseshoe vortices and vortex rings. However, the formation of the vortex rings is extremely important since the formation

78

of the rings is closely related to the change of circulation generated by the lifting body. Such a change may result either from the change of the angle of attack of the lifting surface and/or from the change of velocity of the body. One may also include in the change of angle of attack the alteration of the positions of the flaps of an aircraft. Consequently, an aircraft or a submerged body moving with rapidly changing velocities or at a constant velocity with periodically oscillating lifting surfaces can give rise to vortex rings. Finally, it is worth noting that the changes in velocity and/or the angle of attack of lifting surfaces may precipitate and enhance other demise mechanisms.

2. Demise of the Vortex Pair

The maximum height to which the vortex pair rises has been obtained from the plotted as well as the tabulated data and is shown in Fig. 32 as a function of the stratification parameter Nb_0/V_0. Only those points for which D/b_0 were sufficiently large so as to preclude any free surface effects are shown in Fig. 32. Also shown in this figure are the couple of data points obtained by Tomassian [Ref. 47].

Figure 32 points out several important facts. First, the vortices have a self-limiting effect on their rise, even in an unstratified medium. Second, the stratification imposes further limitation on the maximum height of rise. In all cases, various demise mechanisms bring about the said limitation. These will now be discussed in some detail, bearing in mind the fact that it is in some cases extremely difficult to quantify some of these mechanisms.

The most obvious of all the mechanisms is the so-called aging of the vortices or the diffusion of vorticity by viscous and turbulent actions.

79

MAXIMUM VERTICAL RISE OF VORTICES
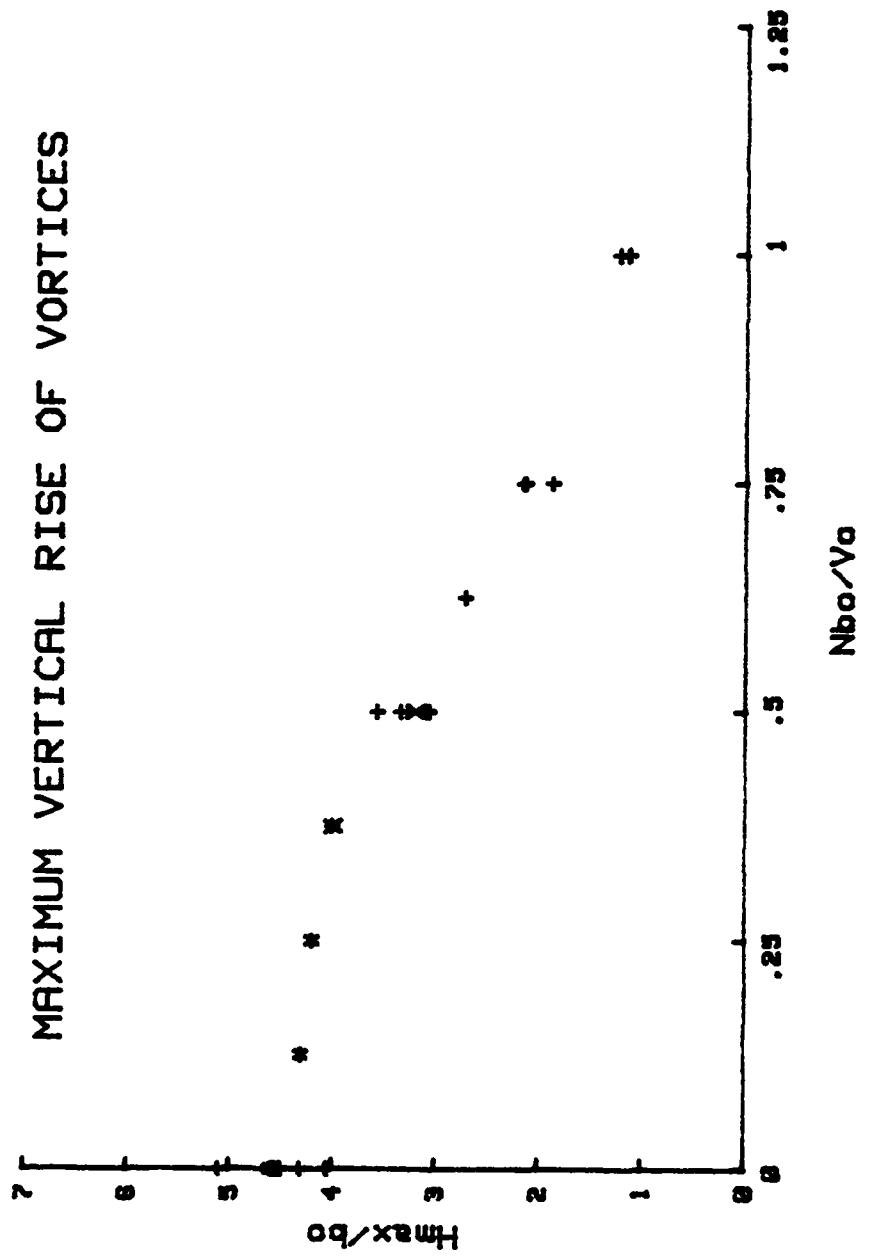
Figure 32. Experimental Data for H_{max}/b_o versus Nb_o/V_o.

It is a well-known fact that a vortex with a given initial vorticity distribution diffuses its vorticity gradually. If the vortices are moving in a stratified medium the density gradient gives rise to opposite-signed vorticity outside the recirculation cell. This vorticity may be entrained into the recirculation cell, thereby reducing the total circulation. The entrainment and detrainment of the recirculation cell have been discussed in detail by Crow [Ref. 51] and by Tombach [Ref. 59], among others, and will not be discussed here further. Suffice it to note that the end result of the aging of vortices is to decrease their upward migration.

The next demise mechanism is that first rigorously analyzed by Crow [Ref. 54] and known either as Crow instability or sinusoidal instability. Crow has shown that two initially parallel trailing vortices are unstable to small perturbations and links at intervals of 8.6 times the initial core spacing b_0. The rings so formed gradually dissipate at a rate dependent on atmospheric conditions. In fact, Crow and Bate [Ref. 55] have shown the role played by turbulence in the sinusoidal instability, the wavelength, and the demise of the entire trailing vortex. In spite of the uncertainties associated with the quantification of the effects of turbulence, the instability analysis of Crow still remains as the only rigorous mathematical model of any one of the demise mechanisms.

In the data shown in Fig. 32, the Crow instability was observed in the trailing vortices for stratification parameters less than about 0.75. At higher stratification parameters, the vortices do not last long enough to experience Crow instability. This raises the important question as to the time required from the inception to the linking of the

vortices in stratified fluids. Such an analysis does not yet exist and the said time will probably be a strong function of the ambient turbulence as in the case of unstratified fluids.

The events following the linking of the vortices are both interesting and complex. The stretching of the vortices, the instability propagating about the rings, the increase of the core size, and the generation of opposite-signed vorticity give rise to as yet incalculable consequences. This aspect of the investigation, like many other interesting problems raised during the course of this investigation, needs further examination, probably through the use of high-speed motion pictures.

The last and certainly one of the most important demise mechanisms to be discussed is the vortex breakdown. When the axial velocity in a vortex becomes nearly equal to the maximum tangential velocity at the edge of the core, the vortex undergoes a rapid transition from supercritical to subcritical flow. This abrupt transition may occur in one of three forms depending on the circulation and the Reynolds number of the ambient flow. These are axisymmetric vortex breakdown, spiral breakdown, and double-helix breakdown [Ref. 7]. The occurrence of the vortex breakdown may be precipitated by an adverse pressure gradient. For example, the swirling flow in a conical diffuser produces vortex breakdown at a distance must closer to upstream than a uniform pipe. Thus in the case of an axisymmetric streamlined body, t e deceleration of the ambient flow at the aft end produces vortex breakdown in the trailing vortex. In the case of the Delta-wings, the breakdown results from the expansion of the core and the reduction of the tangential velocity. The consequence of the

breakdown is not the total annihilation of the vortex, as it was once thought. Observations and measurements have shown that the vortices survive the vortex breakdown and continue to rise. It is not yet known as to how much circulation if left in the vortex following the vortex breakdown or a cascade of breakdowns. In all cases, the trailing vortex may contain one or more velocity maximums with numerous smaller swirls. It appears that the reduction of circulation is more with vortex breakdown than with the other mechanisms.

The data points shown in Fig. 32, particularly for small values of the stratification parameter have resulted from the vortices which had sufficient time to undergo Crow instability and vortex breakdown. Depending on the particular experiment, either the Crow instability or the vortex breakdown occurred first since there was no strong adverse pressure gradient to precipitate the vortex breakdown first. Since the vortex motion resulting from a combination of Crow instability followed by vortex breakdown is not the same as that resulting from vortex breakdown followed by some form of Crow instability, one does expect considerable scatter in H_{max}/b_o. This is evidenced by the data points in Fig. 32, particularly for $Nb_o/V_o = 0$. It must be emphasized that H_{max}/b_o is a measure of the maximum relative height at which the vortex cores have essentially dissipated. It is quite possible that some residual vorticity may still persist in the flow. This vorticity is not expected to have significant consequences relative to the vorticity associated with the trailing vortices prior to the dissipation of the cores. In other words, the vorticity density in the flow field for H/b_o larger than H_{max}/b_o is insignificant relative to H/b_o smaller than H_{max}/b_o.

83

The need to determine the lifespan of vortices and to understand the physics of the demise mechanisms gave rise to several approximate analyses. These will now be discussed in some detail and another approximate analysis will be presented.

Scorer and Davenport [Ref. 50] assumed that the impulse imparted to the vortex pair and the circulation of each vortex remain constant. This resulted in a gradually decreasing distance between the vortices given by:

$$H = \frac{V_0}{AN} \sinh (ANt) \qquad (8)$$

and

$$b = b_0 \frac{1}{\cosh (ANt)} \qquad (9)$$

in which

$$A = 0.67$$

Eliminating time between Eqs. (8) and (9), one has

$$\sqrt{(\frac{b_0}{b})^2 - 1} = \frac{ANH}{V_0} \qquad (10)$$

Scorer and Davenport assumed that the recirculation cell will cease to rise when the vortices annihilate each other by having their cores touch. In other words, assuming $b = 2r_0$, one has from Eq. (10),

$$\frac{H_{max}}{b_0} = \frac{1.492}{Nb_0/V_0}\sqrt{(\frac{b_0}{2r_0})^2 - 1} \tag{11}$$

The above equation yields the maximum relative height in terms of the stratification parameter provided that one has some idea about the core radius, or b_0/r_0. The use of $r_0 = 0.1b_0$ in Eq. (11) results in unrealistically large H_{max}/b_0 values. Various values of b_0/r_0 were examined so as to obtain some correspondence, at least for some ranges of Nb_0/V_0. This resulted in a choice of $b_0/r_0 = 3$. Then Eq. (11) reduces to

$$\frac{H_{max}}{b_0} = \frac{1.67}{Nb_0/V_0} \tag{12}$$

Equation (12) is plotted in Fig. 33 together with the experimental data. Clearly, there are two fundamental difficulties associated with Scorer and Davenport's analysis. First, the assumed core radius of $b_0/3$ is too large to be realistic. Second, as the stratification parameter approaches zero, the analysis predicts increasingly large H_{max}/b_0 values, implying that a trailing vortex in an unstratified infinite fluid medium will never cease to rise. These shortcomings are simple consequences of the fact that the physics associated with the demise mechanisms have not been incorporated into the analysis. Judging from the results of other works since the pioneering work of Scorer and Davenport, one must state in all fairness that it has not yet been possible to incorporate the consequences of turbulence, Crow instability, and vortex breakdown into the analysis. Attempts made to model numerically to include the effect of turbulence will be discussed later.

MAXIMUM VERTICAL RISE OF VORTICES

$$H_{max}/b_o = \frac{2.39}{Nb_o/V_o} \quad [\text{Eq. (15)}]$$

$$H_{max}/b_o = \frac{1.67}{Nb_o/V_o} \quad [\text{Eq. (12)}]$$
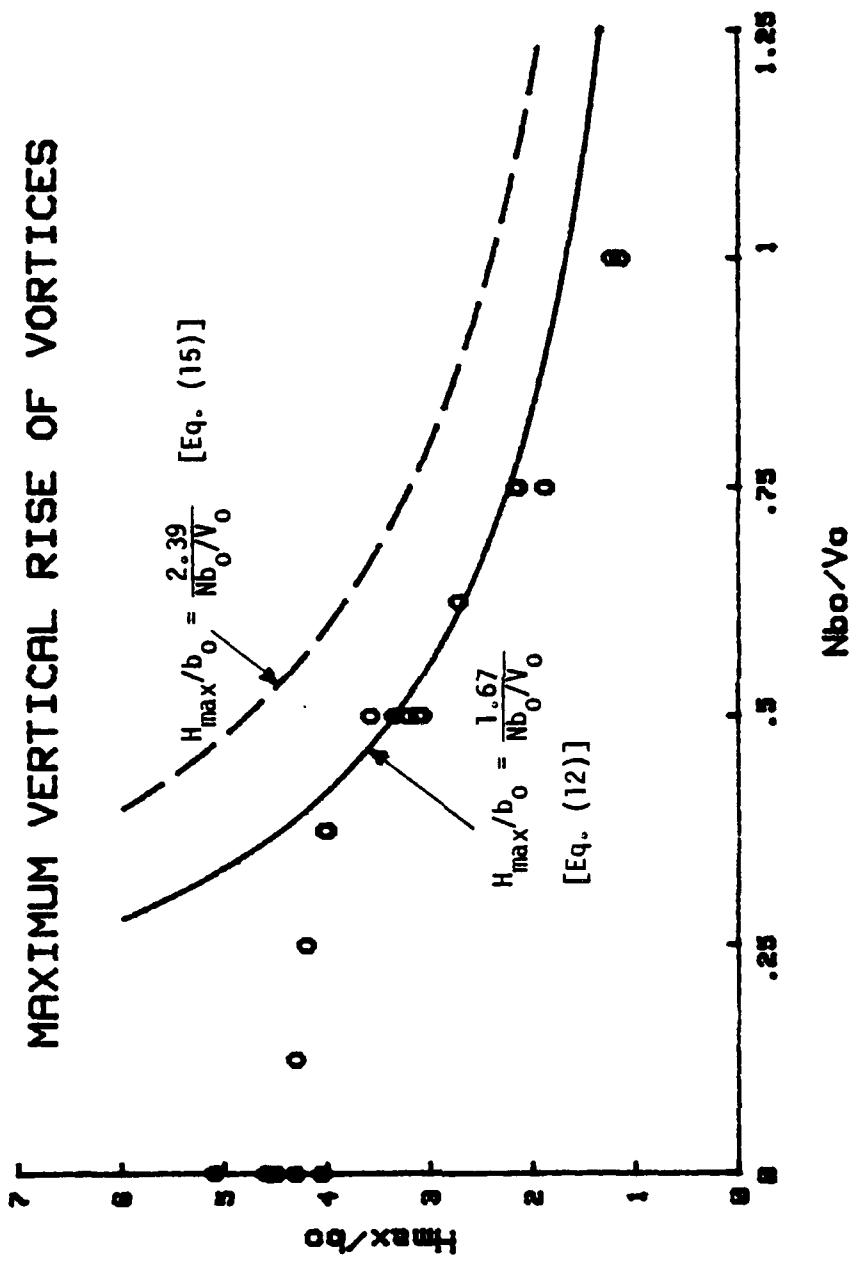
Figure 33. Comparison of the Experimental Data with Eqs. (12) and (15).

86

Another approximate analysis of the ultimate vertical migration of the recirculation cell may be carried out by assuming that the initial kinetic energy of the fluid within the cell is converted to potential energy.

The kinetic energy of the fluid within the recirculation cell is given by [Ref. 62]

$$E = \frac{1}{2\pi} \rho \, \Gamma^2 (\ln \frac{b_0}{r_0} + \frac{1}{4}) \qquad (13)$$

The potential energy of the recirculation cell may be written as

$$P = m b_0^2 \, g \, \Delta\rho \, H_{max} \qquad (14)$$

in which $m b_0^2$ is the area of the recirculation cell and $m = 2.83$. Equating the kinetic and potential energies using $r_0/b_0 = 0.1$, and simplifying, one has

$$H_{max}/b_0 = \frac{2.39}{(N b_0/V_0)} \qquad (15)$$

Equation (15) is shown in Fig. 33 together with Eq. (12) and experimental data. Clearly, Eq. (15) represents the upper bound of the H_{max}/b_0 values since no energy dissipation due to any one of the demise mechanisms has been incorporated into the analysis. Finally, it should be emphasized that the predictions of Eq. (15) could have been partially matched to the experimental data by artificially increasing the relative core radius r_0/b_0. In the foregoing, r_0/b_0 was assumed to have the

experimentally observed value of 0.1 in order to accentuate the energy loss brought about by the complex demise mechanisms.

A third approximate analysis may be carried out by assuming that the vortex separation remains constant, but the strength of the vortices vary with time.

Starting with the analysis of Scorer and Davenport [Ref. 50], i.e., by equating the time rate of change of impulse imparted to the vortex pair to the buoyant force, one has

$$\frac{\partial(\rho \Gamma b_0)}{\partial t} = g m b_0^2 \Delta\rho \tag{16}$$

Assuming $\partial b_0/\partial t = 0$, one has

$$\rho b_0 \frac{d\Gamma}{dt} = g m b_0^2 \rho B z \tag{17}$$

in which $\Delta\rho = \rho B z$ and $B = N^2/g$. Noting that $V = \frac{dz}{dt} = \frac{\Gamma}{2\pi b_0}$, Eq. (17) may be reduced to

$$\frac{\Gamma d\Gamma}{\pi b_0} = g m b_0 B z \, dz \tag{18}$$

Integration of Eq. (18) and rearrangement in terms of the stratification parameter yields

$$\frac{H_{max}}{b_0} = \frac{1.49}{N b_0/V_0} \tag{19}$$

The correspondence between the experimental data and the prediction of

88

Eq. (19) (see Fig. 34) may be somewhat fortuitous because of a number of reasons. The size of the vortex core does not enter into the analysis even though it is known to have an important effect on the life of vortices. Furthermore, as in all other analyses, the known demise mechanisms do not appear in Eq. (19).

All of the foregoing approximate analyses point out emphatically that there are *no simple approximations* with which one can predict the rise of the vortices. One must use experimental data and heuristic reasoning to delineate the role played by various demise mechanisms in the ascent of vortices. This fact is further accentuated by Fig. 35 where the experimental data are shown together with a best fit curve defined by

$$\frac{H_{max}}{b_o} = 4.64 \exp[-1.3(Nb_o/V_o)^2] \tag{20}$$

The particular dependence of H_{max}/b_o on Nb_o/V_o strongly suggests that the phenomena such as turbulence, entrainment and detrainment, Crow instability, and the vortex breakdown play far more complex roles than what may be quantified in a simple approximate analysis.

E. SAILPLANE GENERATED VORTICES

The results obtained with a streamlined body and its lifting surface in stratified and unstratified water will be presented in the following.

Figure 36 shows the normalized vertical distance H/b_o as a function of the relative distance Z/b_o along the direction of motion for three representative model velocities. The reason for the choice of the particular normalizing parameters is that the body proximity does not allow

89

MAXIMUM VERTICAL RISE OF VORTICES

$$H_{max}/b_o = \frac{1.49}{Nb_o/V_o} \text{ , [Eq. (19)]}$$
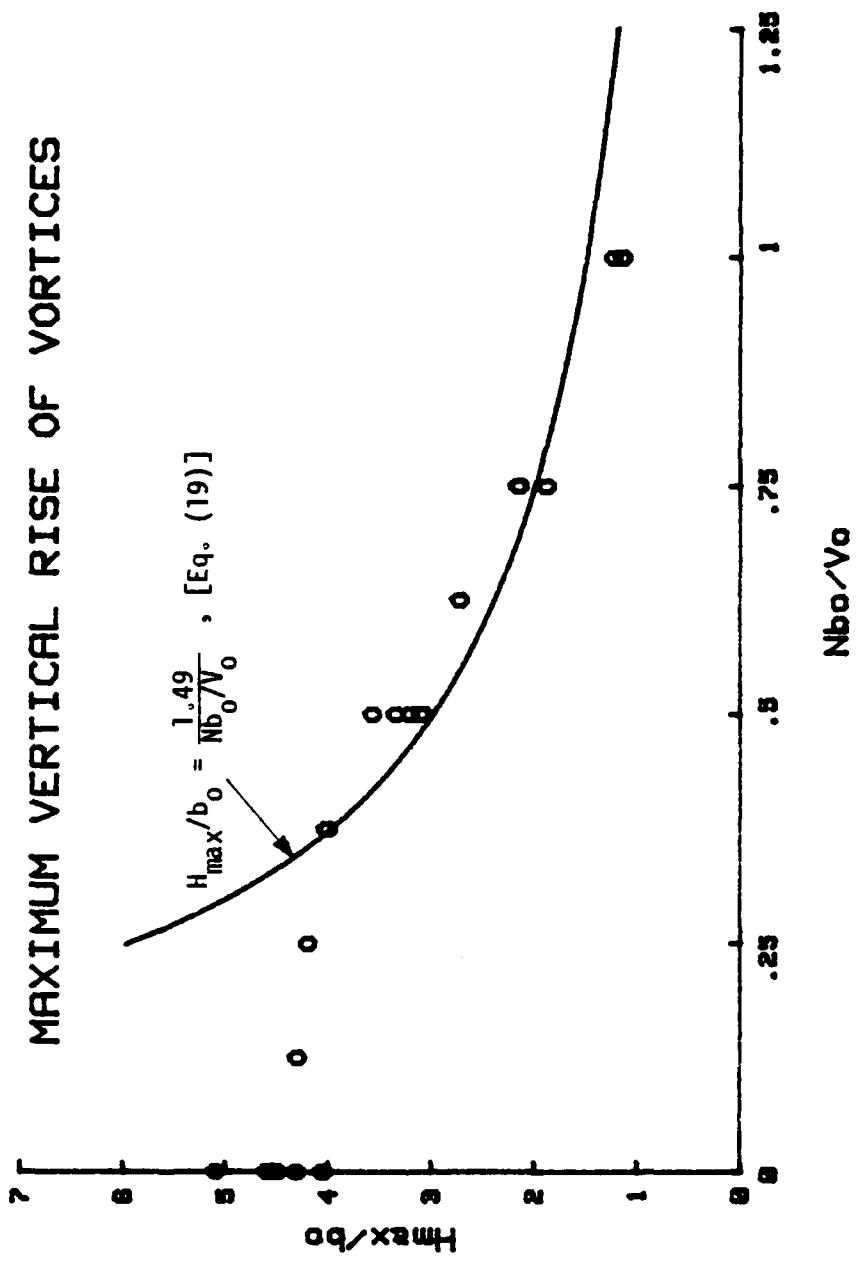
Figure 34. Comparison of the Experimental Data with Eq. (19).
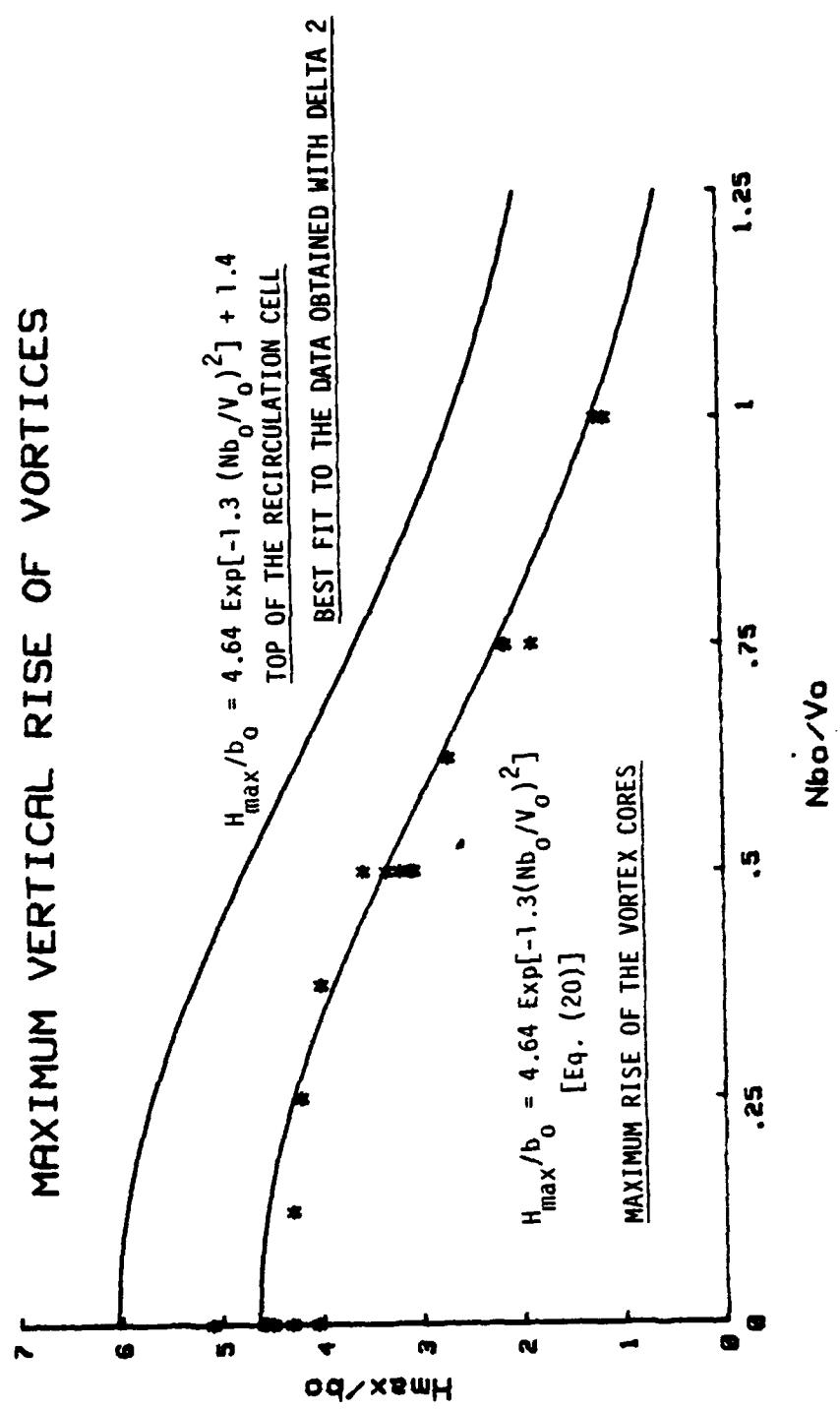
Figure 35. Experimental Data and the Best-Fit Curve [Eq. (20)].
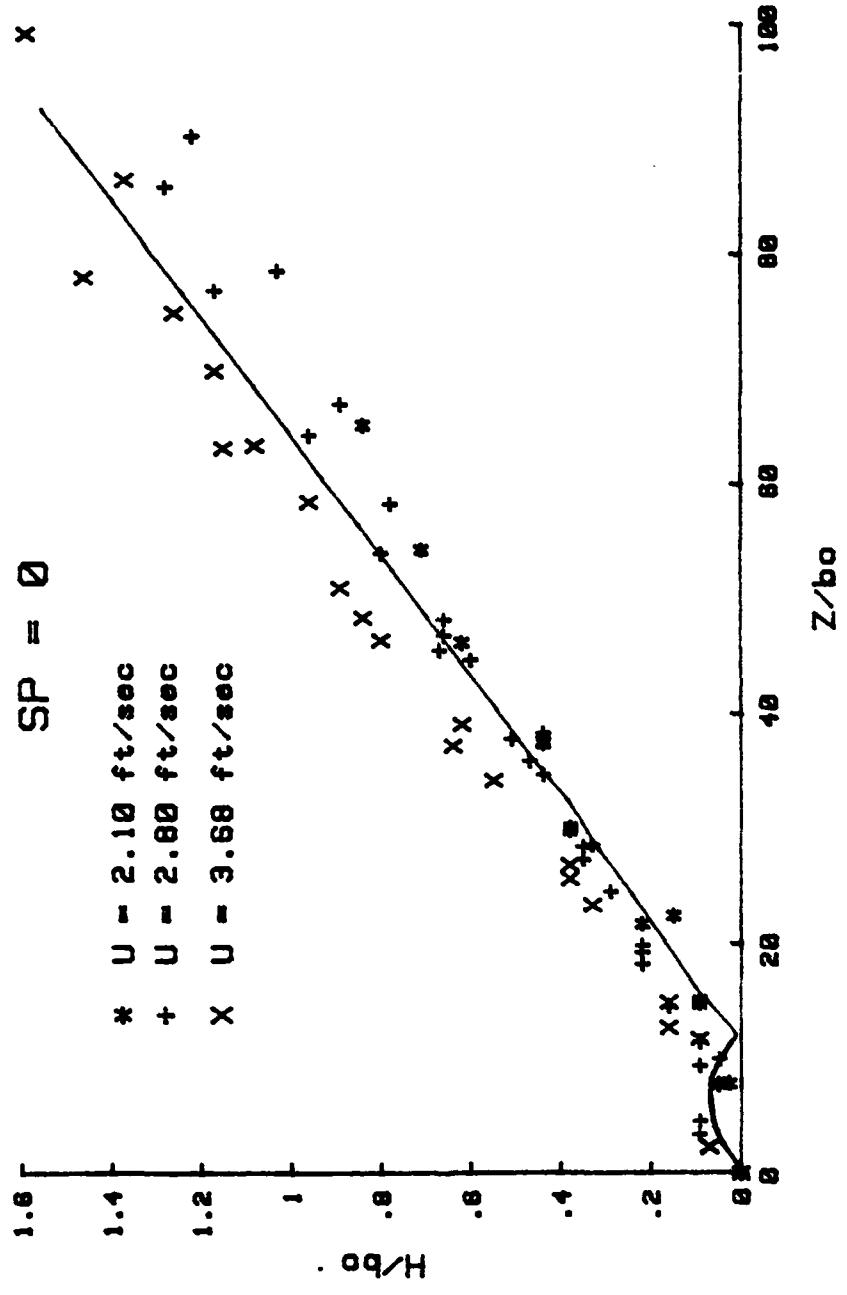
Figure 36. The Rise of the Sailplane Generated Vortices as a Function of Z/b_0 for SP = 0.

the determination of an initial rise velocity V_o. In spite of the scatter, the data show that there is very little or no dip in the path of the trailing vortices as they approach the aft end of the body at $Z/b_o = 14$. Once the vortices are free from the body proximity effects, they continue to rise at a nearly constant velocity. In fact it is this particular rise velocity that is used in Fig. 37 to plot H/b_o as a function of $V_o t/b_o$.

Also shown in Fig. 36 is the analytical result based on ideal line vortices (see Appendix E). The vortex characteristics used in the calculations were those appropriate for the lifting surface of the streamlined body. The predictions of the inviscid flow model come surprisingly close to the experimental data. This may be due to a number of reasons, the most important of which is the use in the calculations of the vortex strength which corresponded to that experimentally determined value after a series of vortex core bursts, i.e., the use of the vortex velocity based on the data shown in Fig. 36.

The exploratory results obtained with one stratification parameter (SP = 0.625) are shown in Figs. 38 and 39. A comparison of these figures with Figs. 36 and 37 show that the stratification inhibits the rise of the vortices as anticipated on the basis of the experiments with Delta-wings. The effects of other stratifications on the evolution of trailing vortices shed from the lifting surfaces of an axisymmetric slender body will have to be examined in light of additional experiments. The determination of the circulation existing in the trailing vortices after the vortex breakdown will enable one to compare with greater confidence the prediction of the numerical models with the results obtained experimentally.

93
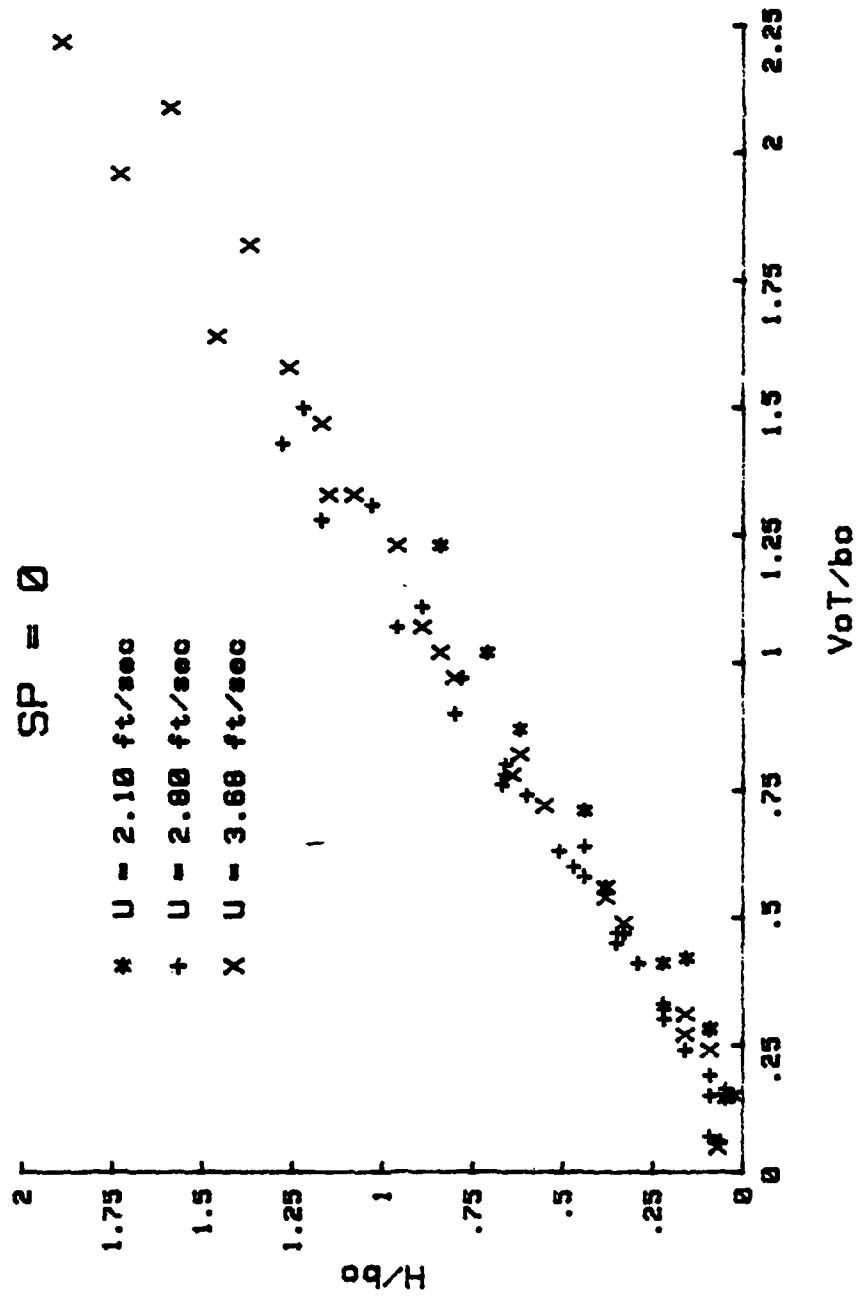
Figure 37. The Rise of the Sailplane Generated Vortices as a Function of $V_0 t/b_0$ for SP = 0.

94
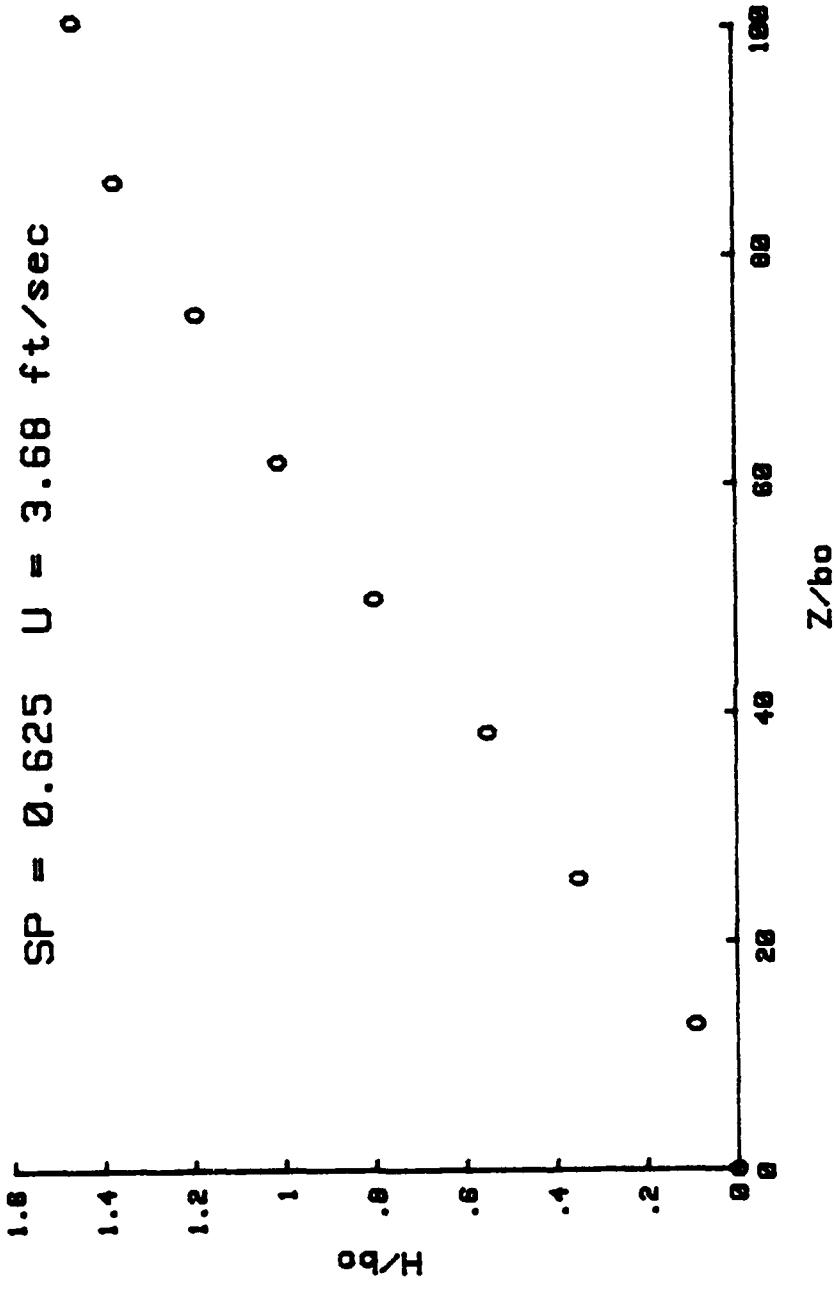
Figure 38. The Rise of the Sailplane Generated Vortices as a Function of Z/b_0 for SP = 0.625.
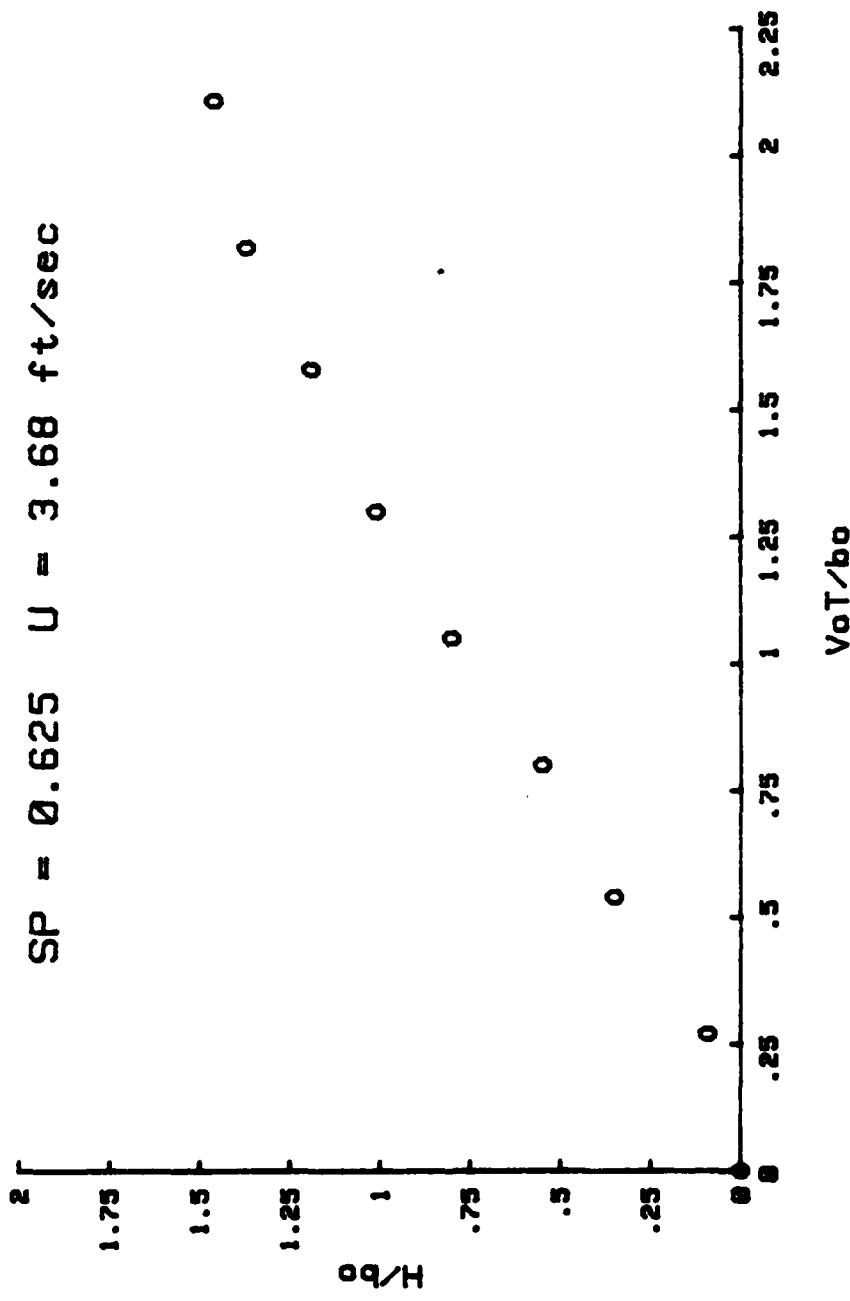
Figure 39. The Rise of the Sailplane Generated Vortices as a Function of V_0t/b_0 for SP = 0.625.

F. NUMERICAL MODEL OF LAMINAR VORTEX PAIR

As discussed in the previous sections, the need to determine the lifespan of vortices and to understand the physics of the demise mechanisms gave rise to several approximate analyses. Numerical methods have been employed only recently using computers to attempt to incorporate the effect of turbulence in the evolution and ultimate demise of the vortex pair. It is hoped that such methods will provide not only a power of prediction of the migration of trailing vortices but also some insight as to the relationship between turbulence and the demise mechanisms. To be sure, there are, at present, no numerical methods dealing with the three-dimensional trailing vortices and the effects of vortex breakdown and Crow instability.

The most advanced numerical methods have been applied to the study of the two-dimensional, unsteady vortex pair. Hecht et al. [Ref. 44], introduced such a model which solves the mean and ensemble-averaged Reynolds stress equations of fluid motion, based on a second-order closure turbulence model. The initial distribution of vorticity was assumed to be Gaussian of the form

$$\zeta = \frac{\pm\Gamma}{\pi\sigma^2} \exp[-(r/\sigma)^2] \tag{21}$$

with $\sigma = 0.25b_0$ (this corresponds to $r_0/b_0 = 0.177$). The initial turbulence distribution was again Gaussian with a spread of $0.25b_0$, and was assumed to be isotropic with a representative integral scale. An upward velocity was employed to follow the vortex descent. A Reynolds number of $V_0 b_0/\nu = 2 \times 10^5$ was assumed for the analysis.

97

The model was validated by comparing the calculated and experimentally determined trajectories of <u>vortex rings</u>. The results of this model for a vortex pair in atmosphere with a stratification parameter of 0.8 are compared in Fig. 40 with those of the Delta-wings in water with a stratification parameter of 0.75. The model matched the experimental data very well, although there are no physical arguments to justify the selected integral scale for turbulence. Furthermore, the value of σ should be about half that assumed.

In a recent paper, Hecht, Bilanin, and Hirsh [Ref. 53] compared the predictions of the aforementioned model with other analytical [Refs. 49, 51, and 59] and experimental results [Ref. 43]. Initial distribution of vorticity was based on the data from Burnham et al. [Ref. 43]. The initial σ used in Eq. (21) was determined to be $0.074b_0$. The integral scale for turbulence was set to a smaller value for this analysis and a sensitivity study of the macroscale effects on vortex descent was presented. The results of this model for SP = 0.67 and $\sigma/b_0 = 0.075$ are compared with the Delta-wing results for SP = 0.625 and SP = 0.75 in Fig. 41. This model does not match the data for $V_0 t/b_0$ greater than about 2.

A better match between the measured and calculated values could have been achieved with $\sigma = 0.25b_0$. But this value is larger than that in trailing vortices by a factor of about 3 relative to the observations of Burnham et al. [Ref. 43]. Of course the integral scale of turbulence could have been adjusted also to achieve more realistic results for $V_0 t/b_0$ larger than about 1.5.

While the numerical models cited above have pioneered in the study of turbulent effects in trailing vortices, the difficulties associated with
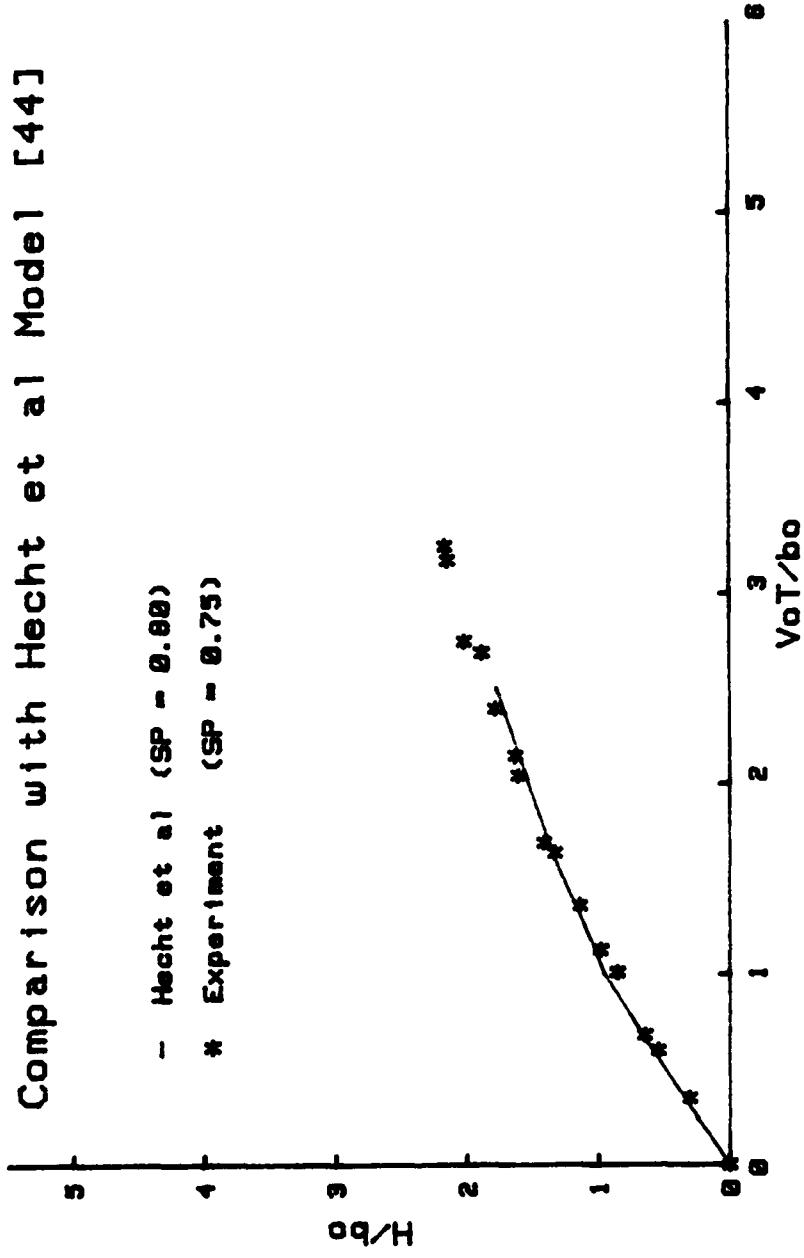
Figure 40. Comparison of Experimental Data with that Predicted by Hecht et al (Ref. 44).

99
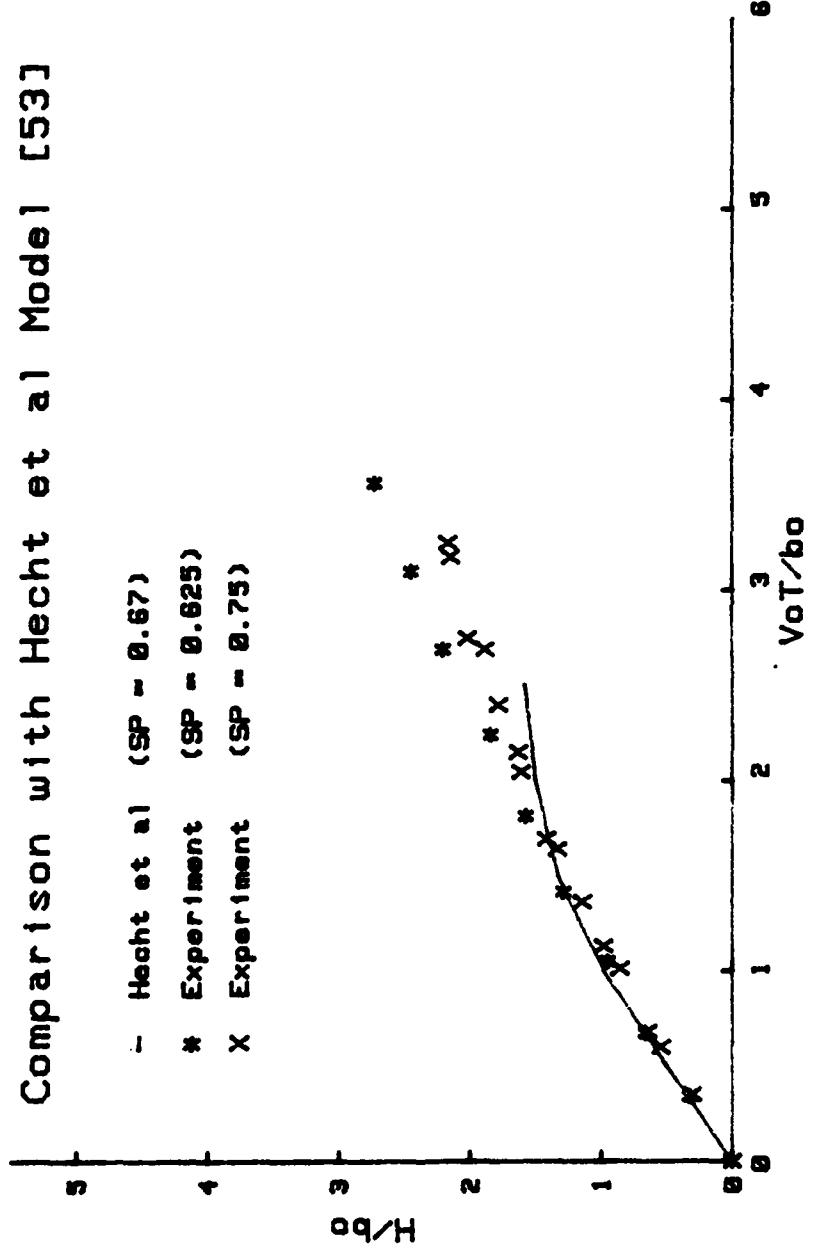
Figure 41. Comparison of Experimental Data with that Predicted by Hecht et al (Ref. 53).

100

the choice of free parameters (σ and the integral scale of turbulence) point out the need for additional work.

In an effort to eventually produce such a fully turbulent flow model to compare the three-dimensional trailing vortex data, gathered from the experimental models in the water basin, a two-dimensional, laminar, unsteady flow numerical model of the vortex pair was developed as part of this investigation.

For this purpose, the Navier-Stokes equations were written as

$$\frac{\partial u}{\partial t} + u \frac{\partial u}{\partial x} + v \frac{\partial u}{\partial y} = 0 - \frac{1}{\rho} \frac{\partial P}{\partial x} + \nu \Delta^2 u \tag{22}$$

$$\frac{\partial v}{\partial t} + u \frac{\partial v}{\partial x} + v \frac{\partial v}{\partial y} = g - \frac{1}{\rho} \frac{\partial P}{\partial y} + \nu \Delta^2 v \tag{23}$$

where the y-axis is assumed to be directed downwards. Eliminating the pressure between the two equations, one has

$$\frac{\partial \zeta}{\partial t} + \frac{\partial (u\zeta)}{\partial x} + \frac{\partial (v\zeta)}{\partial y} = \nu \Delta^2 \zeta - \frac{g}{\rho} \frac{\partial \rho}{\partial x}$$

$$+ \left[\frac{1}{\rho} \frac{\partial \rho}{\partial y} (\nu \Delta^2 u - \frac{Du}{Dt}) - \frac{1}{\rho} \frac{\partial \rho}{\partial x} (\nu \Delta^2 v - \frac{Dv}{Dt}) \right] \tag{24}$$

$$\zeta = \frac{\partial u}{\partial y} - \frac{\partial v}{\partial x} \tag{25}$$

and represents the vorticity. For flows in which the gravitational acceleration is several orders of magnitude larger than the fluid accelerations, the terms in the bracket in Eq. (24) may be neglected. This amount to invoking the Boussinesq hypothesis. Thus, the equation of motion and the equation of continuity may be written as

101

$$\frac{\partial \zeta}{\partial t} + \frac{\partial(u\zeta)}{\partial x} + \frac{\partial(v\zeta)}{\partial y} = \nu\nabla^2\zeta - \frac{g}{\rho_0}\frac{\partial \rho}{\partial x} \tag{26}$$

$$\frac{\partial \rho}{\partial t} + \frac{\partial(u\rho)}{\partial x} + \frac{\partial(v\rho)}{\partial y} = \nu\nabla^2\rho \tag{27}$$

The last term in Eq. (26) represents the effect of the density gradient and gives rise to opposite-signed vorticity.

The equations that were chosen to describe the motion include a Gaussian distribution of the initial vorticity given by

$$\zeta = \frac{\pm\Gamma}{2\pi r_0^2}\exp[-(r^2/2r_0^2)] \tag{28}$$

Boundary values of the u and v velocity components are determined by the Biot-Savart Integrals

$$u(x,y) = \int_A \frac{(y'-y)\zeta(x',y')}{2\pi r^2}\,dx'dy' \tag{29}$$

$$v(x,y) = \int_A \frac{(x-x')\zeta(x',y')}{2\pi r^2}\,dx'dy' \tag{30}$$

Where:

$$r^2 = (x-x')^2 + (y-y')^2$$

x',y' denote the position of vorticity, and

x,y the point where the velocity components are calculated.

The stream-function values around the boundaries and velocity within the field boundaries are calculated from u and v using

102

$$u = \frac{\partial \psi}{\partial y} \; ; \qquad v = - \frac{\partial \psi}{\partial x} \qquad \qquad (31)$$

Field stream-function values are calculated using Poisson's equation

$$\nabla^2 \psi = - \zeta \qquad \qquad (32)$$

The calculations had to be carried out in a finite numerical mesh, as in all other numerical analyses. The appropriate boundary conditions are shown on the boundaries of the quadrant in which the calculations have been performed (see Fig. 42). It should be noted that the conditions $u(0,y) = v(x,0) = 0$ are satisfied automatically by evaluating the Biot-Savart equations in all four quadrants. Furthermore, the symmetry provided by the free surface (x-axis) and by the normal bisecting the vortex pair (y-axis) enable one to confine the domain of calculation to a single quadrant.

Additional details of the analysis are as follows:

(i) The domain of calculation is prescribed;

(ii) The vorticity distribution given by Eq. (28) is assigned to mesh points;

(iii) A particular stratification is assigned to the density distribution;

(iv) Boundary values of velocities are calculated using the Biot-Savart equations;

(v) The boundary values of the stream-function are calculated;

(vi) The flow field values of the stream-function are calculated using Poisson's equation and a successive overrelaxation scheme;

(vii) The velocity field is calculated through the use of the stream-function values.

103

$$\frac{\partial \rho}{\partial y} = 0 \ , \quad v(x,0) = 0$$

x

$$\frac{\partial \rho}{\partial x} = 0$$

$$u(0,y) = 0$$

D O M A I N

O F

C A L C U L A T I O N

$$\frac{\partial^2 \zeta}{\partial x^2} = 0$$

$$\frac{\partial^2 \rho}{\partial x^2} = 0$$

$$\frac{\partial^2 \zeta}{\partial y^2} = 0 \ , \quad \frac{\partial^2 \rho}{\partial y^2} = 0$$

y
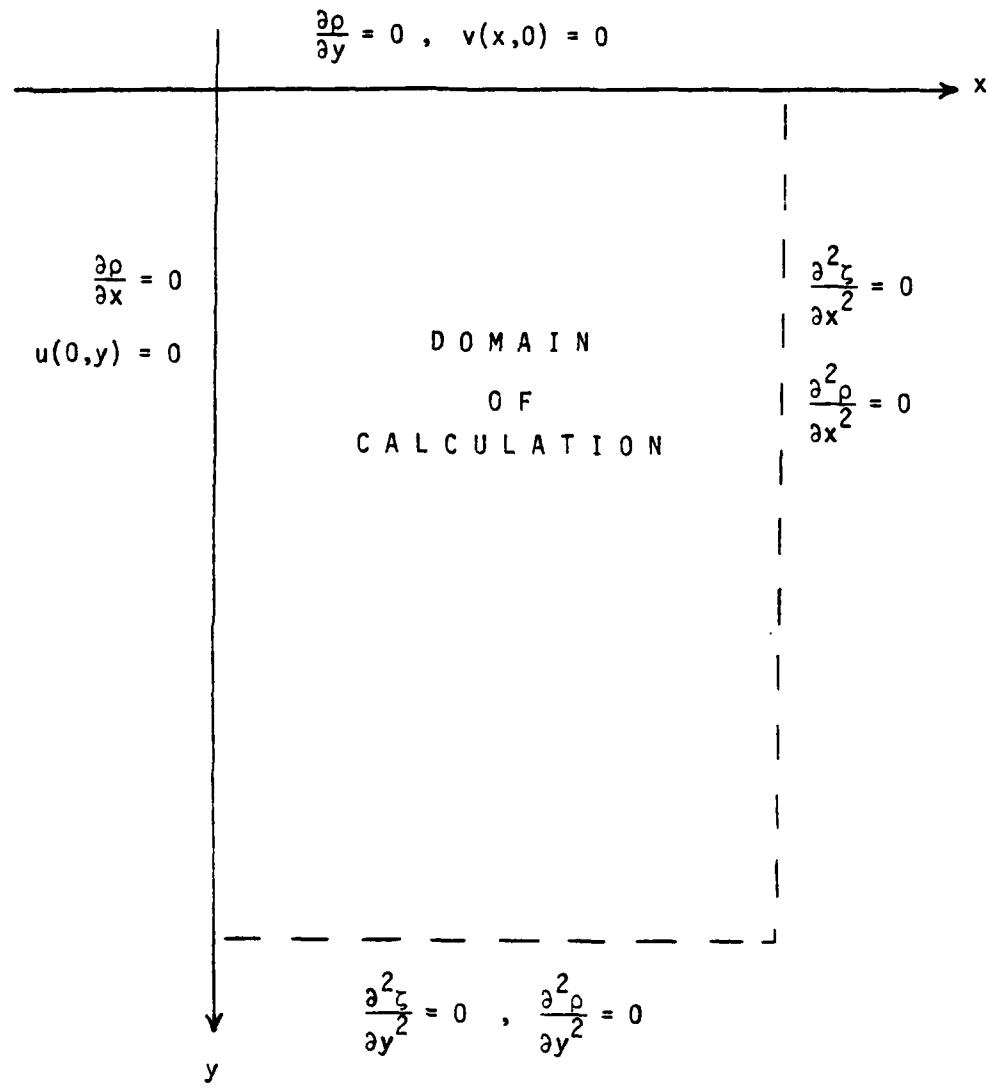
Figure 42.   Computational Field and Boundary Conditions for
the Numerical Model.

104

The foregoing marks the end of the first time step. The successive steps are sequenced as follows:

(i)   The vorticity and density fields are calculated using an upwind-differencing scheme;

(ii) The new center of vorticity is calculated using the square of vorticity as the weighing parameter;

(iii) A vertical velocity is imposed on the field using the velocity calculated from the rate of change of the center of vorticity; and finally,

(iv) The new points at the top of the field are initialized and the vorticity is used to calculate the boundary velocities.

The last step completes the iteration and marks the beginning of a new sequence.

The plots of the streamlines of the flow field for a simulation of the motion of the vortices generated by Delta 1 for SP = 0 are shown in Figs. 43 through 47. The time indicated on each plot is the normalized time $t/(b_0/V_0)$ which is of course identical to its common form $V_0 t/b_0$. In these calculations, D/b_0 was taken to be 4.31, and the initial value of r_0 was assumed to be $0.09b_0$. The calculated values of H/b_0 are compared with those obtained experimentally in Fig. 48. The matching of the two results is surprising in view of the fact that neither turbulence nor any other demise mechanism in conjunction with turbulence was taken into consideration. The surprising agreement between the two results may be attributed to numerical diffusion and to the relative stability of the trailing vortices in unstratified fluids.

Sample streamline plots resulting from the numerical calculation for SP = 0.50 are shown in Figs. 49 through 53 for various values of H/b_0.

105
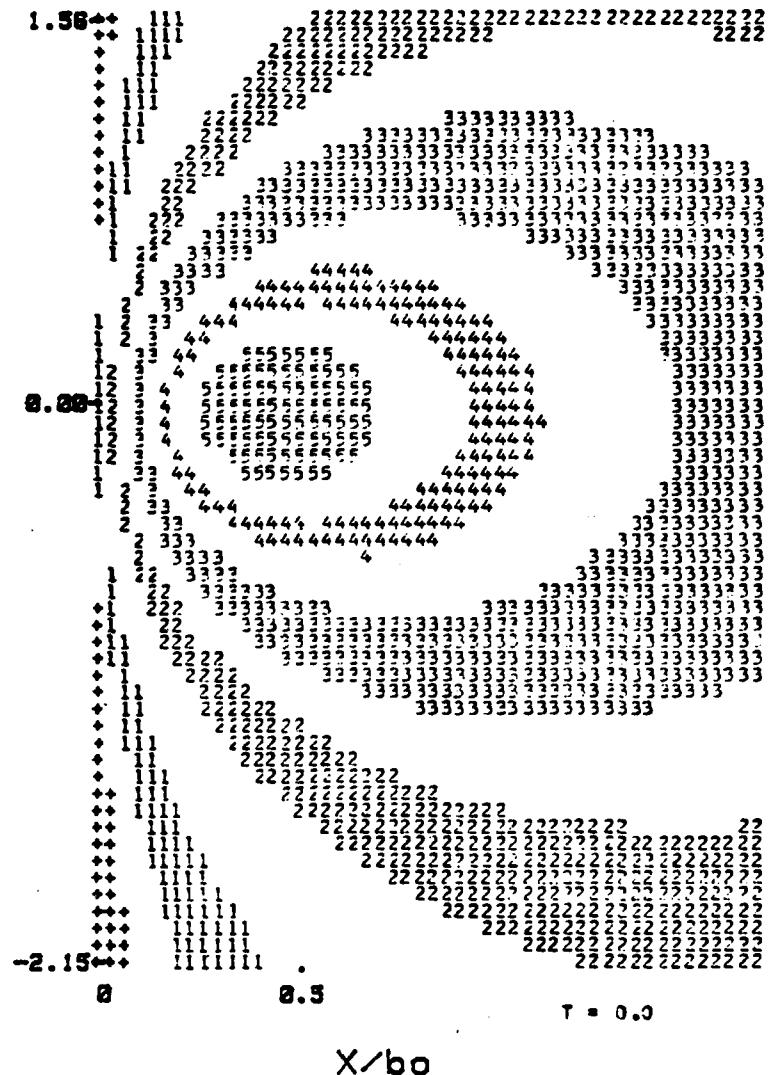
Figure 43. Streamlines of the Numerical Model for SP = 0, $H/b_0 = 0$.
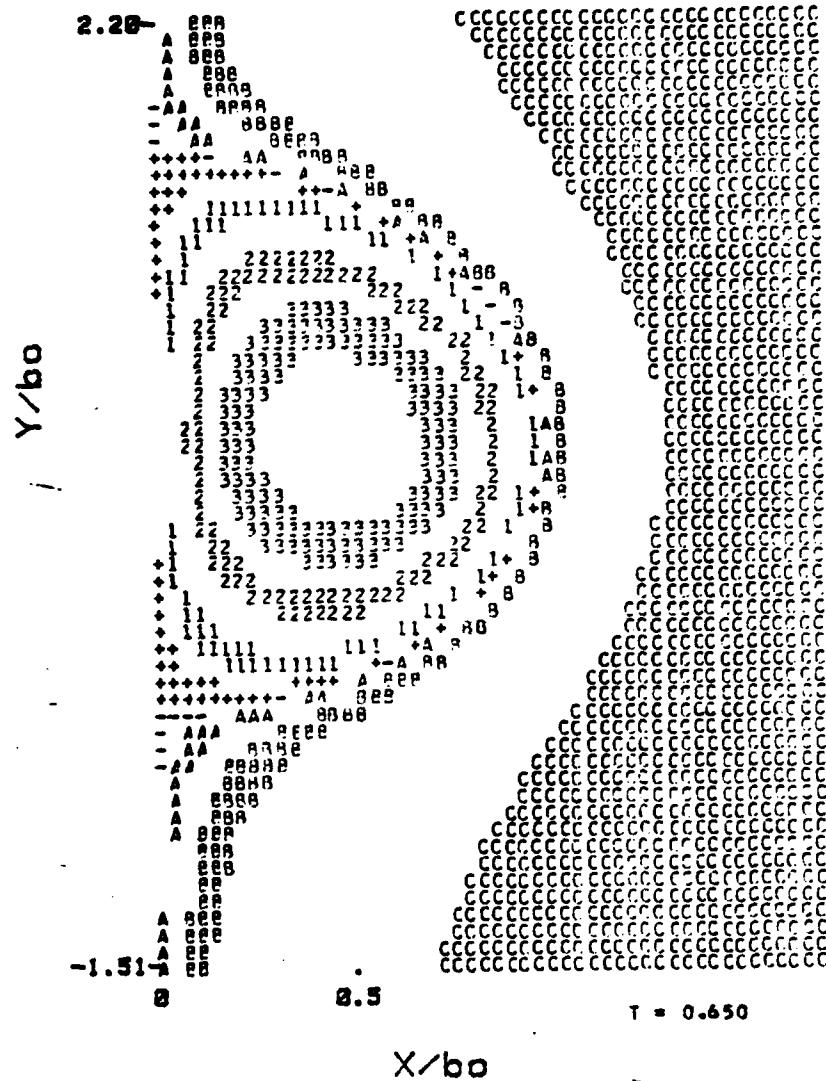
Figure 44. Streamlines of the Numerical Model for
SP = 0, H/b_0 = 0.60.
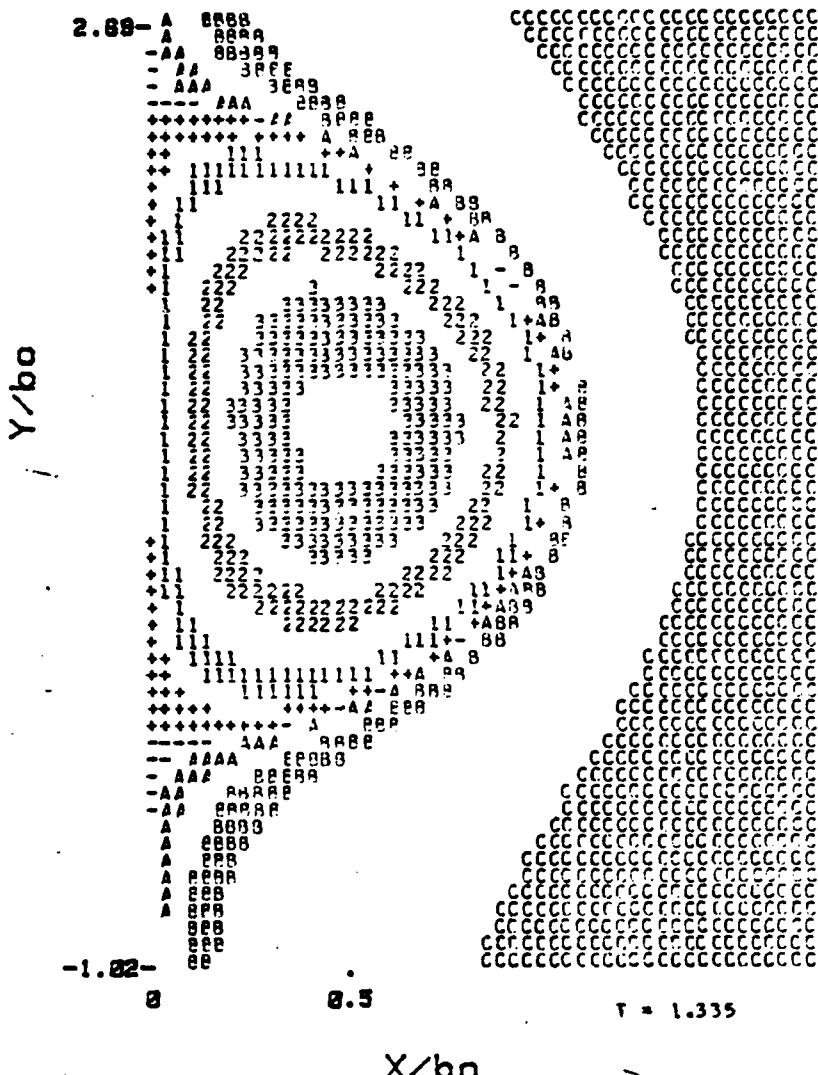
Figure 45.   Streamlines of the Numerical Model for
SP = 0, H/b_0 = 1.13.

108
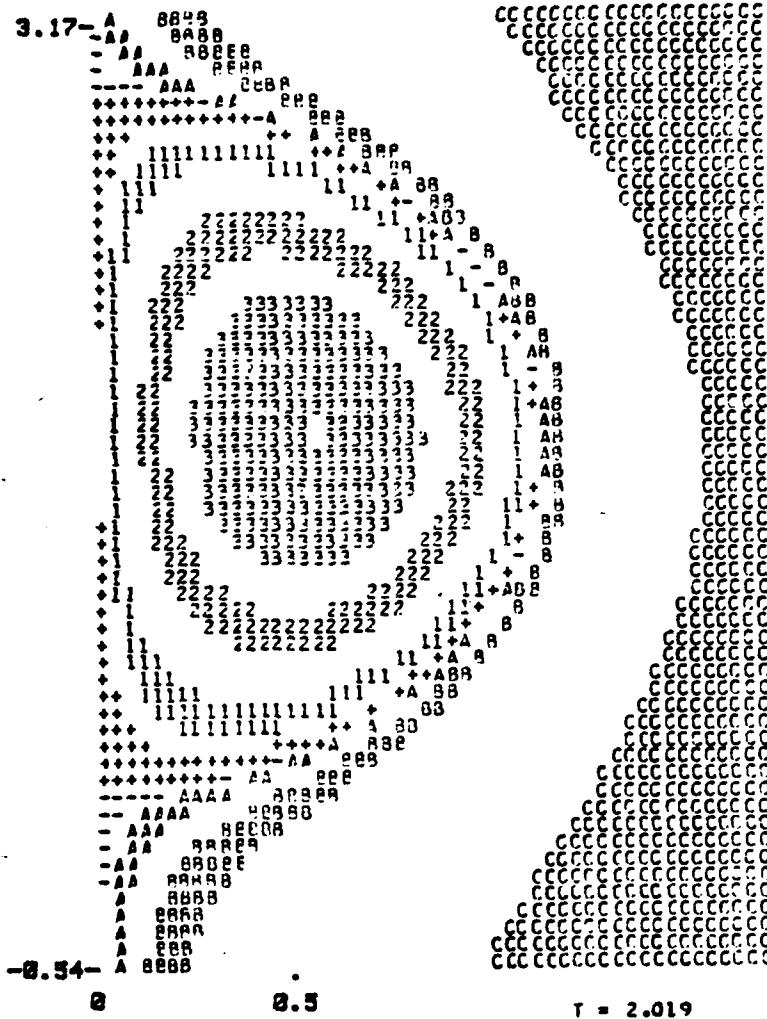
Figure 46.   Streamlines of the Numerical Model for
SP = 0, H/b_0 = 1.59.

SP = 0   H/bo = 2.01
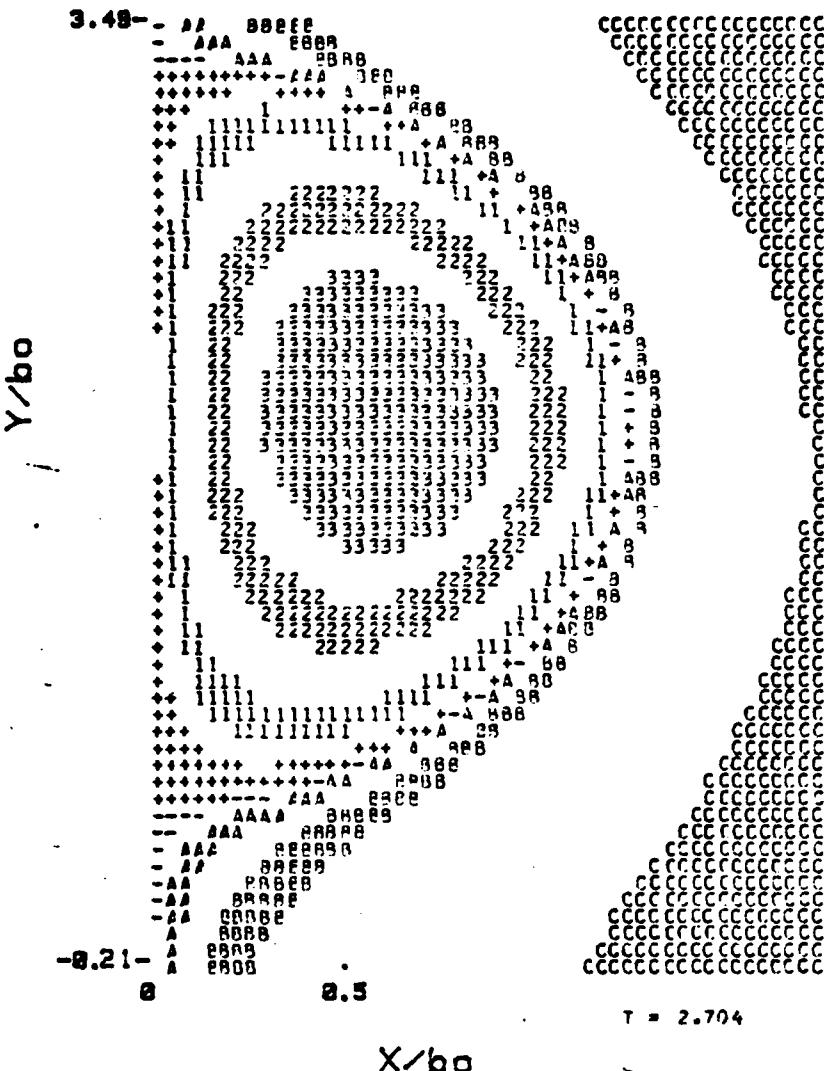
Figure 47. Streamlines of the Numerical Model for
SP = 0, H/b_0 = 2.01.

110
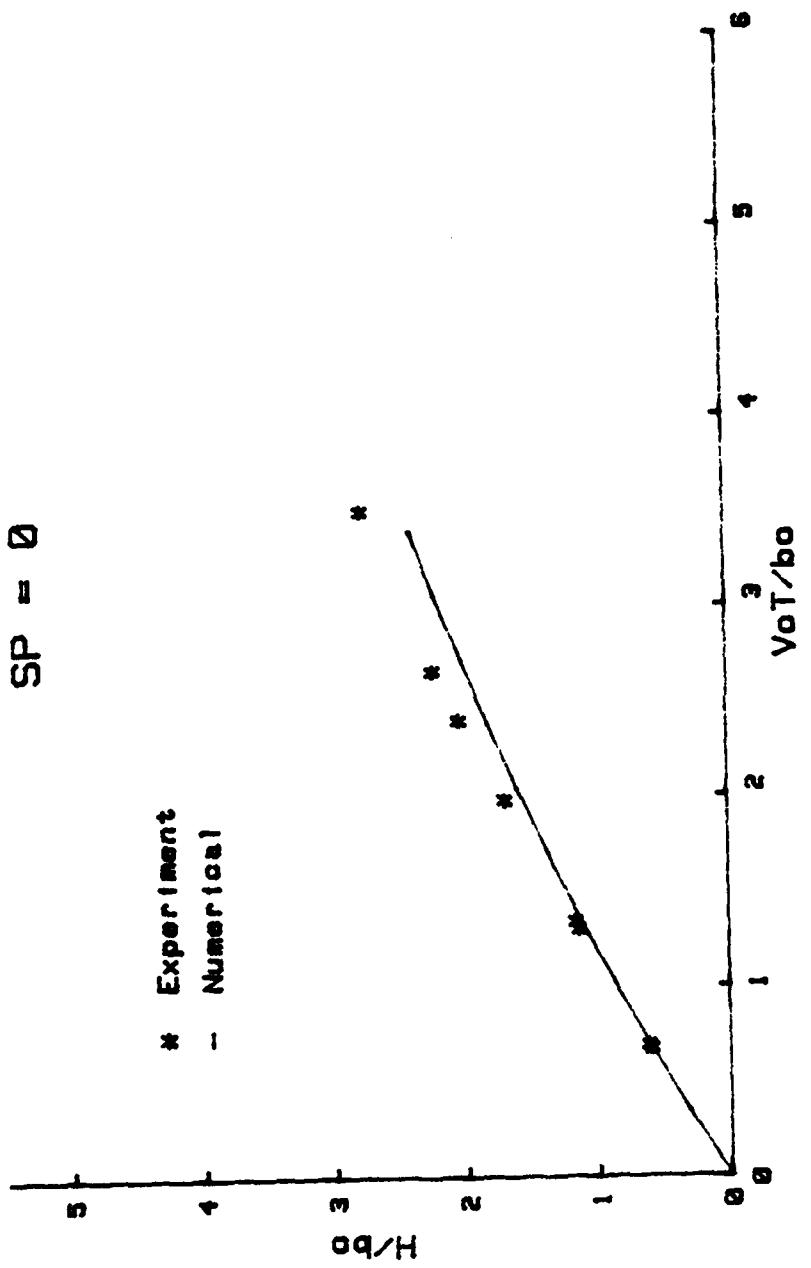
Figure 48. Comparison of Experimental Data with the Predictions of the Numerical Model for SP = 0.
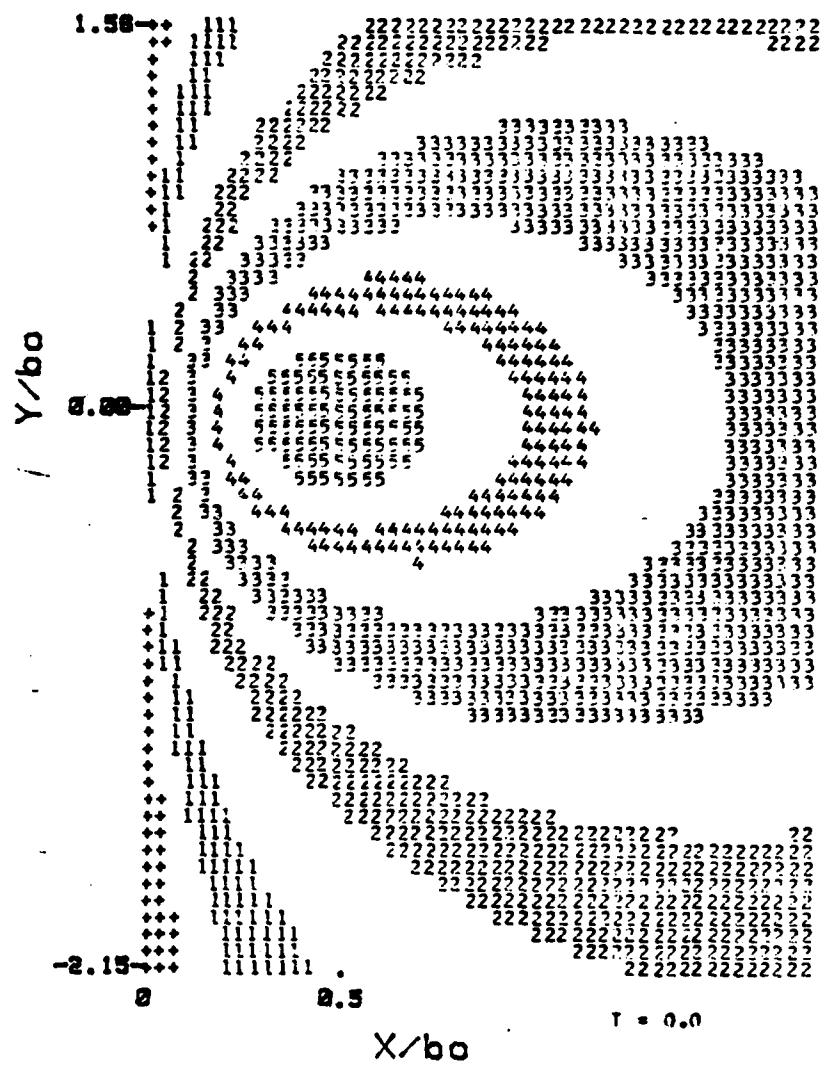
Figure 49.   Streamlines of the Numerical Model for
SP = 0.50, H/b = 0.
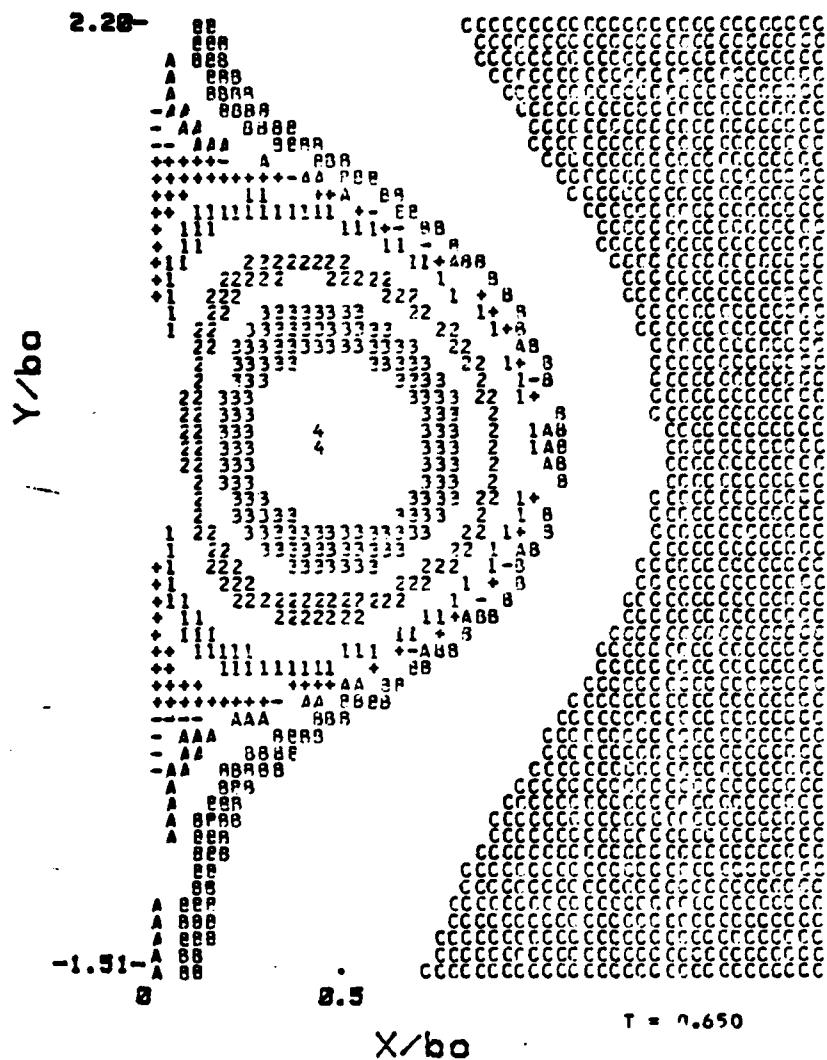
Figure 50. Streamlines of the Numerical Model for SP = 0.50, H/b_0 = 0.61.
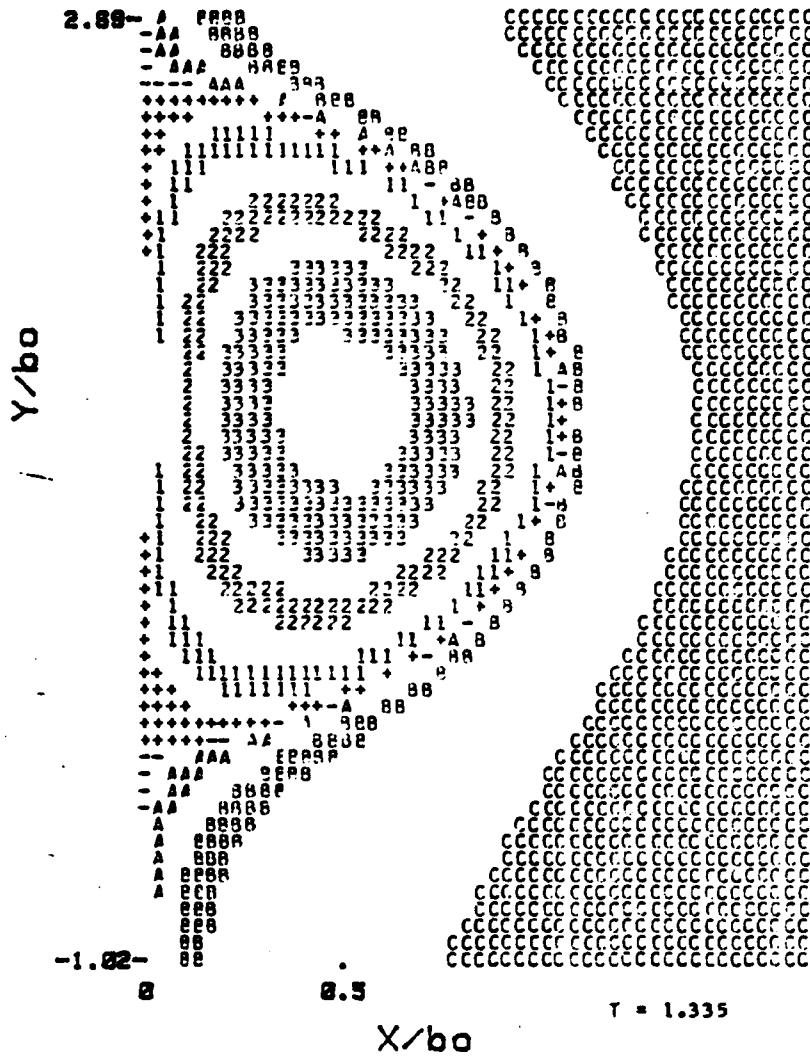
Figure 51. Streamlines of the Numerical Model for
SP = 0.50, H/b$_0$ = 1.17.

114

SP = 0.50   H/bo = 1.70
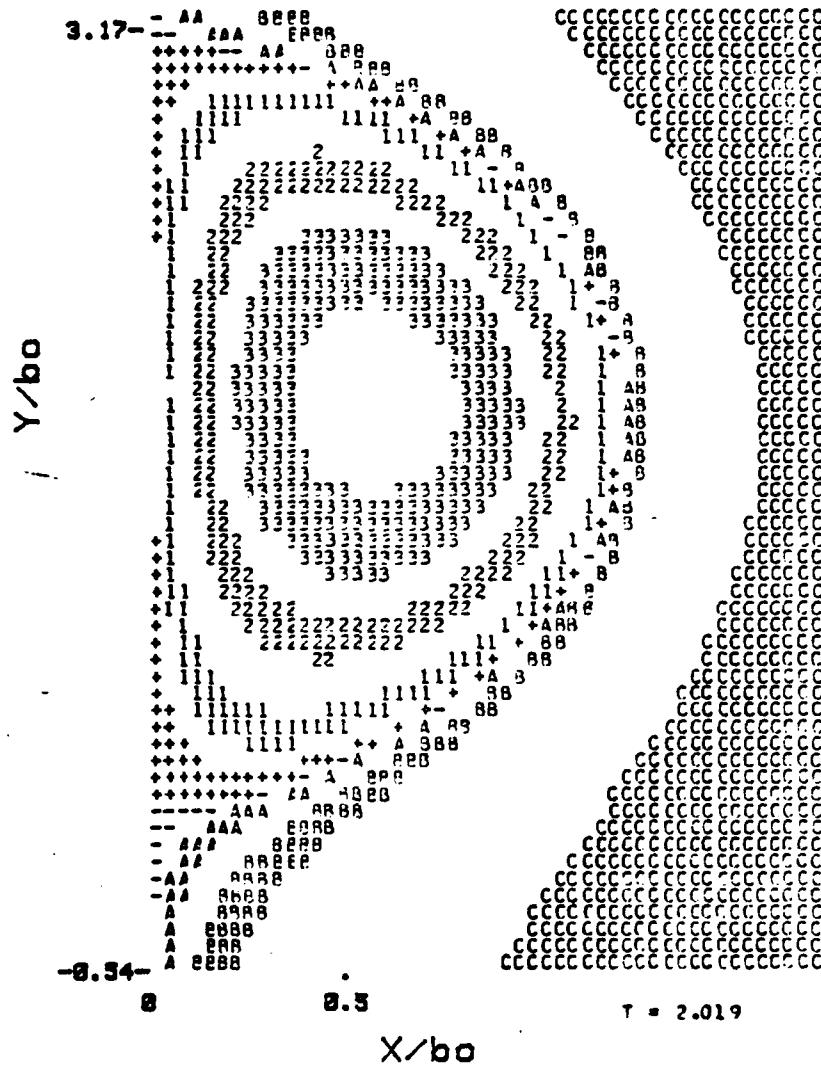
Figure 52. Streamlines of the Numerical Model for
            SP = 0.50, H/b$_o$ = 1.70.

115

SP = 0.50   H/bo = 2.22
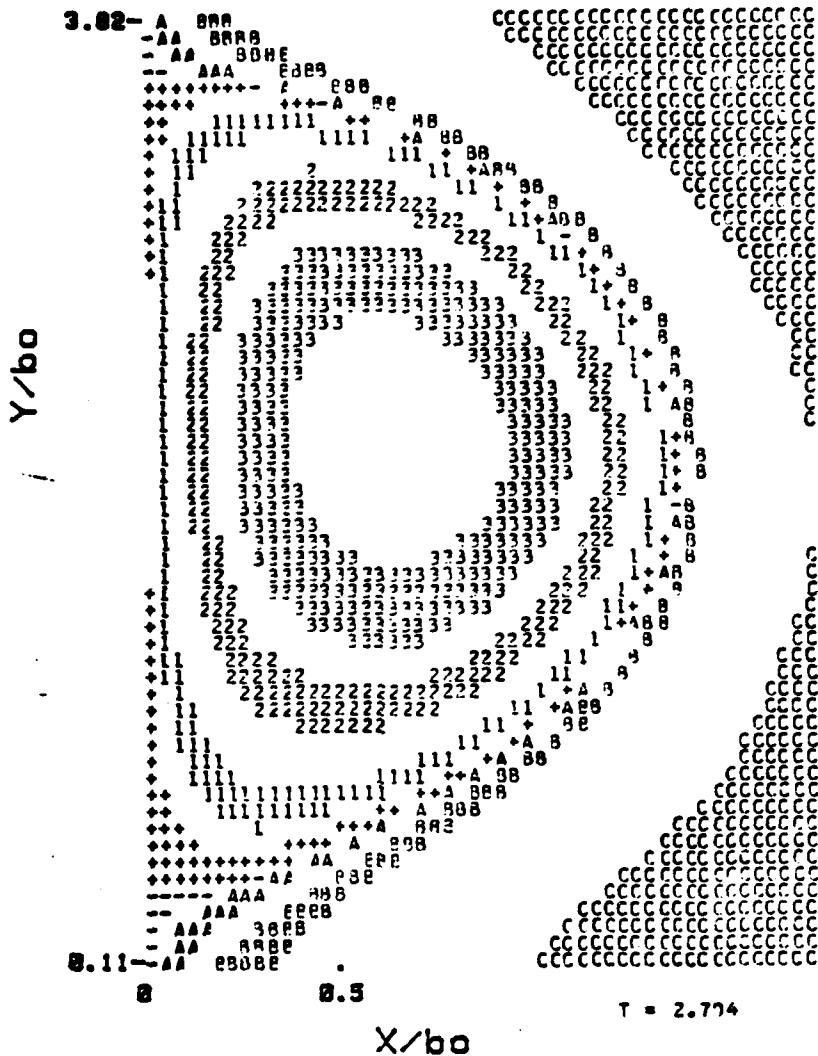
Figure 53.   Streamlines of the Numerical Model for
             SP = 0.50, H/b$_0$ = 2.22.

The comparison with Figs. 43 through 47 show that in the stratified case
the vortices do not split out laterally as much as in the unstratified
case. The reason for this is that the opposite-signed vorticity is
generated, as shown by numerical calculations, outside the lower right
and lower left sides of the recirculation cell. The effect of this
vorticity is to pull the vortices together and thus increase the velocity
of their upward migration. Had turbulent diffusion been present, the
reduction in circulation would have more than offset the effect of opposite-
signed vorticity, thereby slowing the rise of vortices. In laminar
vortices, however, the strength of the vortices changes very slowly and
the vortices accelerate upward in an amount closely related to the magni-
tude of stratification. The foregoing arguments, however qualitative,
point out once again the conflicting conclusions arrived at by various
workers (see Table I).

The experimental and calculated values are compared in Figs. 54 and
55 for SP = 0.50 and SP = 1.0, respectively. The correspondence between
the measured and calculated values is surprisingly good, partly because
of the fact that even the experimental values of H/b_o for the stratified
(SP = 0.50) and unstratified cases do not significantly differ (see Figs.
23 and 27). However, in the case of SP = 1.0 where the experimental data
for SP = 0 and SP = 1.0 show significant differences (see Figs. 23 and 27),
the predictions of the numerical calculation differ significantly from
the experimental data as seen from Fig. 55. As noted earlier, the strong
opposite-signed vorticity generated in this case accelerates the vortices
upward and yields larger H/b_o values. It is interesting to note that at
the early stages of the motion, where the effect of counter-signed
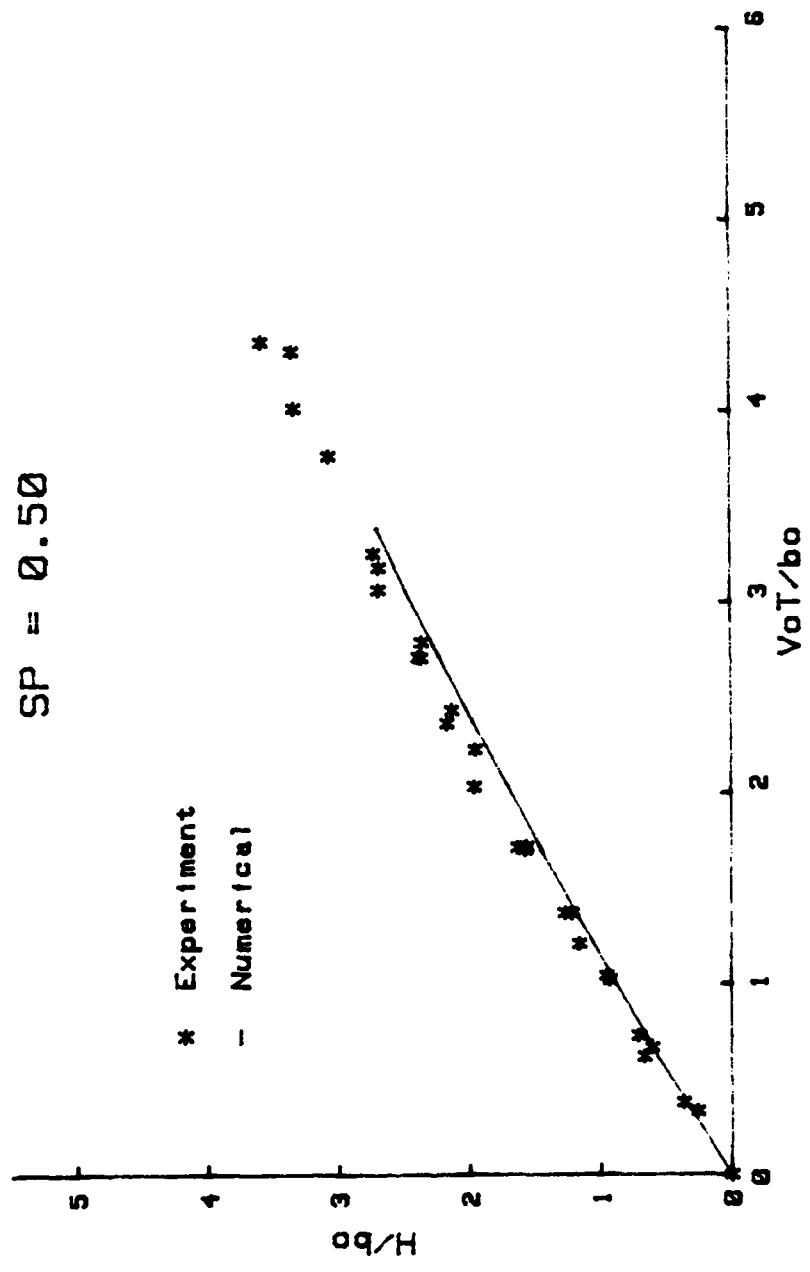
Figure 54. Comparison of Experimental Data with the Predictions of the Numerical Model for SP = 0.50.
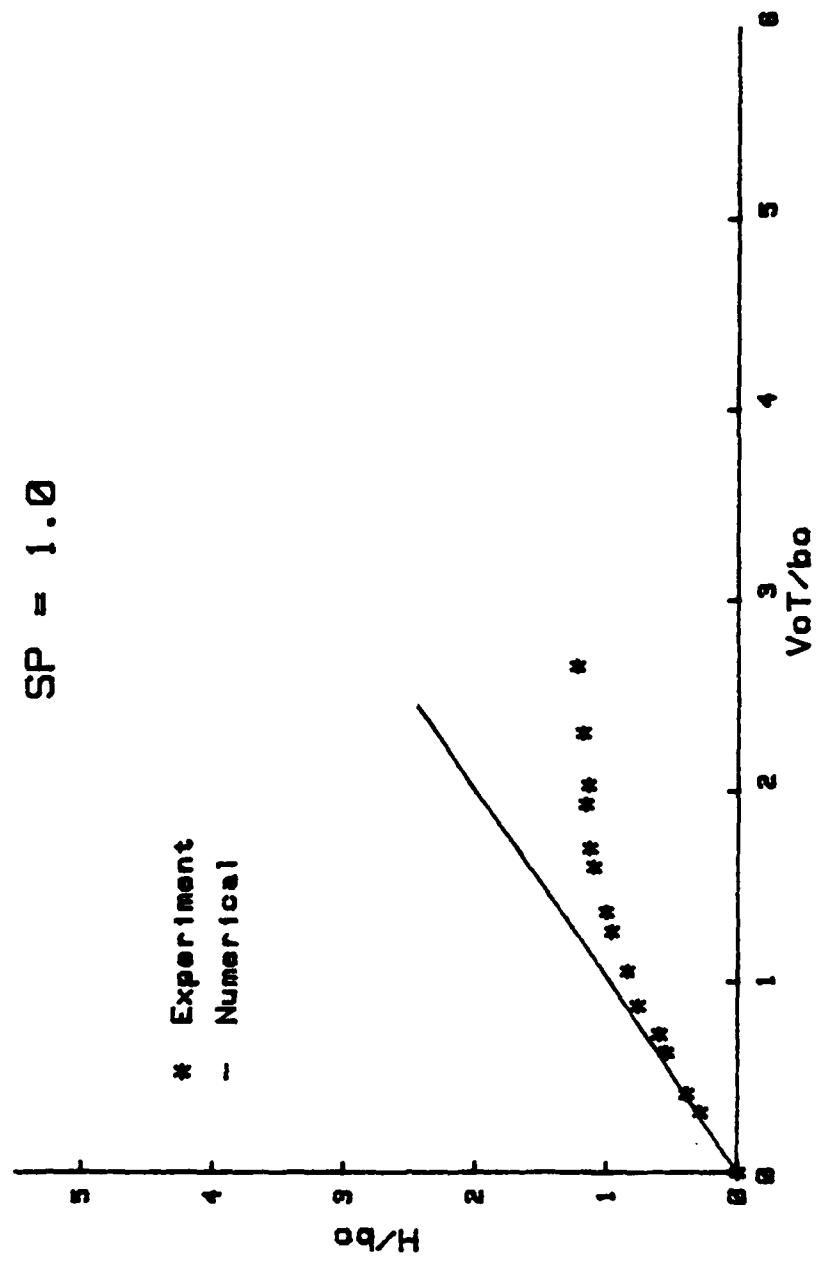
Figure 55. Comparison of Experimental Data with the Predictions of the Numerical Model for SP = 1.0.

119

vorticity is not yet evident, the slope of the numerical prediction is nearly identical to that of the experimental data.

It should be emphasized that the foregoing was only an exploratory numerical investigation of the evolution of a laminar vortex pair. It served to confirm the need for the development of a comprehensive numerical model which is not only true to the underlying physics of the phenomena but also devoid of floating parameters whose values are arbitrarily chosen (e.g., initial vorticity diffusion, r_0/b_0, mesh size, size of calculation domain, etc.). The results also show that turbulence plays an extremely important role in the diffusion of vorticity and thus in the entire life of vortices from their inception to their ultimate demise.

Even when such a comprehensive model is developed it does not now appear that it would be too easy to surmount the difficulties associated with the modeling of the consequences of the Crow instability, vortex breakdown, and the entrainment and detrainment of the recirculation cell. Of course it is not too surprising that such an investigation should require a better understanding of turbulence itself through measurements and calculations of vortical flows.

G. SCALE EFFECTS

The results obtained with Delta wings have shown that the Reynolds number does not play a measurable role in the evolution of the turbulent trailing vortices. Thus, the data presented herein may be used for larger Delta wings provided that the background turbulence is negligible and the stratification is linear. Additional experiments are needed to delineate the effects of the background turbulence and the nonlinearity of the stratification. Such experiments are currently underway.

As to the streamlined body, the Reynolds number of the model is about 800 times smaller than that of a full scale vehicle. In spite of the rather large difference between the Reynolds numbers of the model and the prototype, however, the data presented herein are thought to be valid for the full scale vehicle provided that the background turbulence is negligible and the stratification is nearly linear. This assertion is based on the fact that the boundary layers on the model and its lifting surfaces were rendered turbulent with tripping wires and sand strips. Obviously, this does not preclude the need for full scale experiments for a number of reasons, the most important ones being the effect of background turbulence and the nonlinearity of the stratification.

One must bare in mind that there are fundamental differences between the demise mechanisms of trailing vortices generated by a Delta wing or rectangular wing (in the absence of any body-proximity effects) and those generated by a vehicle and its control surfaces. The demise of the vortices emanating from a Delta wing is primarily due to sinusoidal instability and turbulent diffusion. Thus, the lifespan of these vortices may be strongly affected by the background turbulence [Ref. 55]. The demise of the trailing vortices generated by the lifting surfaces of an axisymmetric body is primarily due to the vortex breakdown. In fact, the data presented herein show that the vortex breakdown (brought about by the body-proximity effects) severely limits the rise of the trailing vortices. The comparison of the data obtained with Delta wings and the streamlined body show that the maximum rise of the cores of the vortices generated by the sail planes of the streamlined body is about 2.5 times smaller than that of the Delta wings. Thus, in the case of vehicles one would be interested not only with the effect of background turbulence and the type of stratification but also with the

121

effect of Reynolds number on the intensity and generation of vortex breakdown or cascade of vortex breakdowns. The previous studies [Refs. 6-8] have shown that the occurrence of vortex breakdown is not materially affected by the Reynolds number (and Mach number) provided that the vortex is initially turbulent. In other words, the background turbulence is not of major importance in the occurrence of vortex breakdown, at least when the breakdown takes place on a single vortex. One cannot ignore the fact that events such as vortex breakdown do not occur simultaneously and symmetrically on a pair of trailing vortices. The mutual induction of vortices and the non-symmetrical occurrence of cascades of vortex breakdown on each vortex may enhance the role played by the background turbulence. Furthermore, the amount of circulation remaining in the recirculation cell following the breakdown may be affected by the background turbulence. The best estimate, at present, is that the intensity of the adverse pressure gradient (i.e., the mean flow field about the body) is fundamentally responsible for the occurrence and the position of the vortex breakdown. The subsequent demise of the vortices may be affected by the background turbulence, mutual induction, and the type of stratification.

It is evident from the foregoing that it would be very desriable to conduct a series of field experiments. In doing so, the data presented herein should serve well for their planning and for the interpretation of the environmental effects on the evolution of the trailing vortices and vortex rings. Clearly, meaningful full scale experiments require, for their interpretation, not only the measurement of the characteristics of vortices but also the quantification of the prevailing environmental conditions.

In summary, the evolution of vortices shed by a body and its control surfaces in a natural environment with non-isotropic background turbulence, currents, shear, wave motion, and stratification is such a complex time-dependent phenomenon which demands quantitative analysis, ingenious experiments, and qualitative descriptions for the purpose of explaining the underlying causes of the physical effects and providing a model by which design and operation can be safely and reasonably performed. Ultimately, the flow field and the vortex motion about full scale vehicles will not be quantified solely due to the knowledge gained through the study of well-posed problems and controlled laboratory experiments alone but rather through the interaction and reasoble marriage of the two approaches: basic studies and full scale experiments.

V. CONCLUSIONS

The investigation reported herein warranted the following conclusions:

1. In unstratified water, the trailing vortices generated by a lifting surface moving at a negative angle of attack rise with time and dissipate ultimately at a finite height (about $H/b_0 = 4.6$). The top of the recirculation cell rises to a normalized height of about $H/b_0 = 6$. This height should not be confused with the height to which the dye in the trailing vortex diffuses after a long period of time.

2. The rate of rise of vortices is always smaller than that predicted theoretically through the use of the inviscid line vortices.

3. The rise of the vortices was shown to be governed by the dimensionless parameters $V_0 t/b_0$, D/b_0, and Nb_0/V_0 (the stratification parameter) for linearly stratified fluids with no background turbulence.

4. The effect of stratification is to reduce the rate of rise of vortices and the maximum height attained by them. In fact, the larger the stratification (i.e., Nb_0/V_0), the smaller the maximum height attained by the vortices.

5. The ultimate demise of the vortices generated by Delta wings is observed to be brought about by sinusoidal instability and turbulent diffusion. The demise of the vortices generated by the lifting surfaces of an axisymmetric body is brought about by a cascade of vortex breakdowns and the turbulent diffusion.

6. The vortices subjected to vortex breakdown rise to a maximum height which is about 2.5 times smaller than those subjected to sinusoidal instability.

7. The results have shown that the body-proximity effects on trailing vortices are very strong and always give rise to vortex breakdown.

8. Various approximate analytical models were considered and all were deemed to be inadequate. None of the approximate models yielded a finite rise height in unstratified water and none considered the effects of the demise mechanisms.

9. An exploratory numerical analysis based on two-dimensional, laminar unsteady flow assumptions was carried out. The predictions of the model were in good agreement in the unstratified case. In the stratified case, the generation of the counter-signed vorticity decreased the vortex span and increased the velocity of the upward migration of the vortices. The predictions of the model could be made more realistic through the inclusion of at least the effects of turbulence and possibly those of other demise mechanisms.

10. The scale effects were examined in as much detail as possible. It is concluded that the scale effects under similar conditions (linear stratification and no background turbulence) are insignificant. However, the demise of the vortices undergoing sinusoidal instability may be strongly affected by the background turbulence. The body-proximity effects and the adverse pressure gradient, rather than the background turbulence, are thought to govern the occurrence and the position of the vortex breakdowns. However, the ultimate demise of the vortices subjected to vortex breakdown may be affected by the background turbulence, in addition to other laboratory and environmental factors such as non-linear stratification, currents, waves, wave-current interactions, wakes of other bodies, shear, etc.

125

LIST OF REFERENCES

1. Olsen, J. H., Goldburg, A. and Rogers, M., "Aircraft Wake Turbulence and its Detection," Plenum Press, New York, 1971.

2. Hallock, J. N. (Ed.), "Proceedings of the Aircraft Wake Vortices Conference," National Technical Information Services, Springfield, VA 22161, 1977.

3. Lanchester, F. W., Aerodynamics, 2nd Ed., London, Constable and Company Ltd., 1909.

4. Pradtl, L., "Tragflugeltheorie," I Metl. Gottingen Nachiuehten, 1918.

5. Betz, A., "Behavior of Vortex Systems," NACA TM 713 (translation from ZAMM, Vol. XII.3, 1932).

6. Sarpkaya, T., "On Stationary and Travelling Vortex Breakdowns," Journal of Fluid Mechanics, Vol. 45, 1971, p. 545.

7. Sarpkaya, T., "Effect of Adverse Pressure Gradient on Vortex Breakdown," AIAA Journal, Vol. 12, 1974, p. 602.

8. Escudier, M. P. and Zehnder, N., "Vortex-Flow Regimes," Journal of Fluid Mechanics, Vol. 115, 1982, p. 105.

9. Gersten, K., "Calculation of Nonlinear Aerodynamic Stability Derivatives of Aeroplanes," AGARD Rep. 342, April 1961.

10. Garner, H. C. and Lehrian, M., "Nonlinear Theory of Steady Forces on Wings with Leading-Edge Flow Separation," Aeronautical Research Council, R & M 3375, Feb. 1963.

11. Pullin, D. K., "Calculations of the Steady Conical Flow Past a Yawed Slender Delta Wing with Leading Edge Separation," Imperial College of Science and Technology, London, Aero Report 72-17, July 1972.

12. Jones, I. P., "Flow Separation from Yawed Delta Wings," Computers and Fluids, Vol. 3, 1975, pp. 155-177.

13. Belotserkovskii, S. M., "Calculation of the Flow Around Wings of Arbitrary Planforms Over a Wide Range of Angles of Attack," NASA TT F-12, 391, 1969.

14. Rehbach, C., "Calculation of Flow Around Zero-Thickness Wings with Evolute Vortex Sheets," NASA TT F-15, 183, 1973.

15. Rehbach, C., "Numerical Investigation of Vortex Sheets Issuing from Separation Line Near the Leading Edge," NASA TT F-15, 530, 1974.

16. Kandil, O. A., "Asymmetric Flow Past Wings at Large Incidence with Small Amplitude Oscillations," AIAA Paper No. 78-1336, August 1978.

17. Kandil, O.A., "State of the Art of Nonlinear Discrete-Vortex Methods for Steady and Unsteady High Angle of Attack Aerodynamics," AGARD CP-247, January 1979.

18. Belotserkovskii, S. M. and Nisht, M. I., "Nonstationary Nonlinear Theory of a Thin Wing of Arbitrary Planform," Mekhanika Zhidkosti Gasa, No. 4, 1974, pp. 100-108.

19. Rom, J., Almosnino, D. and Zorea, C., "Calculation of the Nonlinear Aerodynamic Coefficients of Wings of Various Shapes and their Wakes Including Canard Configurations," 11th Congress of ICAS, Lisbon, Portugal, September 1978.

20. Kandil, O. A., Mook, D. T. and Nayfeh, A. H., "New Convergence Criteria for the Vortex Lattice Models of the Leading-Edge Separation," NASA SP-405, No. 16, May 1976, pp. 285-300.

21. Kelly, S. G., "A Systematic Investigation of the Parameters Affecting the Accuracy of the Vortex-Lattice Method," M. S. Thesis, VPI, Blacksburg, VA, May 1977.

22. Weber, J. A., Brune, G. W., Johnson, F. T., Lu, P., and Rubbert, P. E., "Three-Dimensional Solution of Flows Over Wings with Leading Edge Vortex Separation," AIAA Journal, Vol. 14, 1976, pp. 519-525.

23. Johnson, F. T., Lu, P., Brune, G. W., Weber, J. A., and Rubbert, P. E., "An Improved Method for the Prediction of Completely Three-Dimensional Aerodynamic Load Distributions on Configurations with Leading-Edge Separation," AIAA Paper No. 76-417, 1976.

24. Kuhlman, J. M., "Analytical Studies of Separated Vortex Flow on Highly Swept Wings," NASA CR 3022, Nov. 1978.

25. Reddy, C. S., "Theoretical Study of Aerodynamic Characteristics of Wings Having Vortex Flow," NASA CR 159184, Nov. 1979.

26. Polhamus, E. C., "Technical Evaluation Report on the FDPS on High Angle of Attack Aerodynamics," AGARD AR-145, August 1979.

27. Kandil, O. A., Chu, L. C., and Yates, Jr., E. C., "Hybrid Vortex Method for Lifting Surfaces with Free Vortex Flow," AIAA Paper No. 80-0070, January 1980.

28. Chu, L. C., "A Nonlinear Hybrid-Vortex Method for Wings with Side-Edge Separation," M. S. Thesis, Old Dominion University, Norfolk, VA, 1981.

29. Kaden, H., "Auswicklung einer imstabilen Unstetigkeitsflache," Ingenieur Archiv, Vol. II, 1931, pp. 140-168.

30. Moore, D. W. and Saffman, P. G., "The Motion of a Vortex Filament with Axial Flow," Pil. Trans. Royal Soc., London, Vol. 272, 1972.

31. Brown, C. E. and Michael, W. H., "Effect of Leading Edge Separation on the Life of a Delta Wing," Journal of Aeronautical Sciences, Vol. 31, Oct. 1954, pp. 690-694.

32. Mangler, K. W. and Smith, J. H. B., "Calculation of the Flow Past Slender Delta Wings with Leading Edge Separation," RAE Report 2593, May 1957, Royal Aircraft Establishment, Farnsborough, England.

33. Smith, J. H. B., "Improved Calculations of Leading-Edge Separation from Slender Delta Wings," RAE Report 66070, March 1965, Royal Aircraft Establishment, Farnsborough, England.

34. Moore, D. W., "A Numerical Study of the Roll-up of a Finite Vortex Sheet," Journal of Fluid Mechanics, Vol. 63, 1974, pp. 225-235.

35. Fink, P. T. and Soh, W. K., "Calculation of Vortex Sheets in Unsteady Flow and Applications in Ship Hydrodynamics," 10th Symposium of Naval Hydrodynamics, Camb. MA., 1974.

36. Sarpkaya, T. and Shoaff, R. L., "Inviscid Model of Vortex Shedding by a Circular Cylinder," AIAA Journal, Vol- 17, No. 11, 1979, pp. 1193-1200.

37. Batchelor, G. K., "Axial Flow in Trailing Line Vortices," Journal of Fluid Mechanics, Vol. 20, 1964, pp. 645-658.

38. Spreiter, J. R. and Sacks, A. H., "The Rolling-up of the Trailing Vortex Sheet and its Effect on the Downwash Behind Wings," Journal of Aeronautical Sciences, Vol. 18, 1951, pp. 21-33.

39. Donaldson, C. duP., "A Brief Review of the Aircraft Trailing Vortex Problem," AFOSR-TR-71-1910, May 1971.

40. Jordan, P., "Structure of Betz Vortex Cores," Journal of Aircraft, Vol. 10, 1973, pp. 691-693.

41. Donaldson, C. duP., Snedeker, R. S., and Sullivan, R. D., "A Method of Calculating Aircraft Wake Velocity Profiles and Comparison with Full Scale Experimental Measurements," Journal of Aircraft, Vol. 11, 1974, pp. 547-555.

42. Tombach, I., "Observations of Atmospheric Effects of Vortex Wake Behavior," Journal of Aircraft, Vol. 10, 1973, pp. 641-647.

43. Burnham, D. C., Hallock, J. N., Tombach, I. H., Brashears, M. R., and Barber, M. R., "Ground Based Measurements of a B-747 Aircraft in Various Configurations," U. S. Dept. of Transportation Report FAA-RD-78-146, December 1978.

44. Hecht, A. M., Blanin, A. J., Hirsh, J. E., and Snedeker, R. S., "Turbulent Vortices in Stratified Fluids," _AIAA Journal_, Vol. 18, 1979, pp. 738-746.

45. Maxworthy, T., "The Structure and Stability of Vortex Rings," _Journal of Fluid Mechanics_, Vol. 51, 1972, pp. 15-32.

46. Barker, S. J. and Crow, S. C., "The Motion of a Two-Dimensional Vortex Pair in Ground Effect," _Journal of Fluid Mechanics_, Vol. 82, 1977, pp. 659-671.

47. Tomassian, J. D., "The Motion of a Vortex Pair in a Stratified Medium," Ph. D. Thesis, UCLA, June 1979.

48. Tulin, M. P. and Schwartz, J., "The Motion of Turbulent Vortex Pairs in Homogeneous and Density Stratified Media," Hydronautics Inc., Technical Report No. 231-15, AD-723-184, 1971.

49. Saffman, P. G., "The Motion of a Vortex Pair in Stratified Atmosphere," _Studies in Applied Mathematics_, Vol. II, No. 2, June 1972, pp. 107-119.

50. Scorer, R. S. and Davenport, L. J., "Contrails and Aircraft Downwash," _Journal of Fluid Mechanics_, Vol. 43, 1979, pp. 451-464.

51. Crow, S. C., "Motion of Vortex Pair in a Stably Stratified Fluid," Poseidon Research Report No. 1, May 1974.

52. Widnall, S. E., "The Structure and Dynamics of Vortex Filaments," _Annual Review of Fluid Mechanics_, Vol. 7, 1975, pp. 141-165.

53. Hecht, A. M., Bilanin, A. J., Hirsh, J. E., "Turbulent Trailing Vortices in Stratified Fluids," _AIAA Journal_, Vol. 19, 1981, pp. 691-698.

54. Crow, S. C., "Stability Theory for a Pair of Trailing Vortices," _AIAA Journal_, Vol. 8, 1980, pp. 2172-2179.

55. Crow, S. C. and Bate, E. R. Jr., "Lifespan of Trailing Vortices in a Turbulent Atmosphere," _Journal of Aircraft_, Vol. 13, 1975, pp. 476-482.

56. Chevalier, H., "Flight Test Studies of the Formation and Dissipation of Trailing Vortices," _Journal of Aircraft_, Vol. 10, 1973, pp. 14-18.

57. Costen, R. C., "Drift of Buoyant Wing-Tip Vortices," _Journal of Aircraft_, Vol. 9, June 1972, pp. 406-412.

58. Kuhn, G. D. and Nielsen, J. N., "Analytical Studies of Aircraft Trailing Vortices," AIAA Paper 72-42, 1972.

59. Tombach, I. H., "Transport of a Vortex Wake in a Stably Stratified Atmosphere," Aircraft Wake Turbulence and its Detection, Edited by J. H. Olsen et al., Plenum Press, New York, 1971, pp. 41-57.

60. Narain, J. P. and Uberoi, M. S., "The Motion of a Trailing Vortex Wake in a Stratified Medium," Atmospheric Environment, Vol. 8, 1974, pp. 459-473.

61. Elle, B. J., "An Investigation at Low Speed of the Flow near the Apex of Thin Delta Wings with Sharp Leading Edges," A.R.C. Reports and Memoranda No. 3176, January 1958.

62. Lamb, H. (Sir), Hydrodynamics, Dover Publications, New York (6th ed.), 1945, pp. 221-224.

APPENDIX A

RELATIONSHIP BETWEEN THE AMOUNT OF SALT
AND STRATIFICATION PARAMETER

The stratification parameter is defined as Nb_0/V_0 and is given by

$$\frac{N b_0}{V_0} = \frac{b_0}{V_0} \sqrt{\frac{g}{D} \frac{\Delta \rho}{\rho_0}} \qquad (A-1)$$

where:

N = the Brunt-Vaisala frequency and is defined by

$$N = \left(- \frac{g}{\Delta y} \frac{\Delta \rho}{\rho_0}\right)^{1/2} \qquad (A-2)$$

b_0 = the vortex core separation

g = 32.174 ft/s^2 is the gravitational acceleration

d = the layer thickness in inches

ρ_0 = the fresh water density

$\Delta \rho$ = the change in density between two layers

V_0 = the initial vortex rise velocity.

The ratio of the initial vortex-rise velocity to the model velocity was found to be constant for each model, independent of model velocity, i.e., V_0/U = Constant for a given model.

The brine-water density ρ_n in the n-th layer is related to the concentration C_n by

131

$$\rho_n = \rho_0(1 + 0.71C_n) \qquad \text{(A-3)}$$

where the salt concentration C is defined in general by the following equation as a function of the amount of salt added:

$$\frac{1}{C} = 1 + \frac{W_{Fr.water}}{W_{salt}} \qquad \text{(A-4)}$$

Thus, one has

$$\Delta \rho = \rho_n - \rho_{n-1} = 0.71 \, \rho_0(C_n - C_{n-1})$$

or

$$\frac{\Delta \rho}{\rho_0} = 0.71(C_n - C_{n-1}) \qquad \text{(A-5)}$$

and the Eq. (A-1) becomes,

$$\frac{Nb_0}{V_0} = \frac{b_0}{(V_0/U)U} \sqrt{\frac{0.71 \times g \times (C_n - C_{n-1})}{d}} \qquad \text{(A-6)}$$

Solving Eq. (A-6) with respect to $(C_n - C_{n-1})$ one has

$$C_n - C_{n-1} = (\frac{d}{0.71g}) \times [\frac{(V_0/U)U}{b_0}]^2 \times (\frac{Nb_0}{V_0})^2 \qquad \text{(A-7)}$$

where $n = 1,2,3,\dots$.

Because of the fact that the first layer normally is fresh water without salt, i.e., $C_0 = 0$, one has

132

$$C_1 = \left(\frac{d}{0.71\ g}\right)\ \left[\frac{(V_0/U)U}{b_0}\right]^2\ \left(\frac{Nb_0}{V_0}\right)^2$$

$$C_2 = C_1 + \left(\frac{d}{0.71\ g}\right)\ \left[\frac{(V_0/U)U}{b_0}\right]^2\ \left(\frac{Nb_0}{V_0}\right)^2$$

Hence

$$C_2 = 2C_1$$

$$\text{(A-8)}$$

$$C_n = nC_1$$

Also from Eq. (A-4) one obtains

$$W_{n,salt} = \frac{W_{Fr.water}}{\frac{1}{C_n} - 1} \qquad \text{(A-9)}$$

Combining Eqs. (A-7), (A-8), and (A-9), one has

$$W_{n,salt} = \frac{W_{Fr.water}}{h\left(\frac{d}{0.71\ g}\right) \times \left[\frac{(V_0/U)U}{b_0}\right]^2 \times \left(\frac{Nb_0}{V_0}\right)^2} - 1 \qquad \text{(A-10)}$$

Equation (A-10) gives the amount of salt that has to be added to the n-th layer for a given value of the stratification parameter Nb_0/V_0 and a given layer thickness $d \times W_{Fr.water}$ is the weight of fresh water that is included in layer of thickness D in the water basin, i.e.,

$$W_{Fr.water} = (36)(3)(d)(62.4) = 561.6\ d\ \text{lbs.}$$

133

where d is as previously described. Therefore

$$W_{n,salt} = \frac{561.6 \times d}{(\frac{nd}{12 \times 0.71\ g})[\frac{(V_o/U)U}{b_o}]^2(\frac{Nb_o}{V_o})^2 - 1} \qquad (A-11)$$

For example, for

$Nb_o/V_o = 0.5$, $d = 1"$, $U = 2.05$ ft/sec, and $V_o/U = 0.0391$

$W_{1,salt} = 0.01519$ lbs of salt.

Also, for

$Nb_o/V_o = 1.0$, $d = 1"$, $U = 2.05$ ft/sec, and $V_o/U = 0.0391$

$W_{1,salt} = 0.0607$ lbs of salt, and

$W_{2,salt} = 0.1215$ lbs of salt.

134

APPENDIX B

TEMPERATURE STRATIFICATION EFFECTS

A nonuniform temperature stratification which might result from the temperature difference between the ambient air and the water in the basin could have an adverse effect on the salt stratification and on the accuracy of the data obtained. To this end, an analysis has been carried out by assuming that the basin is full with water at 50 degree temperature, the basin fills at a much faster rate than the rate of heat diffusion, there is no heat transfer between the bottom and side walls of the basin, and the air temperature at the air-water interface is 65 degrees.

The governing equation is the one-dimensional unsteady conduction equation, given by

$$\frac{\partial T}{\partial t} = \alpha_t \frac{\partial^2 T}{\partial x^2} \qquad (B-1)$$

The initial and the boundary conditions are

$$T(x,0) = 50° F = T_0 \qquad (B-2)$$

$$T(L,t) = 65° F = T_\infty \qquad (B-3)$$

$$\frac{\partial T(0,t)}{\partial x} = 0 \qquad (B-4)$$

Letting $\theta = T - T_\infty$, one has

$$\frac{\partial \theta}{\partial t} = \alpha_t \frac{\partial^2 \theta}{\partial x^2} \qquad (B-4)$$

135

and

$$\theta(x,0) = \theta_0 = -15° F \qquad\qquad (B-5)$$

$$\theta(L,t) = 0 \qquad\qquad (B-6)$$

$$\frac{\partial\theta(0,t)}{\partial x} = 0 \qquad\qquad (B-7)$$

A straightforward application of the technique of separation of variables yields

$$T(x,t) = T_\infty + 2\,\theta_0 \sum_{n=0}^{\infty} \frac{(-1)^n}{\lambda_n L}\, e^{-\alpha_t \lambda_n^2 t} \cos \lambda_n x \qquad\qquad (B-8)$$

where

$$\lambda_n = \frac{(2n+1)\pi}{2L} \qquad\qquad (B-9)$$

For the case under consideration, one has

$$t = 4 \text{ hrs}, \quad L = 45 \text{ inches}, \quad \text{and} \quad \alpha_t = 0.00022 \text{ in}^2/\text{sec}$$

The numerical results have shown that the temperature distribution in the basin is affected to a depth of only seven inches after a period of 4 hours. The small temperature gradient between the said depth and the free surface gives rise to a negligible density gradient in all but the regions very close to the free surface, a region which is not of special

136

interest. It is of importance to note that the numerical values used
in the calculations correspond to those encountered in coldest months
of the year. For the majority of the test runs the water temperature
was about 63 degrees compared to the air temperature of 67 degrees. Thus,
the effect of heat conduction on density stratification was several orders
of magnitude smaller than that calculated.

As to the effect of side walls, a lateral temperature gradient may
develop along the side wall since the thermal conductivity of aluminum
is much larger than that of water. However, such a temperature gradient
will have very little or no effect on the vertical gradient and hence on
the motion of trailing vortices. Experiments with dye particles falling
slowly in a vertical plane, extending from wall to wall, have not re-
vealed any natural convection along the side walls. Thus, it is concluded
that the heat transfer in any direction in the basin did not play an
important enough role to affect the results.

APPENDIX C - DELTA 1 TABULATED DATA

AR = 1.47   VERTEX = 39.5 DEG   B = 7.9 inches

bo = 5.58 inches   ALPHA = 12 DEG   Vo/U = 0.0391

U = 3.09 ft/s   U = 2.20 ft/s   U = 1.58 ft/s
D/bo = 2.15   D/bo = 2.15   D/bo = 2.15
Nbo/Vo = 0   Nbo/Vo = 0   Nbo/Vo = 0

VoT/bo	H/bo	VoT/bo	H/bo	VoT/bo	H/bo
0.00	0.00	0.00	0.00	0.00	0.00
.48	.45	.33	.32	.28	.19
1.23	1.02	.68	.54	.49	.41
1.82	1.35	.91	.75	.74	.64
2.58	1.52	1.19	.98	.97	.82
3.11	1.52	1.48	1.14	1.19	1.00
3.63	1.38	1.77	1.35	1.48	1.11
		2.24	1.52	1.85	1.23
		2.63	1.59	1.91	1.39
		3.04	1.59	2.15	1.46

U = 2.20 ft/s   U = 4.04 ft/s   U = 4.04 ft/s
D/bo = 2.15   D/bo = 2.15   D/bo = 2.70
Nbo/Vo = 0   Nbo/Vo = 0   Nbo/Vo = 0

VoT/bo	H/bo	VoT/bo	H/bo	VoT/bo	H/bo
0.00	0.00	0.00	0.00	0.00	0.00
.38	.38	.60	.54	.88	.71
.72	.58	1.17	.98	1.48	1.22
1.24	1.00	1.74	1.31	2.02	1.61
1.58	1.18	2.33	1.46	2.87	1.98
		2.89	1.52	3.51	2.10
		3.43	1.46		
		4.05	1.29		

AR = 1.47   VERTEX = 39.5 DEG   B = 7.9 inches

bo = 5.58 inches   ALPHA = 12 DEG   Vo/U = 0.0391

U = 4.04 ft/s		U = 3.08 ft/s	
D/bo = 2.70		D/bo = 3.24	
Nbo/Vo = 0		Nbo/Vo = 0	
VoT/bo	H/bo	VoT/bo	H/bo
0.00	0.00	0.00	0.00
.88	.71	.44	.47
1.48	1.22	.83	.75
2.02	1.61	1.23	1.11
2.67	1.98	1.80	1.46
3.51	2.18	2.04	1.76
		2.48	2.00
		2.87	2.33
		3.32	2.51
		3.78	2.55

U = 4.04 ft/s		U = 2.20 ft/s	
D/bo = 3.24		D/bo = 3.24	
Nbo/Vo = 0		Nbo/Vo = 0	
VoT/bo	H/bo	VoT/bo	H/bo
0.00	0.00	0.00	0.00
.57	.58	.38	.38
1.14	1.02	.60	.54
1.64	1.47	.91	.79
2.16	1.88	1.22	1.07
2.68	2.20	1.54	1.33
3.22	2.44	1.85	1.54
3.76	2.61	2.15	1.81
4.30	2.61	2.47	2.03
4.86	2.51	2.79	2.25

AR = 1.47   VERTEX = 39.5 DEG   B = 7.9 inches

bo = 5.58 inches   ALPHA = 12 DEG   Vo/U = 0.0391

U = 4.04 ft/s Vo = 0.16 ft/s Nbo/Vo = 0		U = 4.04 ft/s Vo = 0.16 ft/s Nbo/Vo = 0		U = 3.09 ft/s Vo = 0.12 ft/s Nbo/Vo = 0	
VoT/bo	H/bo	VoT/bo	H/bo	VoT/bo	H/bo
0.00	0.00	0.00	0.00	0.00	0.00
.56	.52	.69	.62	.42	.41
1.15	1.07	1.34	1.16	.83	.82
1.72	1.52	1.98	1.69	1.24	1.20
2.31	1.99	2.68	2.23	1.87	1.61
2.89	2.49	3.50	2.76	2.18	2.01
3.45	2.89			2.54	2.40
3.99	3.32			2.99	2.74
4.55	3.68			3.43	3.18
5.10	3.99			4.10	3.47

U = 3.09 ft/s Vo = 0.12 ft/s Nbo/Vo = 0		U = 3.56 ft/s Vo = 0.14 ft/s Nbo/Vo = 0		U = 2.65 ft/s Vo = 0.10 ft/s Nbo/Vo = 0	
VoT/bo	H/bo	VoT/bo	H/bo	VoT/bo	H/bo
0.00	0.00	0.00	0.00	0.00	0.00
.82	.62	.50	.52	.40	.39
1.55	1.46	.99	.93	.82	.75
2.05	1.98	1.48	1.37	1.28	1.16
2.55	2.36	1.97	1.81	1.72	1.59
3.03	2.72	2.50	2.25	2.14	1.95
3.48	3.18	3.02	2.72	2.55	2.39
4.48	3.81	3.53	3.08	3.01	2.70
		4.09	3.38	3.50	3.08
		4.61	3.68	4.00	3.36

AR = 1.47   VERTEX = 39.5 DEG   B = 7.9 inches

bo = 5.58 inches   ALPHA = 12 DEG   Vo/U = 0.0391

U = 2.32 ft/s		U = 2.05 ft/s		U = 2.32 ft/s	
Vo = 0.09 ft/s		Vo = 0.09 ft/s		Vo = 0.09 ft/s	
Nbo/Vo = 0		Nbo/Vo = 0		Nbo/Vo = 0.50	
VoT/bo	H/bo	VoT/bo	H/bo	VoT/bo	H/bo
0.00	0.00	0.00	0.00	0.00	0.00
.66	.66	.46	.48	.33	.26
1.26	1.22	.95	.91	.67	.61
1.87	1.83	1.36	1.29	1.02	.92
2.09	1.95	1.77	1.63	1.37	1.21
2.88	2.38	2.12	1.93	1.72	1.63
3.05	2.70	2.45	2.28	2.44	2.13
3.52	3.12	2.83	2.46	2.79	2.35
4.23	3.32	3.19	2.72	3.19	2.68
4.53	3.52	3.51	2.94		

U = 2.32 ft/s		U = 4.04 ft/s		U = 2.32 ft/s	
Vo = 0.09 ft/s		Vo = 0.15 ft/s		Vo = 0.09 ft/s	
Nbo/Vo = 0		Nbo/Vo = 0.375		Nbo/Vo = 0.50	
VoT/bo	H/bo	VoT/bo	H/bo	VoT/bo	H/bo
0.00	0.00	0.00	0.00	0.00	0.00
.57	.48	.57	.54	.38	.37
1.02	1.00	1.17	1.02	.82	.66
1.49	1.38	1.81	1.54	1.04	.95
1.84	1.68	2.48	2.01	1.37	1.27
2.27	2.03	3.08	2.44	1.78	1.57
2.88	2.33	3.59	2.83	2.04	1.98
3.08	2.67	4.16	3.19	2.37	2.17
3.46	2.93	4.71	3.48	2.72	2.38
4.14	3.31	5.28	3.66	3.07	2.88
				4.02	3.32
				4.37	3.57

AR = 1.47   VERTEX = 39.5 DEG   B = 7.9 inches

bo = 5.58 inches   ALPHA = 12 DEG   Vo/U = 0.0391

U = 3.56 ft/s Vo = 0.14 ft/s Nbo/Vo = 0.50		U = 2.32 ft/s Vo = 0.09 ft/s Nbo/Vo = 0.75		U = 2.32 ft/s Vo = 0.09 ft/s Nbo/Vo = 1.0	
VoT/bo	H/bo	VoT/bo	H/bo	VoT/bo	H/bo
0.00	0.00	0.00	0.00	0.00	0.00
.73	.71	.35	.30	.31	.28
1.21	1.16	.68	.63	.63	.54
1.72	1.56	1.01	.85	.87	.76
2.23	1.95	1.36	1.14	1.26	.96
2.71	2.36	1.69	1.41	1.60	1.10
3.26	2.72	2.05	1.61	1.93	1.16
3.77	3.08	2.40	1.70	2.30	1.18
4.32	3.34	2.75	2.01	2.65	1.23
		3.10	2.14		

U = 2.32 ft/s Vo = 0.09 ft/s Nbo/Vo = 0.625		U = 3.56 ft/s Vo = 0.14 ft/s Nbo/Vo = 0.75		U = 2.32 ft/s Vo = 0.09 ft/s Nbo/Vo = 1.0	
VoT/bo	H/bo	VoT/bo	H/bo	VoT/bo	H/bo
0.00	0.00	0.00	0.00	0.00	0.00
.34	.33	.60	.54	.41	.39
.67	.66	1.13	.98	.72	.59
1.05	.95	1.64	1.33	1.05	.84
1.42	1.29	2.15	1.63	1.37	1.00
1.81	1.58	2.69	1.88	1.78	1.13
2.24	1.84	3.25	2.18	2.03	1.14
2.69	2.20				
3.10	2.44				
3.57	2.72				

APPENDIX D - DELTA 2 TABULATED DATA

AR = 1.69   VERTEX = 50.0 DEG   B = 5.1 inches

bo = 3.70 inches   ALPHA = 10 DEG

U = 4.04 ft/s		U = 3.56 ft/s		U = 3.09 ft/s	
Vo/U = 0.0328		Vo/U = 0.0330		Vo/U = 0.0330	
Nbo/Vo = 0		Nbo/Vo = 0		Nbo/Vo = 0	
VoT/bo	H/bo	VoT/bo	H/bo	VoT/bo	H/bo
0.00	0.00	0.00	0.00	0.00	0.00
.88	.88	.66	.66	.92	.76
1.86	1.72	1.36	1.24	1.58	1.31
2.58	2.28	2.02	1.89	2.06	1.82
3.33	2.88	2.88	2.34	2.66	2.34
4.15	3.34	3.48	2.88	3.25	2.74
5.85	3.96	4.17	3.40	3.83	3.21
5.96	4.25	4.76	3.73	4.43	3.44
6.91	4.73	5.44	4.15	5.02	3.89
8.85	5.88	6.28	4.58	5.68	4.31

U = 4.04 ft/s		U = 2.20 ft/s		U = 2.20 ft/s	
Vo/U = 0.0328		Vo/U = 0.0315		Vo/U = 0.0315	
Nbo/Vo = 0		Nbo/Vo = 0		Nbo/Vo = 0	
VoT/bo	H/bo	VoT/bo	H/bo	VoT/bo	H/bo
0.00	0.00	0.00	0.00	0.00	0.00
.70	.76	.49	.43	.48	.43
1.53	1.49	.92	.82	.97	.92
2.31	2.11	1.34	1.17	1.43	1.34
3.10	2.78	1.75	1.59	1.87	1.72
4.68	3.73	2.16	1.95	2.31	2.11
5.82	4.57	2.58	2.24	2.72	2.41
		3.01	2.57	3.09	2.63
		3.45	2.81	3.48	2.92
		3.87	3.00	3.98	3.24
		5.81	4.85	4.73	3.73
				5.14	4.85

AR = 1.89   VERTEX = 50.0 DEG   B = 5.1 inches

bo = 3.70 inches   ALPHA = 10 DEG

U = 3.09 ft/s		U = 3.09 ft/s		U = 2.20 ft/s	
Vo/U = 0.0326		Vo/U = 0.0326		Vo/U = 0.0326	
Nbo/Vo = 0		Nbo/Vo = 0.50		Nbo/Vo = 0.75	
VoT/bo	H/bo	VoT/bo	H/bo	VoT/bo	H/bo
0.00	0.00	0.00	0.00	0.00	0.00
.71	.76	.64	.64	.37	.36
1.27	1.24	1.26	1.14	.74	.71
1.82	1.76	1.90	1.65	1.13	.97
2.36	2.18	2.47	2.00	1.53	1.26
2.93	2.64	3.05	2.38	1.92	1.47
3.54	3.04	3.66	2.62	2.31	1.68
4.18	3.56	4.26	2.87	2.70	1.81
4.83	3.99	4.88	3.10	3.18	1.84
5.68	4.57			3.52	1.88

U = 4.04 ft/s		U = 3.09 ft/s	
Vo/U = 0.0326		Vo/U = 0.0326	
Nbo/Vo = 0.375		Nbo/Vo = 0.50	
VoT/bo	H/bo	VoT/bo	H/bo
0.00	0.00	0.00	0.00
.97	.94	.61	.64
1.79	1.54	1.20	1.10
2.81	2.14	1.80	1.58
3.48	2.62	2.38	1.97
4.15	3.28	3.00	2.33
4.95	3.82	3.60	2.62
5.83	4.01	4.19	2.94
		4.77	3.07

APPENDIX E

INTERACTION OF TIP AND ROOT VORTICES FOR VARIOUS BODY CONFIGURATIONS

It is a well-known fact that the combination of the body and lifting surfaces may give rise to root vortices in addition to the tip vortices. The occurrence of the tip vortices depend strongly on the manner the lifting surfaces are attached to the body. If and when they occur, they affect the evolution of the tip vortices and hence their ultimate demise. Consequently, it is of special importance to examine in detail, albeit through the use of the inviscid line vortices, the mutual interaction of the two types of vortices for various body shapes.

The analysis described below assumes three different body shapes: (i) a streamlined axisymmetric body with lifting surfaces; (ii) a stream-lined half body [half of that used in (i)] and the identical lifting surfaces; and (iii) only the lifting surfaces protruding above a plane surface (representing a body of infinite radius).

The case (i) was analyzed through the use of image line vortices and the appropriate complex velocity potential (see Fig. 56). The analysis yields the following complex velocity

$$iu+v = \frac{\Gamma_1/2\pi}{(z_1-\frac{a^2}{\bar{z}_1})} + \frac{\Gamma_2/2\pi}{z_1-z_2} - \frac{\Gamma_2/2\pi}{z_1-\frac{a^2}{\bar{z}_2}} + \frac{\Gamma_1/2\pi}{z_1+\bar{z}_1} - \frac{\Gamma_1/2\pi}{z_1+\frac{a^2}{\bar{z}_1}}$$

$$- \frac{\Gamma_2/2\pi}{z_1-\bar{z}_2} + \frac{\Gamma_2/2\pi}{z_1+\frac{a^2}{\bar{z}_2}} + \frac{iA'}{2\pi z_1} \qquad\qquad (E-1)$$

145
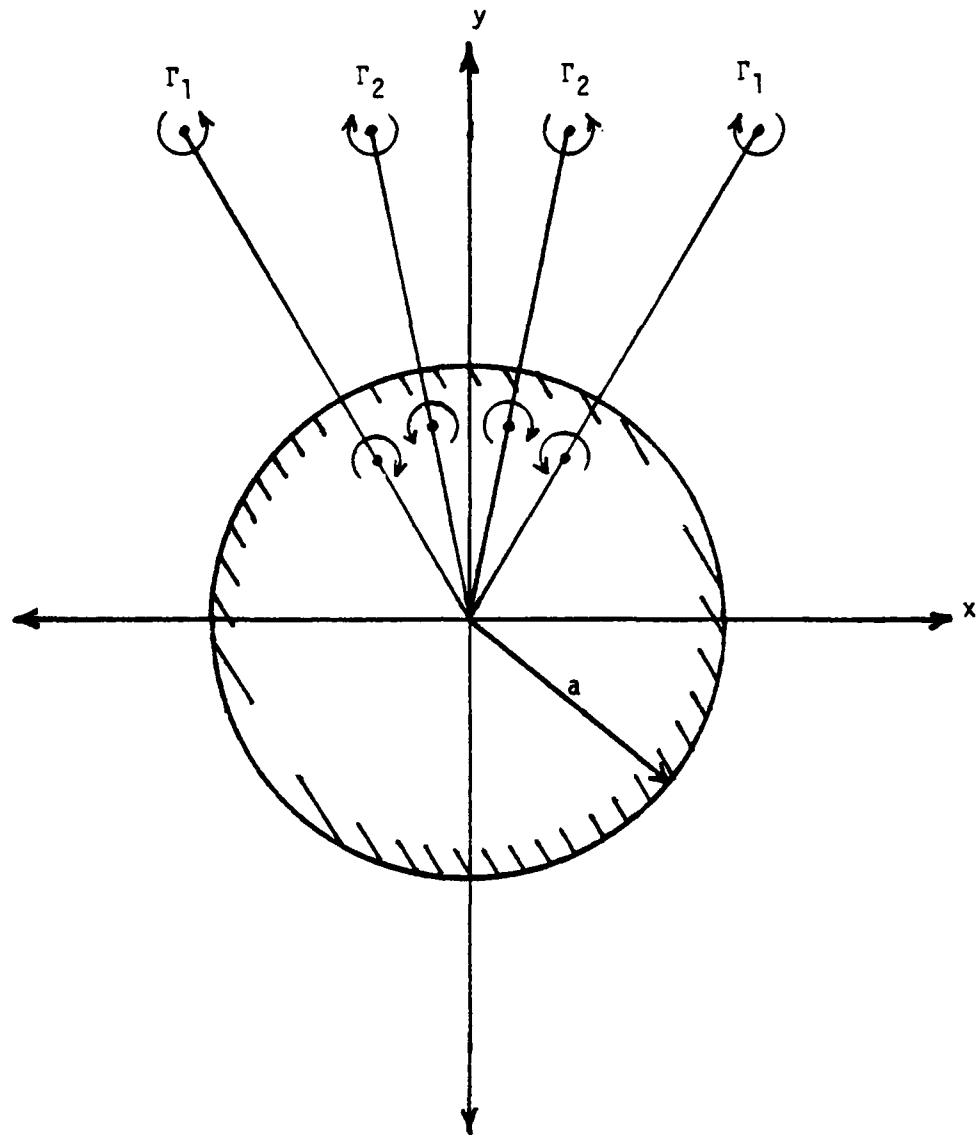
Figure 56. Real and Image Vortices for the
Whole Body Analysis.

where u and v are the x and y components of velocity; $-\Gamma_1$ and Γ_2, the strengths of the tip and root vortices; z_1 and z_2, the complex displacement vector locations of the vortices from the body center; a, the radius of the body (dependent on the distance along the body); and A', the change in body cross-sectional area per unit longitudinal length of the streamline cylindrical body.

Writing

$$u_1^{(n)} + iv_1^{(n)} = \overline{-i(iu_1 + v_1)} \qquad \text{(E-2)}$$

$$\Delta z_1^{(n)} = \frac{1}{2}[3(u_1^{(n)} + iv_2^{(n)}) - (u_1^{(n-1)} + iv_i^{(n-1)})]\Delta t \qquad \text{(E-3)}$$

and

$$z_1^{(n)} = z_1^{(n-1)} + \Delta z_1^{(n)} \qquad \text{(E-4)}$$

where Δt is the time step, the vortex positions were calculated as a function of time. Clearly, the values superscripted by (n-1) represent those previous to those superscripted by n. The value of A' depends on the specific shape of the body under consideration.

The results are shown in Figs. 57 and 58 for the tip and root vortices. In these figures, Y/b_0 represents the normalized height of the vortices as measured from the streamlined body and Z/b_0, the normalized distance along the body, starting at the tip of the lifting surface. Figure 57 shows the vortex positions shortly after their formation while they are under the significant influence of the potential flow generated
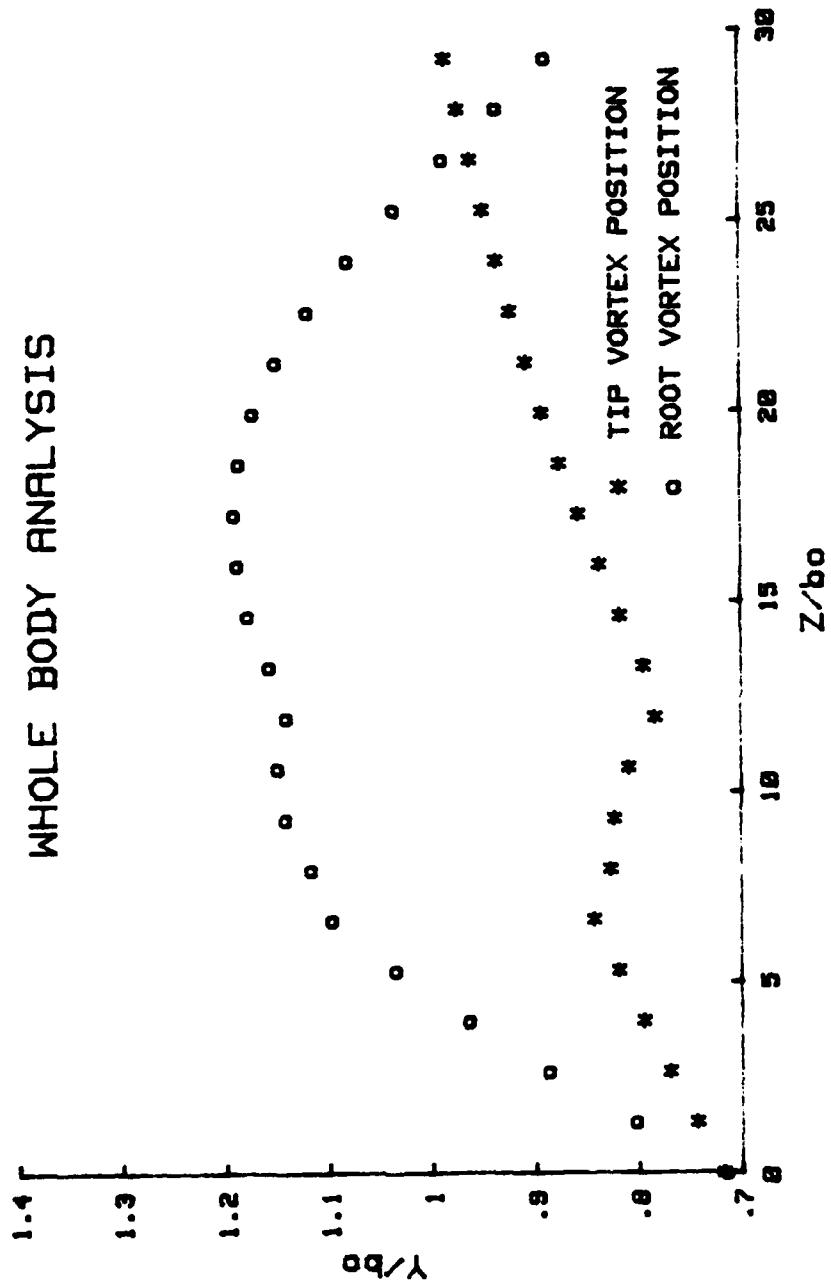
Figure 57. Positions of Tip and Root Vortices for the Whole Body
(Near the Lifting Surface).
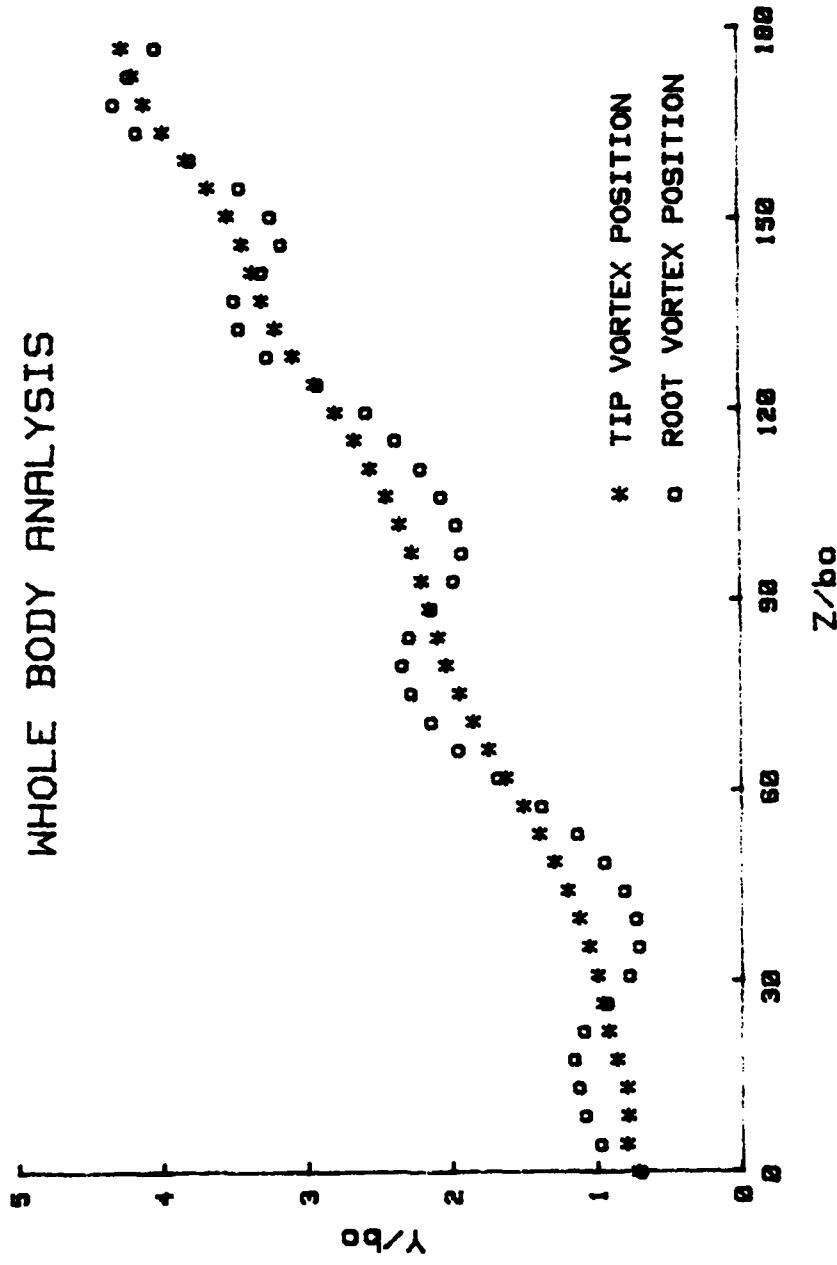
Figure 58. Positions of Tip and Root Vortices for the Whole Body (Away from the Lifting Surface).

by the body. It should be noted that the tip vortex dips near $Z/b_0 = 14$ where the streamlined body terminates. In other words, the potential flow about the aft end of the body pulls the tip vortices toward the body. Beyond the end of the body, the four vortices are under each other's mutual induction only, without body effects. Figure 58 shows the long term interaction between the tip and root vortices (of course assuming that the vortices retain their inviscid character). Clearly, the tip and root vortices rotate about each other. Real vortices are not expected to survive such a continuous rotation.

The case (ii), (the half-body problem), was analyzed in the same manner through the use of the vortex system shown in Fig. 59. The following complex velocity was used to obtain the velocity of the tip vortex in the first quadrant

$$
\begin{aligned}
iu_1 + v_1 = &\frac{\Gamma_1/2\pi}{z_1 - \frac{a^2}{\bar{z}_1}} + \frac{\Gamma_2/2\pi}{z_1 - z_2} - \frac{\Gamma_2/2\pi}{z_1 - \frac{a^2}{\bar{z}_2}} + \frac{\Gamma_1/2\pi}{z_1 + \bar{z}_1} - \frac{\Gamma_1/2\pi}{z_1 + \frac{a^2}{\bar{z}_1}} - \frac{\Gamma_2/2\pi}{z_1 + \bar{z}_2} \\[2ex]
&+ \frac{\Gamma_2/2\pi}{z_1 + \frac{a^2}{\bar{z}_2}} - \frac{\Gamma_1/2\pi}{z_1 + z_1} + \frac{\Gamma_1/2\pi}{z_1 + \frac{a^2}{\bar{z}_1}} + \frac{\Gamma_2/2\pi}{z_1 + z_2} - \frac{\Gamma_2/2\pi}{z_1 + \frac{a^2}{\bar{z}_2}} + \frac{\Gamma_1/2\pi}{z_1 - \bar{z}_1} \quad \text{(E-5)} \\[2ex]
&- \frac{\Gamma_1/2\pi}{z_1 - \frac{a^2}{z_1}} - \frac{\Gamma_2/2\pi}{z_1 - \bar{z}_2} + \frac{\Gamma_2/2\pi}{z_1 - \frac{a^2}{\bar{z}_2}} + \frac{iA'}{2\pi z_1}
\end{aligned}
$$

in which every parameter has the previously ascribed meaning to it.

The results of the half body analysis are presented in Figs. 60 and 61. The vortex positions are very close to those calculated for the

150
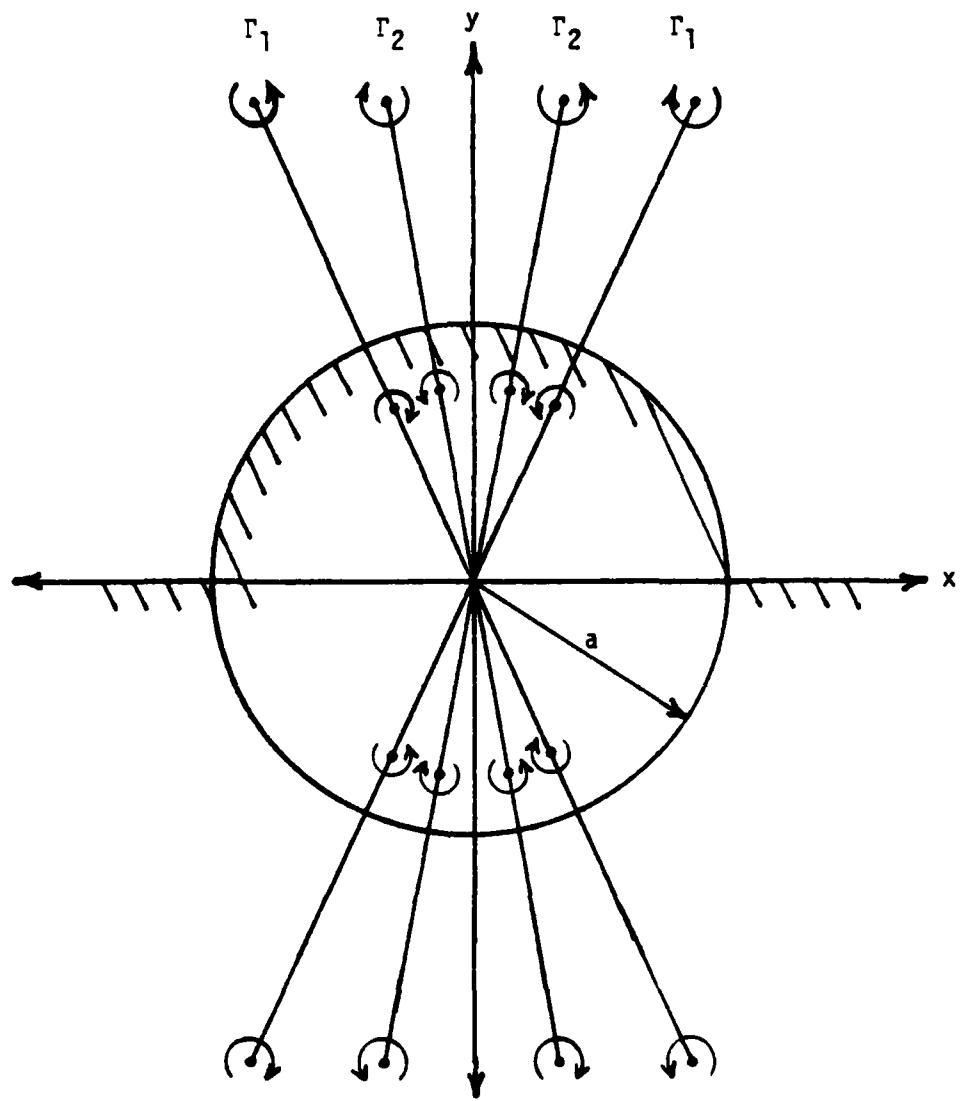
Figure 59. Real and Image Vortices for the
Half Body Analysis.
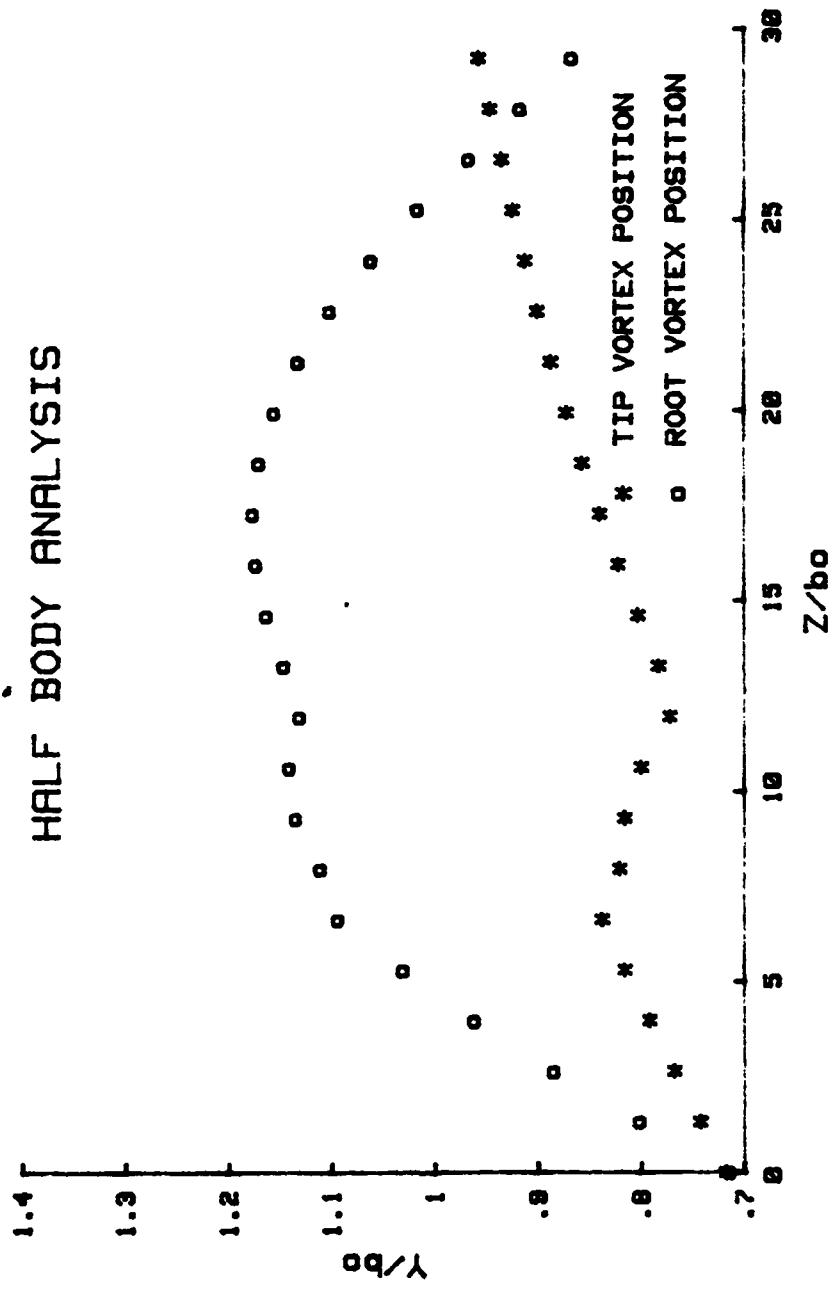
Figure 60. Positions of Tip and Root Vortices for the Half Body
(Near the Lifting Surface).

152
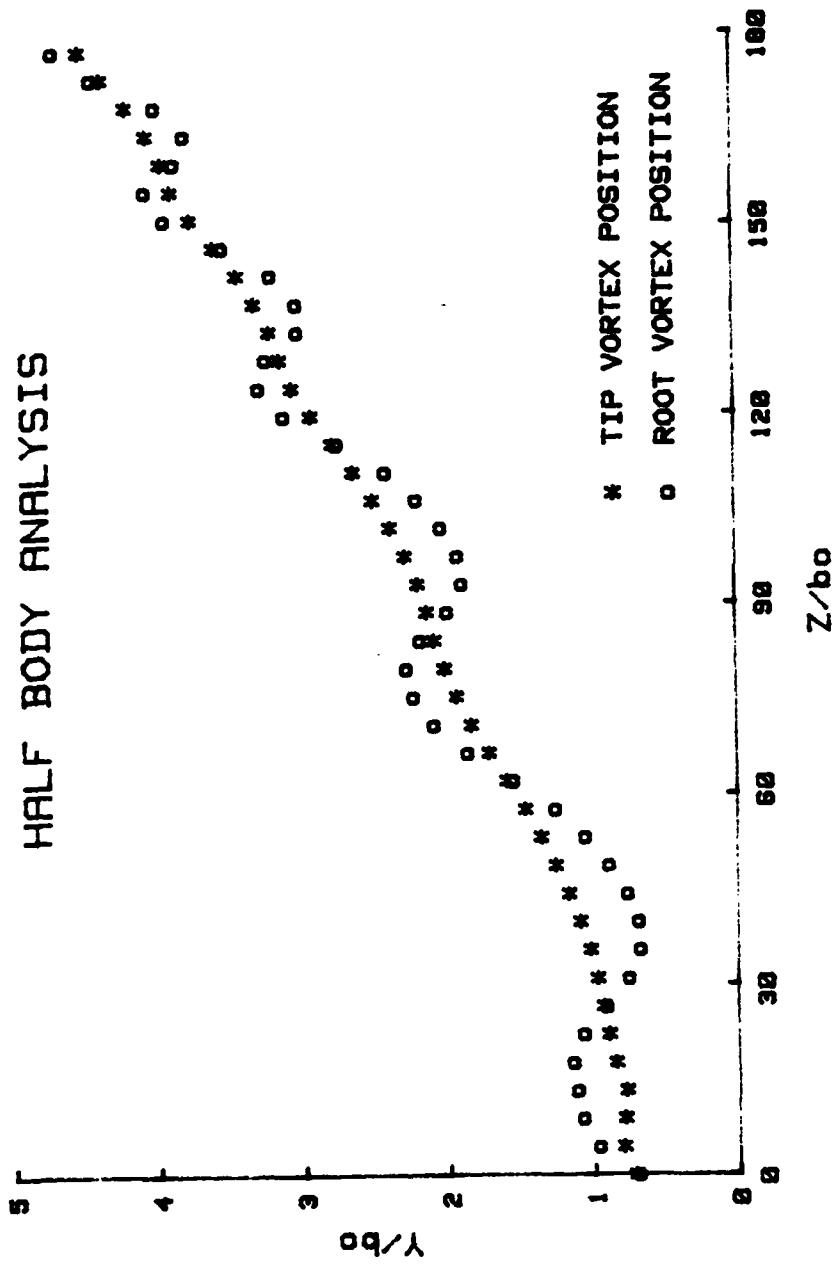
Figure 61. Positions of Tip and Root Vortices for the Half Body (Away from the Lifting Surface).

153

whole body, particularly shortly after the formation of the vortices.
Thus, one may conclude from a hydrodynamic as well as practical point
of view that the half body closely models the whole body while providing
additional experimental flexibilities (e.g., larger depth to body diameter,
mounting of the test body, etc.).

The plane-wall analysis, i.e., case (iii), was carried out through the
use of simple images as shown in Fig. 62. The following complex velocity
describes the velocity of the tip vortex in the first quadrant:

$$iu_1 + v_1 = \frac{\Gamma_1/2\pi}{z_1 + \bar{z}_1} + \frac{\Gamma_1/2\pi}{z_1 - \bar{z}_1} - \frac{\Gamma_1/2\pi}{z_1 + z_1} + \frac{\Gamma_2/2\pi}{z_1 - z_2} - \frac{\Gamma_2/2\pi}{z_1 + \bar{z}_2} - \frac{\Gamma_2/2\pi}{z_1 - \bar{z}_2}$$

$$+ \frac{\Gamma_2/2\pi}{z_1 + z_2} \qquad\qquad (E-6)$$

Once again, identical values of the parameters were used in order to
compare the results of the three cases.

Figures 63 and 64 show the results of the plane-wall analysis. It
is clear from a comparison of Figs. 63 and 64 with Figs. 57 and 58 that
the absence of the body gives rise to significant differences in the
evolution of the vortices. Also, the dipping of the tip vortex at $Z/b_0 = 14$
is not possible without the streamlined body. Clearly, the half-body
configuration models much more closely the whole-body behavior than the
plane-wall model.

The foregoing analysis is limited by such assumptions as inviscid
line vortices, instantaneous vortex roll-up, no boundary layer along the
body, etc. Nevertheless, the hydrodynamic effects of the body are strong
enough to discourage the use of the plane-wall model in the experiments.
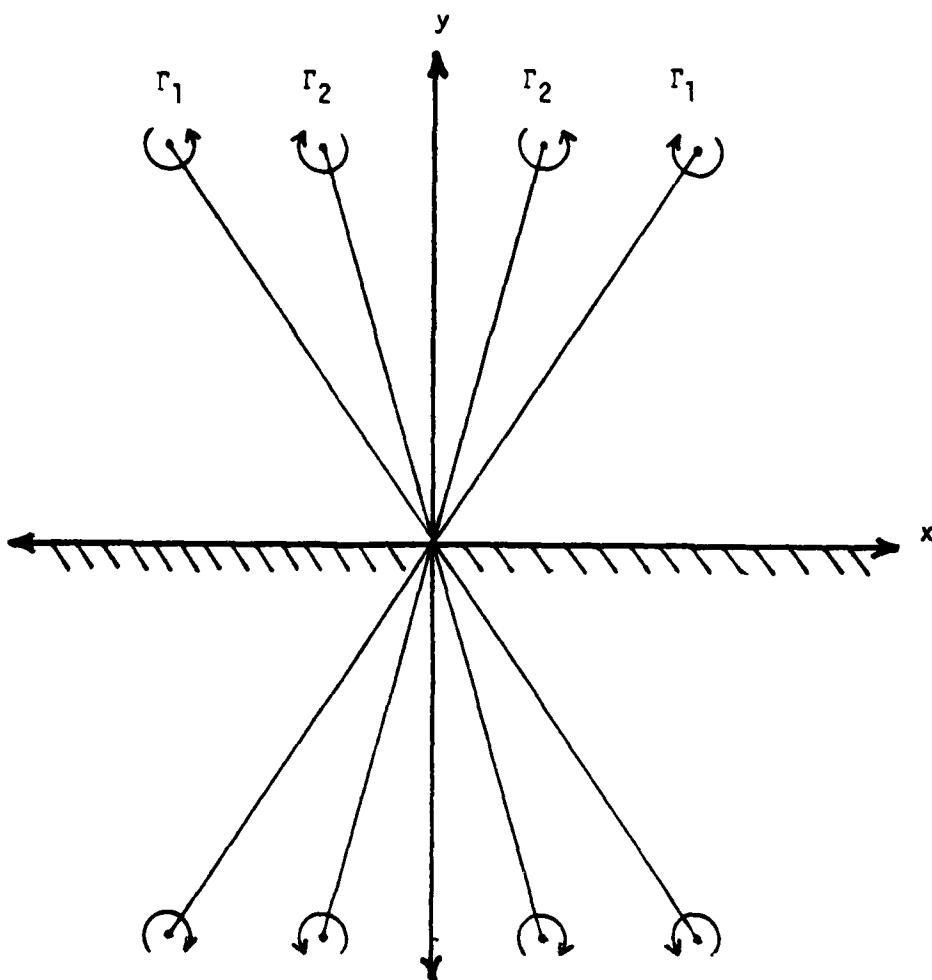
Figure 62. Real and Image Vortices for the
Plane Wall Analysis.
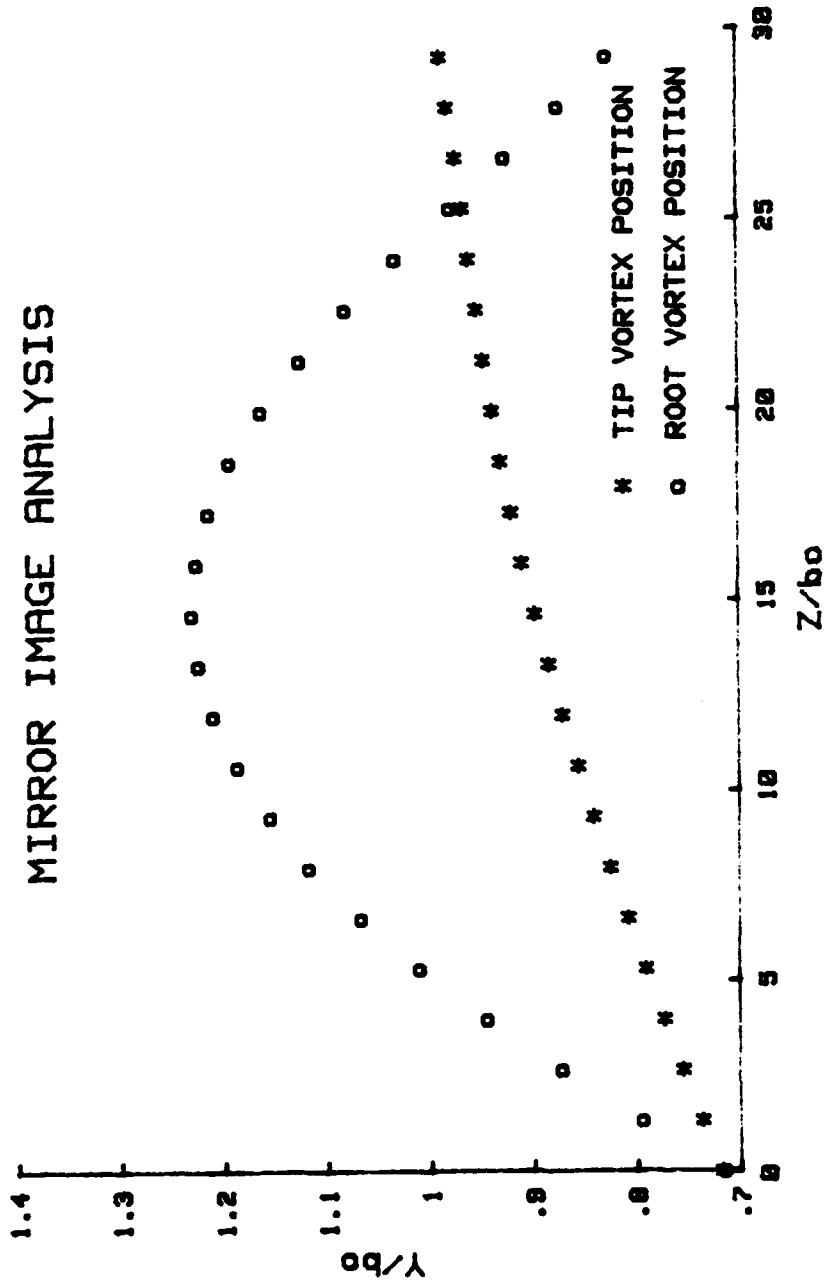
Figure 63. Positions of Tip and Root Vortices For the Plane Wall Analysis
(Near the Lifting Surface).

156
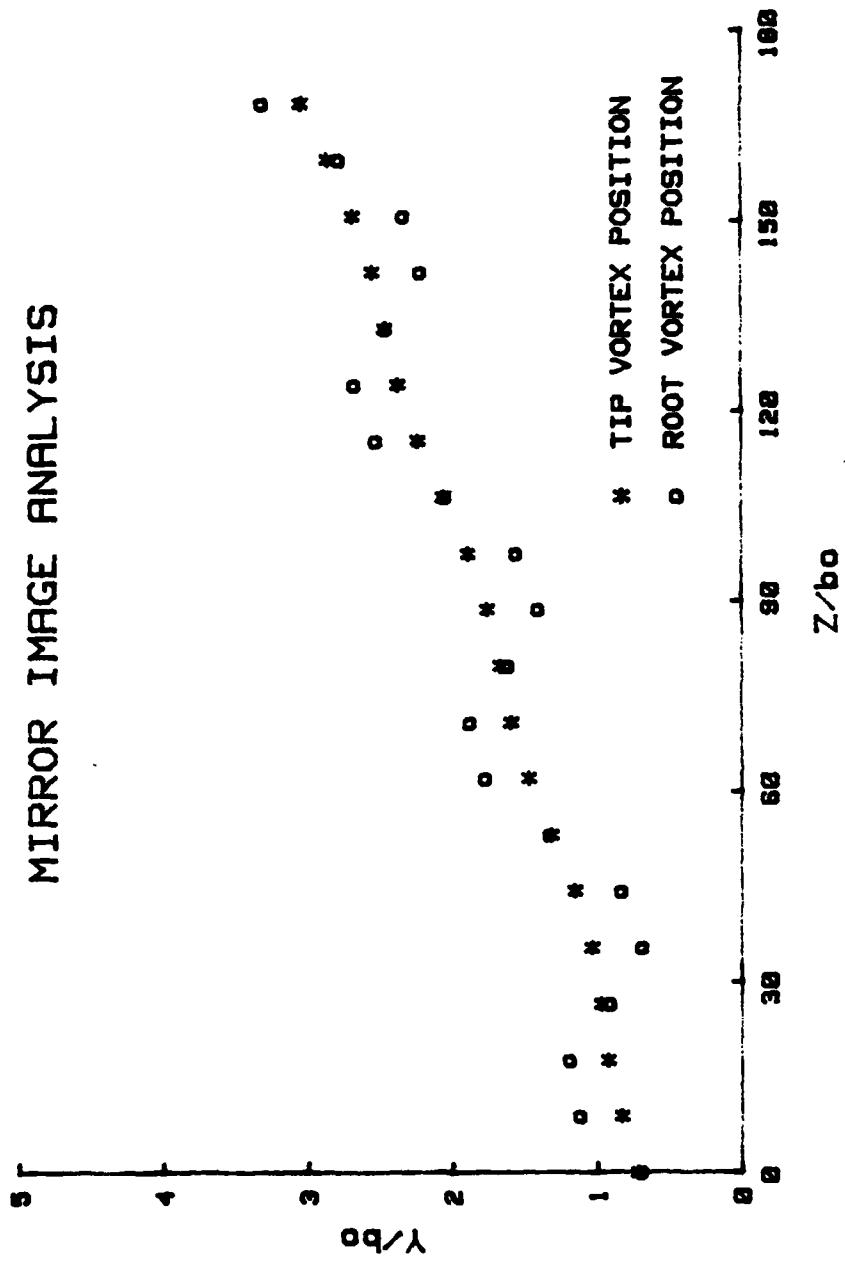
Figure 64. Positions of Tip and Root Vortices for the Plane Wall Analysis (Away from the Lifting Surface).

The prediction of the spiralling of the tip and root vortices from the analysis of the whole or half body required the determination of the specific conditions under which the two said vortices cannot spiral about each other. Such an analysis was carried out only for the simple case shown in Fig. 65 where the body effects are ignored. The use of the complex function for the two real vortices and their images together with the condition of no spiralling yielded

$$\alpha = \beta \frac{3 + \beta^2}{1 + 3\beta^2} \tag{E-7}$$

where $\alpha = |\Gamma_1/\Gamma_2|$ and $\beta = x_1/x_2$. Clearly, there exists a region delineated by certain values of α and β in which the vortices do not rotate about each other. The conditions under which the vortices do rotate about each other may be exploited for more rapid demise of the vortices. However, it remains to be seen as to how and under which conditions the root vortices are generated. This information could only come from experiments and is very much related to the lift carrying capacity of the lifting surfaces and of the body to which they are attached.
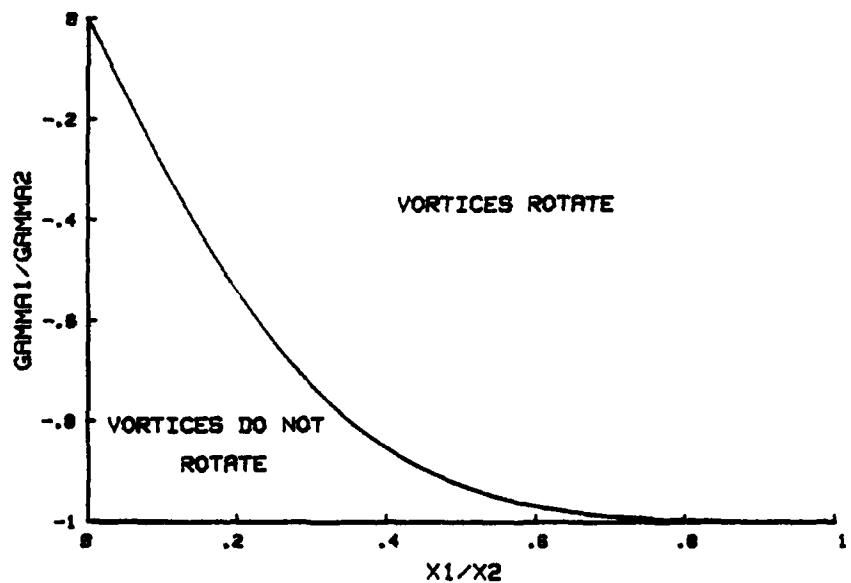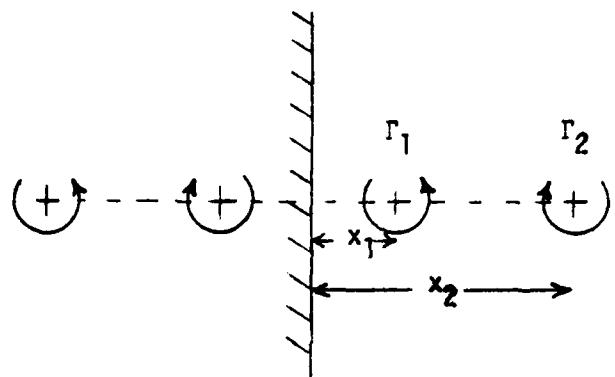
Figure 65. The Analysis of No-Rotation Condition of the Tip and
Root Vortices.

159

INITIAL DISTRIBUTION LIST

No. Copies

Dr. Arthur J. Bruckheim   1
DARPA/TTO
1400 Wilson Blvd.
Arlington, VA 22209

Chief of Naval Operations
OP-95T, Room 5D616
The Pentagon
Washington, DC 20350
Attn: Dr. Jack Breedlove   1
Attn: Dr. A. Andreassen   1

Commander
Department of the Navy
Strategic Systems Project Office
Washington, DC 20376
Attn: Dr. Philip Selwyn (SP2023)   1

Chief of Naval Operations
OP-021, Room 4D544
The Pentagon
Washington, DC 20350
Attn: Dr. Ed Harper   1

Dr. Irwin E. Alber   1
Arete Associates
P.O. Box 350
Encino, CA 91316

Dr. Steve Crow   1
Poseidon Research
1299 Ocean Avenue
Suite 821
Santa Monica, CA 90401

Dr. Wasyl Wasylkiwskyj   1
Physical Dynamics, Inc.
Suite 1620
1300 N. 17th Street
Arlington, VA 22209

Dr. Richard Hoglund   1
ORI, Inc.
1400 Spring Street
Silver Spring, MD 70910

Dr. Denny Ko   1
Dynamics Technology, Inc.
22939 Hawthorne Blvd.
Suite 200
Torrance, CA 90505

Dr. C. D. Donaldson   1
Aeronautical Research Associates of Princeton, Inc.
1800 Old Meadow Road
Suite 114
McLean, VA 22102

Applied Physics Laboratory
The John Hopkins University
Johns Hopkins Road
Laurel, MD 20810
Attn: Dr. L. Crawford   1
Attn: Dr. H. Gilreath   1
Attn: Dr. G. Merritt   1
Attn: Dr. Gary Smith   1
Attn: Dr. Tom Taylor   1
Attn: Dr. D. Wenstrand   1

Dr. Dennis Holliday   1
R&D Associates
4640 Admiralty Way
Marina del Rey, CA 90291

Dr. Don LeVine   1
JASON Program Office
The MITRE Corporation
1820 Dolley Madison Blvd.
McLean, VA 22102

Flow Research
21414 68th Ave. South
Kent, WA 98031
Attn: Peter Liu   1

Continuum Dynamics
P. O. Box 3073
32 Nassau St.
Princeton, NJ 08540
Attn: Alan Bilanin   1

Defense Technical Information Center   2
Attn: DTK-DDA-2
Building 5
Cameron Station
Alexandria, VA 22314

Dr. T. Sarpkaya   10
Code 69SL
Mechanical Engineering
Naval Postgraduate School
Monterey, CA 93940

Office of Research Administration   1
Code 012A
Naval Postgraduate School
Monterey, CA 93940

Library, Code 0142   4
Naval Postgraduate School
Monterey, CA 93940

Chairman, Mechanical Engineering   1
Code 69
Naval Postgraduate School
Monterey, CA 93940